

**HEAT TRANSFER AND
CONDENSATION OF WATER
VAPOUR FROM HUMID AIR IN
COMPACT HEAT EXCHANGERS**

Mohammad Saraireh

A thesis submitted in fulfilment of the requirements of the Degree of
Doctor of Philosophy

at

School of Engineering and Science
Faculty of Health, Engineering and Science
Victoria University
Melbourne, Australia

February 2012

ABSTRACT

In this thesis, an experimental and simulation study of heat transfer in water-to-air compact-plate heat exchanger is presented. A compact-plate heat exchanger made of polypropylene, in which flow pattern is maintained as counter-current, was constructed to conduct the experiments. Experiments were conducted for different operation conditions of hot and cold fluids, in which hot water is considered hot streams and air is considered cold streams. The thermal performance of the plate heat exchanger was analysed using the experimental data. Computational fluid dynamics (CFD) package FLUENT[®] was used to predict the fluid flow and heat transfer in the plate heat exchanger and to study the transient response of the system to changes of inlet temperature for both fluids. The results of the heat rejection rate are presented for the heat exchanger, which is simulated according to the configuration of the plate heat exchanger used in the experiments. The model was also simulated at different operation conditions and compared with experimental data. The simulated results are in good agreement with experimental results.

When the heat exchangers are used as condensers, vapour condensation occurs in the heat exchangers. To enhance our physical understanding of condensation, a new mathematical model for the condensation of water vapour from humid air in a heat exchanger is presented. The mathematical model is developed using heat and mass balances in a plate heat exchanger in which a mixture of water vapour and non-condensable gas (air) is cooled by liquid water. Numerical predictions of condensation rate, heat flux and outlet water temperature in the plate heat exchanger

are compared with experimental results from the literature and good agreement is found. The model is also used for tube condensers to predict the condensation rate, the bulk temperatures of the coolant and the gas-vapour mixture, and the inside and outside surface temperatures of the condenser wall. The predicted results for the counter-flow tube condensers are compared with three sets of published experimental data. The results from this study show that when modelling vapour condensation in the presence of non-condensable gas, a simple model for the mixture channel alone is not sufficient, since neither the temperature nor the heat flux at the wall separating the mixture and the coolant can be assumed constant. The results also show that the wall temperature in the coolant channel can be quite high because of the resistance of heat transfer, and careful modelling of the heat transfer in the coolant channel is needed to achieve good agreement between the model predictions and the experimental results.

Finally, CFD simulations of heat and mass transfer involving the condensation of vapour in the presence of non-condensable gases in plate heat exchanger are presented. The simulations were carried out using FLUENT[®]. Convective heat and mass transfer and vapour condensation at a constant wall temperature are investigated for a plane channel with the aim of comparing the CFD results with well-established correlations. CFD simulations of heat and mass transfer and water-vapour condensation in the presence of non-condensable air are then carried out for constant heat transfer coefficients for the condensation wall and coolant with different mass fractions of water vapour and inlet velocities. The predictions obtained from this are compared with experimental data and reasonable agreement is found for the condensation rates of water vapour and heat flux. Finally, the condensation of the water vapour is simulated in a heat exchanger including both the cooling water and

vapour-air mixture channels separated by solid walls. This simulation is unique and close to reality and no assumptions are required for the temperature or heat transfer coefficient at the condensing wall. The difficulties of simultaneously simulating a gas mixture and liquid flowing in separate channels using commercially available CFD software are discussed and strategies to overcome these difficulties are outlined. Results from this simulation are presented and compared with available experimental results.

DECLARATION

I, Mohammad Saraireh, declare that the PhD thesis entitled ‘Heat transfer and condensation of water vapour from humid air in compact heat exchangers’ is no more than 100,000 words in length including quotations and exclusive of tables, figures, appendices, bibliography, references and footnotes. This thesis contains no material that has been submitted previously, in whole or in part, for the award of any other academic degree or diploma. Except where otherwise indicated, this thesis is my own work.

Signature:



Date: 29/08/2012

ACKNOWLEDGEMENTS

I would like to take this opportunity to acknowledge those who have supported me during my candidature. Firstly, I would like to thank my supervisors, Associate Professor Jun-De Li and Professor Graham Thorpe, for giving me this opportunity, for their constant support and encouragement throughout, and for their belief that I would complete my candidature.

I would also like to thank my colleagues and all the members of the School of Engineering and Science at Victoria University of Technology for their help and support.

Finally, I wish to thank my family. My appreciation extends to my parents for their encouragement and support, and to my brothers and sister.

LIST OF PUBLICATIONS

Conference papers

Saraireh, M, Li, JD & Thorpe, GR 2010, 'Modelling of heat and mass transfer involving vapour condensation in the presence of non-condensable gases', *17th Australasian fluid mechanics conference*, Auckland, New Zealand.

Saraireh, M, Thorpe, G & Li, J-D 2011, 'Simulation of heat and mass transfer involving vapour condensation in the presence of non-condensable gases in plane channels', *ASME conference proceedings*, T10026-T10026-10.

Journal paper

Li, J-D, Saraireh, M & Thorpe, G 2011, 'Condensation of vapour in the presence of non-condensable gas in condensers', *International Journal of Heat and Mass Transfer*, vol. 54, pp. 4078–4089.

NOMENCLATURE

B_m	dimensionless driving force based on mass fractions
C_p	specific heat ($J kg^{-1} K^{-1}$)
C	concentration ($kg m^{-3}$)
d	diameter of the inner pipe (m)
D	diffusivity ($m^2 s^{-1}$)
$D_{i,m}$	diffusion coefficient for species i in the mixture ($m^2 s^{-1}$)
$D_{T,i}$	thermal diffusion coefficient ($m^2 s^{-1}$)
E	energy (J)
f	Fanning friction factor
g	acceleration due to gravity ($m s^{-2}$)
G_b	generation of turbulence kinetic energy due to buoyancy
G_k	generation of turbulence kinetic energy due to mean velocity gradients
G	mixture mass flux ($kg m^{-2} s^{-1}$)
Gr	Grashof number
H	heat transfer coefficient ($W m^{-2} K^{-1}$)
h_v	specific enthalpy of the vapour ($J kg^{-1}$)
h_f	specific enthalpy of the condensate ($J kg^{-1}$)
$h_{fg,i}$	latent heat of water vapour at the interface ($J kg^{-1}$)

\vec{J}_i	diffusion flux of species i ($kg\ m^{-2}s^{-1}$)
k	thermal conductivity ($W\ m^{-1}K^{-1}$)
k	turbulence energy ($m^2\ s^{-2}$)
K	mass transfer coefficient ($m\ s^{-1}$)
L	length of the pipe (m)
M	molecular weight
\dot{m}	mass flow rate ($kg\ s^{-1}$)
\dot{m}_{cond}	mass condensation rate, ($kg\ s^{-1}$)
\dot{m}''	mass flux ($kg\ m^{-2}s^{-1}$)
Nu	Nusselt number
Pr	Prandtl number $\left(Pr = \frac{C_p \mu}{k} \right)$
P	pressure (Pa)
P_v	saturation vapour pressure (Pa)
q''	heat flux ($W\ m^{-2}$)
Q_s	sensible heat (W)
Q_l	latent heat (W)
Ra	Rayleigh number
Re	Reynolds number
R_i	net rate of production of species i
r_i	tube inner radius (m)
r_o	condenser tube outer radius (m)

Sc	Schmidt number
Sc_t	turbulent Schmidt number
Sh	Sherwood number
S_k, S_ε	source terms in Equations 5.1 and 5.2, respectively
S_i	source term in Equation 5.3
S_h	volumetric heat source ($W m^{-3}$)
t	time (s)
T	temperature ($^{\circ}C$)
$T_{out,w}$	outlet water temperature ($^{\circ}C$)
$T_{in,w}$	inlet water temperature ($^{\circ}C$)
T_∞	dry bulb temperature ($^{\circ}C$)
U	bulk velocity ($m s^{-1}$)
u, v, w	velocity components ($m s^{-1}$)
V	velocity ($m s^{-1}$)
x	distance from the inlet (m)
x_0	initial entrance length (m)
Y	mass fraction
y	lateral position (m)

Greek symbols

β	thermal expansion coefficient
α	thermal diffusivity ($m^2 s^{-1}$)
$\alpha_k, \alpha_\varepsilon$	inverse effective Prandtl numbers for k and ε , respectively
δ	thickness of condensate film (m)
δ_s	thickness of solid wall (m)
ε	roughness height (m)
ε	dissipation in Equations 5.1 and 5.2 ($m^2 s^{-3}$)
μ	dynamic viscosity ($kg m^{-1} s^{-1}$)
μ_t	turbulent viscosity ($kg m^{-1} s^{-1}$)
μ_{eff}	effective viscosity ($kg m^{-1} s^{-1}$)
ρ	density ($kg m^{-3}$)
ϖ	specific humidity
τ_g	interfacial shear stress ($N m^{-2}$)
τ	stress tensor ($N m^{-2}$)

Subscripts

a	air
c	condensate
f, i	film interface
f	film
g	gas

i, j	species
l	liquid
o	without suction
r	roughness
s	solid, smooth
t	developing
v	vapour
av	air-vapour
v, i	water vapour at the air-liquid interface
v, b	water vapour in the air-vapour mixture
w	water
w, w	at the wall
wb	wet bulb

Abbreviations

CFD	computational fluid dynamics
HTC	heat transfer coefficient
UDF	user-defined functions
UDS	user-defined scalar
UJV	ustav jaderneho vyzkumu (Nuclear Research Institute)

TABLE OF CONTENTS

Abstract.....	i
Declaration.....	iv
Acknowledgements	v
List of Publications	vi
Nomenclature	vii
Table of Contents	xii
List of Figures.....	xvii
List of Tables	xxiv
Chapter 1: Introduction	1
1.1. Introduction.....	1
1.2. Research Objectives.....	3
1.3. Thesis Layout.....	4
Chapter 2: Literature Review.....	5
2.1. Polymer Heat Exchangers.....	5
2.2. Theoretical Studies of Condensation	7
2.3. Experimental Studies of Condensation.....	9
2.4. Heat and Mass Transfer with Condensation	11
2.5. Simulation of Condensation Using CFD	14
2.6. Conclusion	16

Chapter 3: Experimental and Numerical Study of Heat Transfer in Compact

Heat Exchangers	18
3.1. Introduction.....	18
3.2. The Compact Heat Exchanger	19
3.2.1. Experimental Setup	21
3.2.2. Water and Air Supply System	22
3.2.3. Measurement System.....	24
3.3. Experiment Procedure.....	26
3.4. Data Reduction	27
3.5. CFD Simulation	29
3.5.1. The Governing Equations.....	30
3.5.1.1. <i>The Continuity Equation</i>	30
3.5.1.2. <i>The Momentum Equation</i>	31
3.5.1.3. <i>The Energy Equation</i>	31
3.5.2. Geometry Creation	33
3.5.3. Boundary Conditions.....	35
3.5.3.1. <i>Inlet Boundary Conditions</i>	35
3.5.3.2. <i>Outlet Boundary Conditions</i>	35
3.5.3.3. <i>Wall Boundary Conditions</i>	35
3.5.3.4. <i>Periodic Boundary Conditions</i>	36
3.5.3.5. <i>Symmetry Boundary Conditions</i>	36
3.5.4. Grid Independence and Meshing.....	37
3.5.5. Working Fluid Properties	38
3.5.6. Solid Properties	38
3.5.7. Solver.....	39

3.6. Results and Discussion	39
3.6.1. Experimental Results.....	39
3.6.2. Simulation Results.....	44
3.6.2.1. <i>Flow Visualisation</i>	44
3.6.2.2. <i>Temperature Distribution</i>	46
3.6.2.3. <i>Velocity Distribution</i>	48
3.7. Validation of Simulation Results with Experimental Results	49
3.8. Comparison of the Heat Rejection Rate between Aluminium Alloy and Polypropylene Compact Heat Exchanger	51
3.9. Transient Response of the Polypropylene Plate Compact Heat Exchanger to Inlet Temperature Change.....	52
3.10. Conclusions.....	54
Chapter 4: Mathematical Model of Condensing Heat Exchanger	56
4.1. Mathematical Model of Heat Exchanger with Condensation.....	56
4.1.1. Heat and Mass Transfer Analysis.....	58
4.1.1.1. <i>Heat Balance on the Air-Vapour Mixture</i>	58
4.1.1.2. <i>Force and Momentum Balance on the Condensate Film</i>	60
4.1.1.3. <i>Heat Transfer at the Solid Wall</i>	62
4.1.1.4. <i>Heat Transfer in the Cooling Channel</i>	62
4.2. Mathematical Model of Tube Condenser	63
4.3. Models and Formulations of Heat and Mass Transfer.....	66
4.3.2. Suction Effect Consideration.....	68
4.3.3. Developing Flow Consideration.....	70
4.3.4. Roughness Effect Consideration	71
4.3.5. Thermophysical Properties.....	72

4.3.6. Buoyancy Effect	73
4.4. Numerical Solution Procedures	74
4.5. Results and Discussion	79
4.5.1. Comparison of Model Predictions for Condensation in Plate Heat Exchanger with Existing Experimental Results.....	79
4.5.2. Comparison of Model Predictions for Condensation in Tube with Existing Experimental Results.....	83
4.5.2.1. <i>Condensation Rate</i>	86
4.5.2.2. <i>Temperature</i>	89
4.6. Discussion and Conclusions	102
Chapter 5: CFD Simulation of Condensing Heat Exchanger	105
5.1. Governing Equations and Turbulence Modelling.....	105
5.1.1. Turbulence Equations	105
5.1.2. Species Transport Equations	106
5.2. Simulation of Condensation.....	107
5.2.1. The Experiments of Ambrosini et al. (2008) and the Benchmark Tests ..	107
5.2.1.1. <i>Step 0</i>	110
5.2.1.2. <i>Step 1</i>	118
5.2.1.3. <i>Step 2</i>	120
5.3. Conclusions and Discussion	126
Chapter 6: Conclusions and Recommendations	128
6.1. Conclusions.....	128
6.2. Recommendations.....	131
References.....	132

Appendices.....	143
Appendix A: Tables of Experimental Data.....	143
Appendix B: Thermophysical Properties of Fluids	148

LIST OF FIGURES

Figure 3.1: Schematic of the plate heat exchanger.	20
Figure 3.2: Photograph of the compact-plate heat exchanger.....	21
Figure 3.3: Photograph of the experimental setup for water-to-air heat exchanger test.	22
Figure 3.4: XF 192S pump for circulating water.....	23
Figure 3.5: Speed controller.....	24
Figure 3.6: The data acquisition system.	25
Figure 3.7: Schematic of the inputs required in FLUENT [®] and some outputs.....	30
Figure 3.8: Plate heat exchange geometry.	33
Figure 3.9: Domain dimensions and boundary conditions used in this study.	34
Figure 3.10: Grid independence test.	37
Figure 3.11: Comparison of the heat rejection rate at various air and water mass flow rates (results from Victoria University laboratory).....	40

Figure 3.12: Temperature of water entering and leaving the compact heat exchanger and the ambient air temperature for the period 24 to 25 January 2011 (results from Yallourn power station).....	41
Figure 3.13: Heat rejected by the polypropylene compact heat exchanger for the period 24 to 25 January 2011.	42
Figure 3.14: Temperature of water entering and leaving the compact heat exchanger and the ambient air temperature for the period 15 to 24 February 2011.	43
Figure 3.15: Heat rejected by the compact heat exchanger for the period 15 to 24 February 2011.	43
Figure 3.16: Flow visualisation inside the plate heat exchanger that indicates the decrease in temperature in the direction of flow.	44
Figure 3.17: Flow visualisation inside the plate heat exchange for air channel that indicates the increase in temperature in the direction of flow.	45
Figure 3.18: Temperature distribution inside the water channel.	46
Figure 3.19: Temperature distribution over plate surface of the plate heat exchanger.	47
Figure 3.20: Velocity streamline inside the water channel. Water enters at the top left-hand corner and leaves at the bottom left-hand corner.....	48

Figure 3.21: Comparison of the measured and simulated values of the heat rejection rates for the compact heat exchanger at water flow rate of 0.25 kg/s.	49
Figure 3.22: Comparison of the measured and simulated values of the heat rejection rates for the compact heat exchanger for the period 24 to 25 January 2011.	50
Figure 3.23: Comparison of the measured and simulated values of the heat rejection rates for the period 25 to 27 January 2011.	50
Figure 3.24: Transient response of water stream.	53
Figure 3.25: Transient response of air stream.	54
Figure 4.1: Schematic diagram of the small element in considering control volume analysis.	57
Figure 4.2: Schematic diagram of a tube condenser.	64
Figure 4.3: Comparison of the predicted and experimental heat flux for all the tests of Ambrosini et al. (2008).	81
Figure 4.4: Comparison of the predicted and experimental values of condensation rate for all the tests of Ambrosini et al. (2008).	82
Figure 4.5: Comparison of the predicted and experimental values of outlet water temperature $T_{w,out}$ for all the tests of Ambrosini et al. (2008).	83

Figure 4.6: Comparison of the predicted condensation rates with the experimental results of Siddique (1992), runs 1, 6, 7, 11, 13 and 17.	87
Figure 4.7: Comparison of the predicted condensation rates with the experimental results of Kuhn (1995), runs 2.1-12, 2.2-1, 2.2-8, 3.1-2, 3.3-4, 3.5-4, 4.5-3 and 4.5-5.	88
Figure 4.8: Comparison of the predicted condensation rates with the experimental results of Tanrikut and Yesin (1998), runs 2.3.1, 3.3.1, 3.4.1, 4.3.1 and 5.4.1.....	88
Figure 4.9: Comparison of the predicted temperatures of cooling water, wall and air-vapour mixture with the experimental results of Siddique (1992), run 7.	90
Figure 4.10: Comparison of the predicted temperatures of cooling water, wall and air-vapour mixture with those measured by Siddique (1992), run 11.....	90
Figure 4.11: Comparison of the predicted temperatures of cooling water, water and air-vapour mixture with those measured by Siddique (1992), run 17.....	91
Figure 4.12: Comparison of the predicted temperatures of cooling water, water and air-vapour mixture with those measured by Siddique (1992), run 26.....	91

Figure 4.13: Comparison of the predicted heat flux with the experimental results of Siddique (1992), run 26.	93
Figure 4.14: Comparison of the predicted temperatures of cooling water, air- vapour mixture, inner wall and outer wall with the experimental results of Kuhn (1995), run 2.1-12.	95
Figure 4.15: Comparison of the predicted temperatures of cooling water, air- vapour mixture, inner wall and outer wall with the experimental results of Kuhn (1995), run 2.2-8.	96
Figure 4.16: Comparison of the predicted temperatures of cooling water, air- vapour mixture, inner wall and outer wall with the experimental results of Kuhn (1995), run 3.5-4.	96
Figure 4.17: Comparison of the predicted temperatures of cooling water, mixture, inner wall and outer wall with the experimental results of Kuhn (1995), run 4.5-5.	97
Figure 4.18: Comparison of predicted heat flux with the experiment results of Kuhn (1995), run 2.1-12.	98
Figure 4.19: Comparison of the predicted temperatures of cooling water, wall and air-vapour mixture with the experimental results of Tanrikut and Yesin (1998), run 2.3.1.	99

Figure 4.20: Comparison of the predicted temperatures of cooling water, wall and air vapour mixture with the experimental results of Tanrikut and Yesin (1998), run 3.3.1.....	99
Figure 4.21: Comparison of the predicted temperatures of cooling water, wall and air-vapour mixture with the experimental results of Tanrikut and Yesin (1998), run 3.4.1.....	100
Figure 4.22: Comparison of the predicted temperatures of cooling water, wall and air-vapour mixture with the experimental results of Tanrikut and Yesin (1998), run 5.4.1.....	100
Figure 5.1: Experimental test section (Ambrosini et al. 2008).....	108
Figure 5.2: Computational domain and grid for steps 0 and 1.....	110
Figure 5.3: Grid independence test.....	111
Figure 5.4: Results obtained for two heat transfer cases in step 0: (A) T30-V3, (B) T30-V6.....	116
Figure 5.5: Results obtained for two heat and mass transfer cases in step 0: (a) T30-V3, (b) T30-V6.....	117
Figure 5.6: Comparison of calculated and experimental values of heat flux.....	119
Figure 5.7: Comparison of calculated and experimental values of condensation rate.....	119

Figure 5.8: Computational domain for step 2. 121

Figure 5.9: Comparison of calculated and experimental values of condensation
rate from step 2. 125

Figure 5.10: Comparison of calculated and experimental values of heat flux from
step 2. 126

LIST OF TABLES

Table 3.1: Test runs.....	27
Table 3.2: Comparison of the heat rejection rate between Polypropylene and Aluminium heat exchanger.	52
Table 4.1: Experimental conditions from Ambrosini et al. (2008).....	80
Table 4.2: Experimental runs used for comparison with predictions.	84
Table 5.1. Experimental conditions of tests 1–5 conducted by Ambrosini et al. (2008).	109

CHAPTER 1: INTRODUCTION

1.1. Introduction

In this thesis, the research includes three major parts: an experimental and simulation study of heat transfer in polypropylene compact-plate heat exchanger; a mathematical model of condensation of water vapour from humid air in plate and tube condensers; and a simulation study of heat and mass transfer in vapour condensation in the presence of non-condensable gas using computational fluid dynamics (CFD) software FLUENT[®] for plate condensers.

Heat exchangers are used to transfer heat from one fluid to another in such diverse applications as refrigeration, ventilation and air-conditioning systems, power generation, the manufacturing and space industries, and environmental engineering. Although there are a wide variety of heat exchangers in the market, the present work focuses on counter-current polymer compact-plate heat exchangers. Their excellent heat transfer characteristics, easy fabrication and maintenance, low weight, excellent corrosion resistance and cost competitiveness has made the polymer compact heat exchanger an important choice for engineering applications. Thus, the present thesis begins by investigating the experiments of heat transfer in a compact-plate heat exchanger made of polypropylene for water-to-air heat exchange.

When the heat exchangers are used as condensers, vapour condensation can occur in the heat exchangers. Condensation plays a key role in systems such as air conditioning, power plants, refrigeration, reactor safety, aerospace and desalination. Environmental and economic pressures are driving the need to design increasingly efficient systems. As a result, we need to increase our understanding of condensation.

Condensation is initiated and sustained when the temperature of a surface is maintained below the dew-point temperature of the surrounding vapour. In the process, a condensate is formed with the liberation of latent heat. The process may take place in one of two modes, namely film condensation or drop-wise condensation. In film condensation, the surface is completely wetted by the condensate and is blanketed by a liquid film of increasing thickness as it flows downward under the influence of gravity. Conversely, in drop-wise condensation, the surface is not fully wetted by the condensate and droplets slide downward after they attain a certain size. It is difficult to sustain drop-wise condensation, which may be achieved initially on some surfaces, and the process usually converts to film condensation after some time. Therefore, it is customary to assume film condensation in the design of condensers (Bum-Jin et al. 2004).

Computational modelling, such as that performed by CFD software FLUENT[®], has received much attention in recent years, becoming increasingly popular as an alternative approach to cope with real-world problems. Computational modelling can provide detailed information about the fluid flow and heat and mass transfer mechanism. Further, numerical methods are more flexible and much cheaper, as they give the opportunity for testing new methods before they are executed through

experiments, which are often costly. Thus, it is important to use this technology in the modelling and simulation of heat transfer and condensation in heat exchangers.

1.2. Research Objectives

The first objective of the present work is to introduce an experiment and numerical simulation of heat transfer in a counter-current polypropylene compact-plate heat exchanger for water-to-air heat exchange. To achieve this, a compact heat exchanger was fabricated and experiments were set up to examine the heat rejection rate in the heat exchanger. The validation of the experiment results with the simulation results from CFD is presented.

The second objective of this research is to study the condensation of water vapour from humid air in a heat exchanger. To this end, a mathematical model of air-vapour mixture to water heat exchanger, taking into account condensation of water vapour, is formulated. Such a model allows for a better understanding of the condensation of water vapour and the coupling of heat and mass transfer.

CFD is used to simulate the condensation problem in a heat exchanger. The simulation examines the process of heat and mass transfer that is involved in condensation. The results from the mathematical model and CFD software are validated with the available experimental data from the literature.

1.3. Thesis Layout

This thesis is divided into the following chapters:

Chapter Two

This chapter contains a review of previous work of polymer heat exchangers, and theoretical and experimental studies of condensation.

Chapter Three

This chapter presents the experimental and simulation study of heat transfer in a water-to-air counter-flow polypropylene compact-plate heat exchanger.

Chapter Four

A new mathematical model of condensation in plate and tube condensers is introduced in this chapter, and a comparison between the present work and experimental data reported in the literature is presented.

Chapter Five

A CFD simulation and results of condensation in a plate heat exchanger are presented.

Chapter Six

This chapter presents the conclusions of the research and makes recommendations for future work.

CHAPTER 2: LITERATURE REVIEW

2.1. Polymer Heat Exchangers

Using polymer heat exchangers to transfer thermal energy has received considerable attention from researchers. Perry, Dietz and Shannon (1983) used thin polymer film heat exchangers for large-scale operations, such as in converting saline or salty water to pure water. Schnon (1988) designed a plastic film plate heat exchanger for the recovery or dissipation of heat energy in buildings. Polymer heat exchangers can also be used for heat recovery in the chemical process, or in electrical power and other industries. This type of heat exchanger is designed for operation at low absolute pressures, for example, from 1370 kPa to 2060 kPa maximum.

Several polymeric materials for use in condensing heat exchangers attached to high efficiency gas fired furnaces were studied by Bigg, Stickford and Talbert (1989). Fluorinated ethylene propylene shrink film coverings, glass fibre reinforced poly (phenylene sulphide) extruded tubes and poly (ether imide) tubes were some of the materials that were studied. These polymers showed no evidence of degradation after 10,000 cycles in a gas fired condensing heat exchanger. Heat transfer and pressure drop in gas-to-air plastic heat exchanges was studied by Hetsroni and Mosyak (1994). Polymer materials such as polyethylene, polyester and poly vinylidene chloride were tested and heat transfer coefficients (HTCs) of 80–90 W m⁻² K⁻¹ were reported.

Another study on heat transfer and pressure drop in air-to-air and water-to-water compact cross-flow plate heat exchangers made of poly (ether ether ketone) (PEEK) was conducted by Jachuck and Ranshaw (1994). They recognised that this new generation of polymers could play a key role in the development of a new class of compact heat exchangers, which could be cheaper, lighter and more corrosion resistance than metal heat exchangers. Air-to-water heat transfer experiments in cross-flow plate heat exchangers made of polypropylene were described by Brouwers and Van der Geld (1996), who reported heat transfer coefficient of around $55 \text{ W m}^{-2} \text{ K}^{-1}$.

A plastic heat exchanger made from polypropylene (PP) and polyvinylidene fluoride (PVDF) was constructed by Davidson et al. (1999) to produce solar collectors for heating swimming pools. They concluded that the maximum pressure of the PP heat exchanger was 200 kPa at 80°C and that the PVDF heat exchanger could withstand 600 kPa at 100°C. Polymer plate heat exchanger made from PVDF and PP is used extensively in heating and ventilation systems, such as in car radiators. It is a form of constructed prototype plate exchanger using 60 plates measuring 45cm × 45cm. The unit transfer 26.4kW heat and it operates successfully at 75°C with 6.5 bar differential pressure (Reay, 2000).

The use of polymeric hollow fibre heat exchangers as a new type of heat exchanger for lower temperature and pressure applications was proposed by Zarkadas and Sirkar (2004). They recognised that the polymeric materials could offer many advantages over metals in the construction of heat exchangers. First, they are less expensive and easier to

shape than metals. Further, the energy required to produce a unit mass of plastics is lower than that of metals, making them environmentally attractive.

Polymer film compact heat exchangers (PFCHE) made from PEEK for use in the fuel-cell industry were studied by Zaheed and Jachuck (2005). They concluded that using PFCHE brings several benefits over the metallic fuel-cell designs in terms of overall performance, energy and cost saving.

2.2. Theoretical Studies of Condensation

The field of condensation owes its current state to the pioneering work of Nusselt (1916), who predicted, from a simplified theoretical analysis, the HTC of stationary pure vapour in film condensation on a vertical flat plate. Improvements and modifications to Nusselt's theoretical solution have been made by a number of researchers. For example, Bromley (1952) assumed a linear temperature distribution in the liquid film model. Subsequently, Rohsenow (1973) and others considered the effect of interfacial shear stress on both condensation flow and the characteristic of vapour velocity diminishing along the length of a tube. These investigations were concerned with condensation of pure vapour.

In many industrial operations, some amount of non-condensable gas may exist in vapours. It was well recognised that the presence of non-condensable gas in vapours could greatly reduce condensation heat transfer and deteriorate the performance of devices. Seminal studies on this topic were conducted by Sparrow and Lin (1964),

Minkowycz and Sparrow (1966) and Sparrow, Minkowycz and Saddy (1967). They explored analytically the condensation of gases containing non-condensable gases in forced convection flow along a horizontal flat plate. Following their studies, a number of publications were devoted to the condensation of gas mixtures in laminar or turbulent flow along horizontal, vertical or inclined plates, inside or outside tubes and in tube bundles.

For example, Patankar and Sparrow (1979) studied film condensation in the presence of non-condensable gas on a vertical fin that was attached to a cooled vertical plate or cylinder. A physically meaningful similarity solution of the problem was formulated and numerically evaluated, and a finite difference marching solution of the governing equations for conjugate problem was performed. Further, Webb and Wanniarachchi (1980) developed a one-dimensional numerical model to predict the effect of non-condensable gases in a 10-row by 10-column finned tube heat exchanger by solving the Colburn and Hougen (1934) equation for refrigerant R-11 and air mixture. An iterative solution procedure was applied to solve the equation. The modelling results were not verified with measured data.

A solution showing the effects of a non-condensable gas on the film-wise condensation of a vapour-gas mixture with turbulent flow in a vertical tube using the heat and mass transfer analogy was presented by Wang and Tu (1988). They found that the reduction in heat transfer due to the non-condensable gas was more significant at low pressures and in mixtures flowing with low Reynolds numbers.

Karapantsios, Kostoglou and Karabelas (1995) measured local condensation rates during the direct-contact condensation of water vapour from a mixture with air. The influence of the film Reynolds number was discussed. They found that an increase in the film Reynolds number increases the condensation HTC. However, with the presence of non-condensable gas, the condensation HTC decreases. The effect of the presence of a non-condensable gas, such as air on condensation rate for external condensation for the cases of stagnant as well as flowing vapour, was theoretically investigated by Dharma Rao et al. (2002).

2.3. Experimental Studies of Condensation

Condensation has been experimentally studied by many researchers. Lebedev, Baklastov and Sergazin (1969) performed an experimental study of combined heat and mass transfer in the condensation of vapour from humid air on a flat plate. They found that the condensation heat transfer increases with the relative humidity and the velocity of the air.

An experimental study of condensation in vertical tubes was performed by Siddique (1992), who used the experimental apparatus of an open cooling water circuit and an open non-condensable gas/steam loop for forced convection condition. The condenser tube dimensions were 50.8 mm OD, 46.0 mm ID and 2.54 m effective length. They concluded that the local HTC depends strongly on the mixture Reynolds number, increasing as the Reynolds number increases.

Kim and Kang (1993) and Karapantsios et al. (1995) measured the condensation heat transfer rate for steam–air mixtures in direct contact with the sub-cooled water layers. The condensation HTC's were found to be dependent not only on the steam concentration but also on the wave characteristics of the falling liquid layer.

Condensation of vapours in the presence of non-condense gas on a short horizontal tube was studied by Mamyoda and Asano (1994). They compared their analysis with their own experimental data. Satisfactory agreement was obtained between their experimental results and a mathematical model. Kuhn (1995) performed an experimental study of condensation by using a 3.37 m long seamless stainless steel tube with a 50.8 mm OD and 1.65 mm wall thickness for steam/air and steam/helium.

Experiments with gas-vapour mixtures in the presence of non-condensable gas were conducted by Ganzevles and Van der Geld (2002) to study the importance of the Marangoni effect in actual condensation processes for a compact polymer heat exchanger. The heat resistances were taken into consideration and the heat resistance of the condensate was quantified. The study introduces Nusselt and Sherwood numbers and friction factors based on a characteristic length scale valid in drop-wise condensation. New correlations were obtained from the experiments with a variety of process conditions.

An experimental study was conducted by Tanrikut and Yesin (2005) for steam condensation in the presence of air flowing downward in a vertical tube of 2.15 m with 33/39 mm ID/OD, and cold water flowing upward inside the jacket pipe of 2.133 m and

81.2/89 mm ID/OD. They presented both the temperature profile of the coolant in the jacket pipe and the mixture temperature in the condenser tube.

The use of condensing heat exchangers to recover water vapour from flue gas at coal-fired power plants was studied by Levy et al. (2008b, 2008a). Pilot scale heat transfer tests were performed to determine the relationship between flue-gas moisture concentration, heat exchanger design and operating conditions, and water-vapour condensation rate.

2.4. Heat and Mass Transfer with Condensation

The analysis by heat and mass transfer analogy in situations with condensation has been described by many researchers. Colburn and Hougen (1934) were the first to develop a theory for condensation mass transfer that was controlled by the mass concentration gradient through non-condensable layer. They described the heat transfer process as the sum of sensible heat and latent heat flows. Much later, Corradini (1984) added a correction factor that accounts for the suction effect at high mass transfer rates across the liquid-gas interface. Then, Kim and Corradini (1990) incorporated the effects of film roughness on the gas phase heat and mass transfer for a flat plate.

An analytical study of condensation in a vertical tube using the analogy between heat and mass transfer was conducted by Siddique, Golay and Kazimi (1994). Their model included the effects of developing flow, condensate film roughness, suction and property variation in the gas phase. Pele, Baudoin and Barrand (1994) studied the effect

of the flow rate of saturated humid air on the laminar film-wise condensation inside a vertical cooled pipe during turbulent forced convection. They found that the local condensate HTC decreases along the length of the pipe.

Heat and mass transfer of air-water-vapour mixture in a cross flow heat exchanger was investigated theoretically and experimentally by Brouwers and Van der Geld (1996). From comparing the results, it was found that the heat exchanger model could predict the rate of heat transfer and condensation phenomenon. A theoretical prediction of heat and mass transfer in a vertical tube condenser from steam and non-condensable gas mixture was derived by Dehbi and Guentay (1997). An algebraic equation for the film thickness was derived. Then, mass and heat transfer analogy were invoked to deduce the condensation rate.

According to Takarada et al. (1997), the analogy between the heat and mass transfer is applicable at low concentrations of vapour. Takarada et al. (1997) and Volchkov, Terekhov and Terekhov (2004) theoretically investigated the problem of condensation of humid air by solving integral boundary layer equations of energy and diffusion and using analogy between heat and mass transfer processes.

Terekhov, Terekhov and Sharov (1998) presented a computational analysis of combined heat and mass transfer in condensation of water vapour from moist air on a wall. Desrayaud and Lauriat (2001) studied condensation of water vapour from humid air in a vertical channel. They derived a new correlation for the latent and sensible Nusselt

number and demonstrated the heat and mass transfer analogy between the sensible Nusselt number and Sherwood number.

The problem of condensation of vapours on a vertical fin in the presence of non-condensable gas making use of the analogy between heat and mass transfer was tackled by Sarma et al. (2001).

Oh and Revankar (2006) developed a pure steam condensation model and an empiricism-free or minimum empirical mechanistic model for the vapour/non-condensable mixture condensation. In the model for the mixture, they used general momentum, heat and mass transport relations derived using an analytic method, and considered the surface suction effect. They found from experiments that the condensation HTC decreases with the presence of a non-condensable gas. They also developed a theoretical model for the annular film-wise condensation with non-condensable gas using heat and mass transfer analogy.

Groff, Ormiston and Soliman (2007) presented a numerical solution of film condensation from vapour-gas mixtures in vertical tubes, and solved the complete parabolic governing equations in both the liquid and gas phases, with no need for additional correlation equations for interfacial heat and mass transfer.

More recently, Lee and Kim (2008) developed a theoretical model by improving Siddique et al.'s (1994) analytical model and investigated steam condensation heat transfer in the presence of air or nitrogen gas in a vertical tube. Their results showed

that the effects of the non-condensable gas became weak as the condenser tube diameter decreased because of interfacial shear stress.

2.5. Simulation of Condensation Using CFD

Simulation of condensation using computer programs such as CFD software has been studied by researchers over the last 30 years. Lux et al. (1983) presented a computer model that could predict the performance of a condensing heat exchanger with circular tubes. This model ignored the effect of condensation and diffusion processes. Malalasekera et al. (1993) used CFD to model the heat transfer and the flow in the secondary heat exchanger of a condensing boiler. However, the diffusion process of water vapour in non-condensing gases and water-vapour condensation were not considered in his work.

Valencia (2004) carried out a CFD simulation for the condensation of water vapour and acids on the plate using a commercial code, FLUENT, and a user-defined subroutine. A numerical simulation using the commercial code and a simulation based on empirical correlations using the Engineering Equation Solver was carried out for a two dimensional (2D) vertical water-cooled plate. Experiments were conducted for the condensation of nitric acid, sulphuric acid and water vapour in the presence of air on a vertical water-cooled plate. The discrepancies between experiments and simulation are in a range of 7–25% depending on the combustion conditions and the average surface temperature of the plate.

Many film condensation models in the presence of non-condensable gases were presented by Martin-Valdepenas et al. (2005). Four models were implemented in a CFD code and compared with experimental data. They improved the code for simulating the gas mixing process in large containment buildings involving steam.

A new mechanistic model for the prediction of condensation in the presence of non-condensable gas using a commercial computational fluid dynamic code, CFX-4, was presented by Karkoszka and Anglart (2006). The model was based on a solution of the conservation equation for the vapour phase and the transport equation for the non-condensable gas. A reasonable agreement between the calculated and measured HTC was obtained.

Ambrosini et al. (2008) used the commercial CFD code FLUENT[®] for the numerical simulation of condensation of an air-steam mixture on a flat wall in a vertical square channel. They divided the problem into two steps: step 0 was to model the condensation on an isothermal flat plate and step 1 was to model the condensation in the CONAN Facility (at the Università di Pisa, Italy). The condenser wall and the coolant channel were modelled using conjugate heat transfer and secondary coolant was replaced by using equivalent heat transfer conductance. Ambrosini et al. (2008) found that the model of the condensation on an isothermal flat plate agreed reasonably well with existing correlations, but that the CFD model of the condensation in step 1 showed larger errors in condensation rates and heat flux, especially from near the entrance of the water-vapour-gas mixture.

Benelmir, Mokraoui and Souayed (2009) performed a simulation of water-vapour condensation in the presence of non-condensable gas between two vertical plane plates and in a plate fin-and-tube heat exchanger in a stationary mode using FLUENT software. They found that the condensation rate and the HTC increase with the inlet velocity of the mixture.

2.6. Conclusion

Polymer compact heat exchangers have been applied successfully in many applications over the years. They are becoming increasingly prevalent in the industry due to advances in the development of polymers and a better understanding of their properties. In this research, experiments and simulation of heat transfer in a counter-flow polypropylene compact heat exchanger are conducted and analysed. Here, the compact heat exchanger is designed to reject waste heat by using ambient air to cool warm water, which can be used as an alternative for cooling towers and metal heat exchangers. Simulation of the heat transfer in the heat exchanger is performed using FLUENT[®] to obtain the heat rejected by the heat exchanger, and the results are compared with the experimental data to validate the model.

The literature review revealed that theoretical and computational predictions of vapour condensation and heat transfer in the presence of non-condensable gas have focused on the gas-and-vapour mixture. The cooling of the gas-vapour mixture is usually calculated by assuming a constant wall temperature or a constant heat flux at the wall. In condensers, this wall temperature or heat flux at the wall is in general not known a

priori, and the temperature of the cooling fluid (for example, water) has normally been used as an approximation for the wall temperature. This may be a valid approximation when the mass flow rate of the cooling water is much larger than that of the gas-vapour mixture or when the mass fraction of the water vapour in the gas-vapour mixture is low. However, a better approach is to solve the heat and mass balance on the cooling water and the gas-vapour steams simultaneously.

In this study, we derive equations for the heat and mass balance of a heat exchanger involving water-vapour condensation in gas-vapour mixture flows with water as cooling fluid. The equations, in combination with many theoretical models for heat and mass transfer, are solved numerically. CFD software FLUENT[®] is used to simulate condensation in the heat exchanger for a more realistic model. The predictions are compared with available experimental results where experimental details can be accessed from the literature.

CHAPTER 3: EXPERIMENTAL AND NUMERICAL STUDY OF HEAT TRANSFER IN COMPACT HEAT EXCHANGERS

3.1. Introduction

Many of the available and commercially used heat exchangers are made from metals such as aluminium and stainless steel. Although metals are good conductor of heat, it also brings disadvantages in terms of cost, weight, corrosion and fouling. This has promoted the need to develop alternative heat exchangers made from polymer materials. The use of polymer heat exchangers offers substantial cost and weight savings, and polymers resist corrosion and fouling, giving them the advantage over metal heat exchangers.

The objective of this chapter is to introduce an experimental and numerical study of heat transfer in a new counter-flow compact-plate heat exchanger made of polypropylene. Experiments on heat transfer in the compact heat exchanger are conducted under various conditions for water-to-air heat exchange. Heat rejection rates in the polypropylene compact heat exchanger are obtained for various test conditions. The effect of inlet conditions such as water flow rates and air mass flow rates are discussed.

To validate the experimental results, a three-dimensional (3D) simulation using CFD software FLUENT[®] is performed for the heat exchanger.

3.2. The Compact Heat Exchanger

The plate heat exchanger is shown schematically in Figure 3.1 and a photograph of the compact heat exchanger is given in Figure 3.2. It is a counter-flow parallel-plate heat exchanger made of polypropylene. The heat exchanger consists of 250 parallel polypropylene fluted boards sealed together, producing 249 narrow parallel-flow channels. The gap between the two neighbouring boards is 0.8 mm. Hot water flows through the gaps. Each narrow channel contains an obstacle of the same material with a dimension of 225 mm × 20 mm × 0.6 mm to change the flow pattern to achieve uniform distribution of the flow inside the channels and enhance heat transfer. The plates have a height and width of 609 mm each. The total available heat exchange area of the polymer compact heat exchanger is 184.70 m². Polypropylene fluted boards are used as the material for constructing the heat exchanger. Each board has two thin sheets that become the plates and the plates are jointed together by the fluted walls. Each board of 609 mm wide has 227 small square fluted channels. These channels are mainly for holding the thin sheet together and provide support so that the board can withstand some pressure.

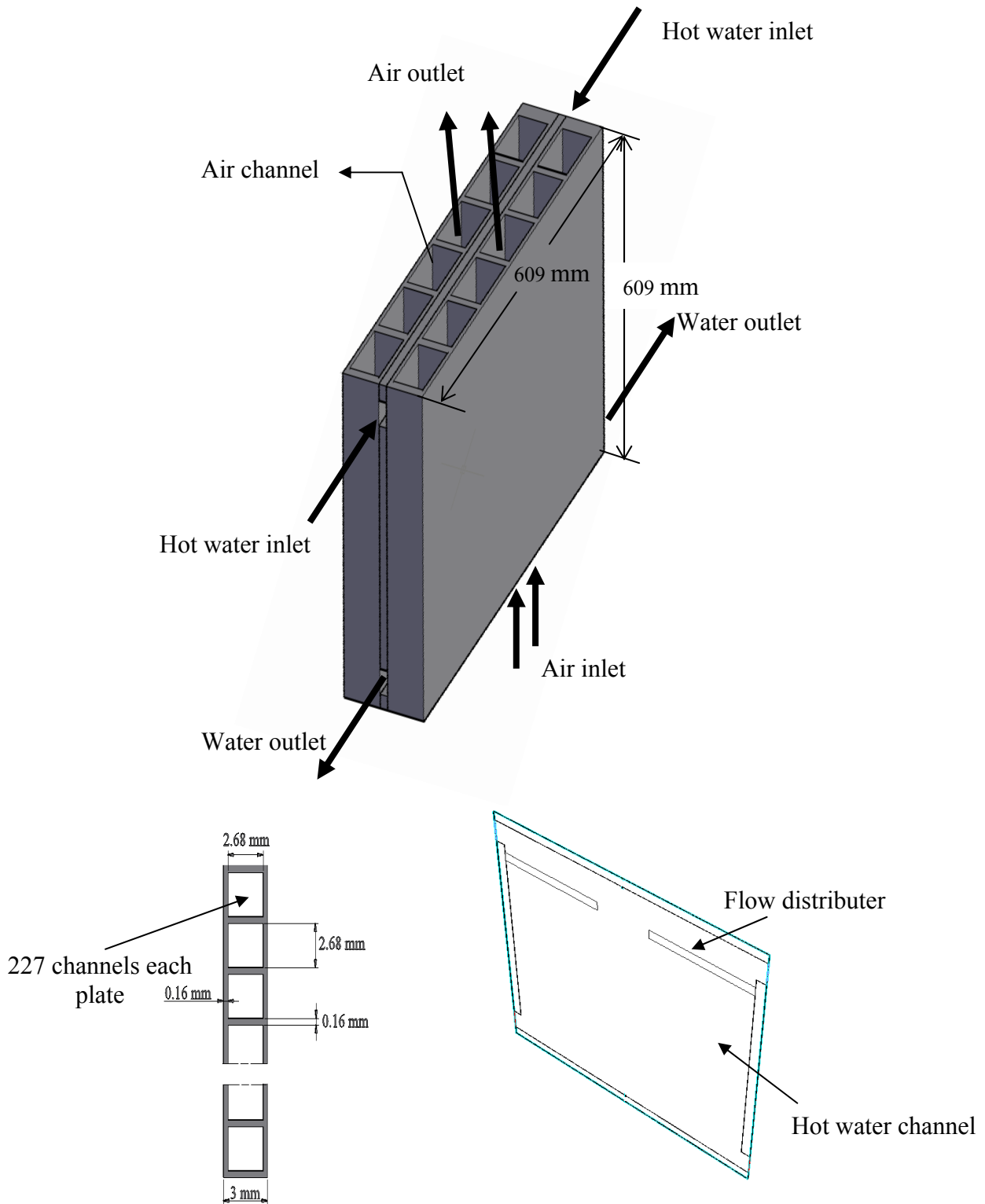


Figure 3.1: Schematic of the plate heat exchanger.

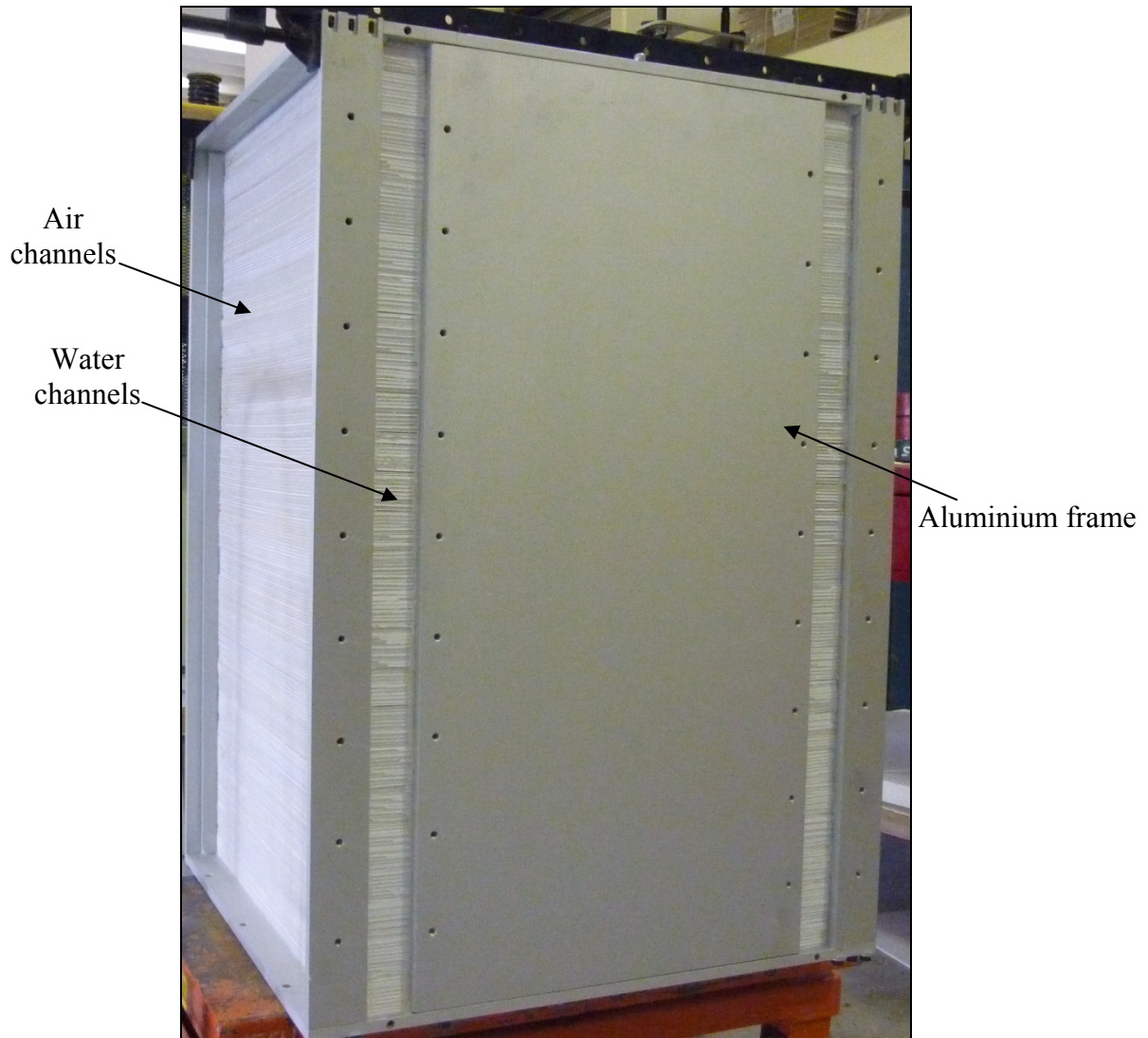


Figure 3.2: Photograph of the compact-plate heat exchanger.

3.2.1. Experimental Setup

Experiments of heat transfer in the compact-plate heat exchanger were conducted under various conditions for water-to-air heat exchange. The experiments were conducted at Victoria University laboratory and Yallourn power station. The Yallourn power station has three cooling towers, water from the towers cools the steam coming from the turbine so it can be pumped back to the boilers to be reheated to steam and again goes to

drive the turbine. The overall experimental setup is shown in Figure 3.3. The experimental setup consisted of the compact-plate heat exchanger, hot water supply system, air supply system and measurement system.

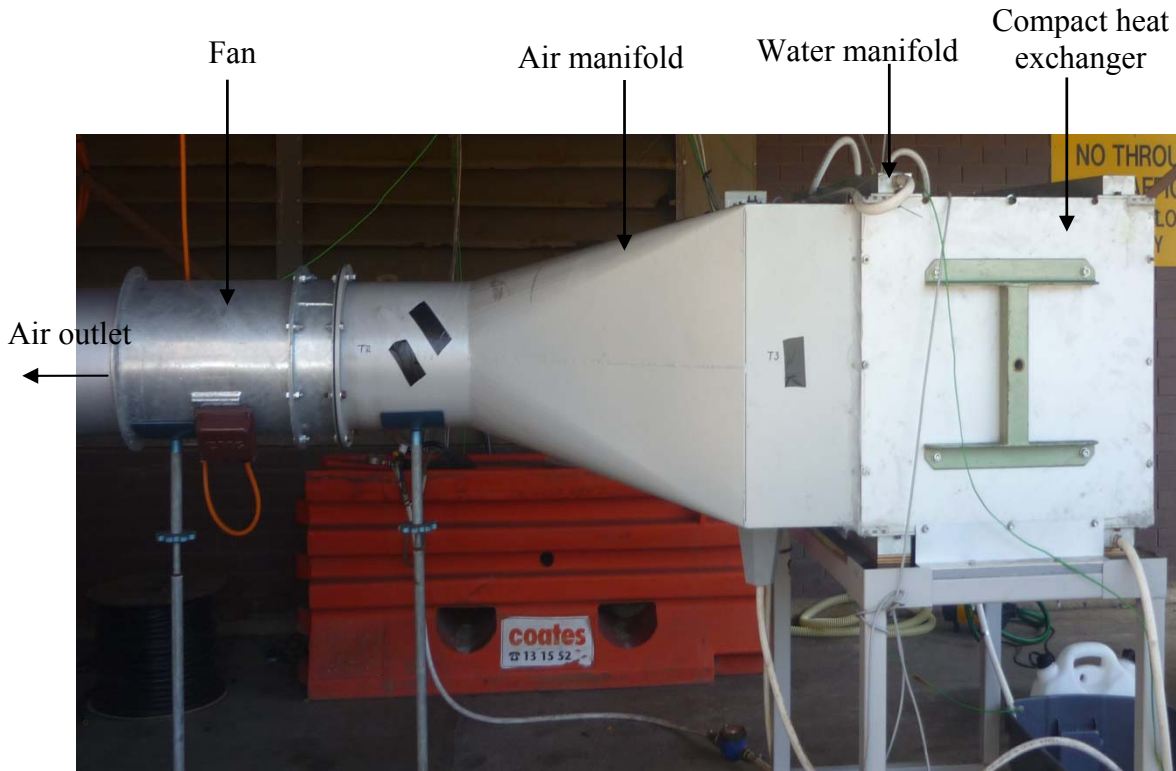


Figure 3.3: Photograph of the experimental setup for water-to-air heat exchanger test.

3.2.2. Water and Air Supply System

During the experiments at Victoria University laboratory, the hot water was supplied by a BOSCH 32Q hot water system, which can provide 32 l/min of hot water with a temperature range of 37–80°C. A XF 192S pump from DAVEY, as shown in Figure 3.4, was used to circulate the water from a bucket under the compact heat exchanger through the hot water system and then to the compact heat exchanger. This construction

method has the advantage of keeping the inlet pressure of the hot water into the heat exchanger at less than 30 kPa to eliminate the possibility of water leaking in the heat exchanger. At the experiments conducted at Yallourn power station, the hot water was taken from the condensate of the power plant direct to the heat exchanger. Manifolds at the inlet and exit of the heat exchanger were used to distribute the water. A valve before the inlet of the heat exchanger was used to adjust the desired inlet flow rate of the water.



Figure 3.4: XF 192S pump for circulating water.

An electrical fan with a power of 0.37 kW, which was attached at the exit of the air manifold, was used to provide a uniform air stream through the compact heat exchanger (see Figure 3.1). A filter was installed in front of the heat exchanger to remove dust from the air. The fan speed can be adjusted by a speed controller as shown in Figure

3.5, with a range of 10–50 Hz. The air flows through the air channels in the compact heat exchanger in counter direction with the hot water, and then flows out the experimental rig via a flow duct installed after the fan.



Figure 3.5: Speed controller.

3.2.3. Measurement System

Figure 3.6 shows a photograph of the data acquisition system that was used to collect the experimental data during the test. The hardware used was DI-718BX Series and the

software used was WinDaq ®. All the measurements of temperatures, flow rates and pressure were read by the data acquisition system and stored on a computer hard drive.

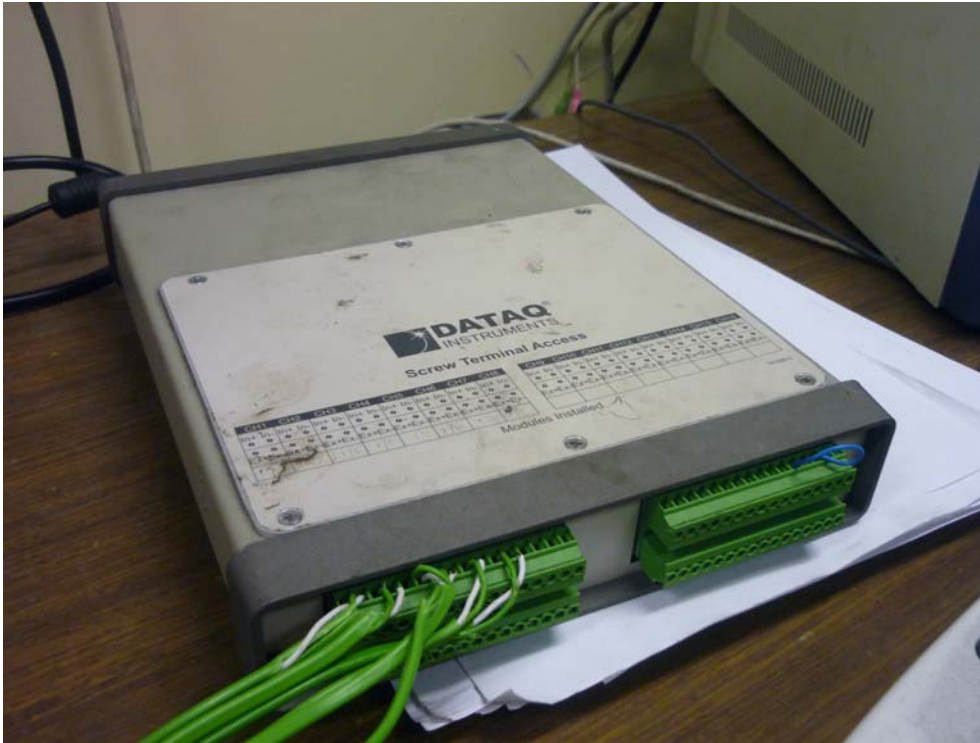


Figure 3.6: The data acquisition system.

Thermocouples, flow meters and pressure transmitters were used to measure the air and hot water temperatures, hot water flow rate and the pressure differences of the air, respectively. Air and water temperatures were measured using K-type thermocouples, which were inserted at the inlet and outlet of the air and hot water flow hoses. The thermocouples were calibrated against a mercury thermometer by using ice and boiling water to specify the low and high calibration values of the thermocouples and then applying them to the data acquisition software. The thermocouples were also calibrated after the tests using a secondary standard thermometer with an accuracy of 0.1°C. The flow rate of the hot water was measured with a flow meter (type RS 257-133). The flow-rate measurements were accurate to 0.0075 l/s.

A pressure regulator was also installed to control the pressure of the water at the inlet of the heat exchanger. A differential pressure transmitter (model FCO332) was used to measure the pressure differences of the air across the compact heat exchanger. The accuracy of the pressure transmitter was 0.25% of reading value. The pressure drop on the inlet air nozzle was measured with a pressure sensor (164PC01D37) to obtain the airflow rate through the test section. The pressure sensor was calibrated against a high-precision manometer with an accuracy of 0.1 Pa. The atmospheric pressure was determined using a barometer mounted near the experimental apparatus to determine the density of the air passing through the nozzle.

3.3. Experiment Procedure

First, the experiments of water-to-air heat exchange in the polypropylene compact heat exchanger were conducted at Victoria University laboratory under the conditions of various airflow rates and hot water flow rates. The parameters of each test are listed in Table 3.1. Then, experiments at Yallourn power station, Australia, were conducted under a wide range of conditions of inlet water temperature, ambient air temperature and hot water mass flow rate. The supply inlet temperature of the water varied between 36 and 48°C. The inlet temperature of the air varied between 11 and 25°C. The flow rate of water ranged from 0.12 to 0.19 l/s and the flow rate of air was about 1.4 kg/s. Appendix A shows the tables of the experimental data from the tests at Yallourn power station.

Table 3.1: Test runs.

Flow rate of hot water (l/s)	Mass flow rate of air (kg/s)	Inlet temperature of water (°C)	Inlet temperature of air (ambient) (°C)
0.10	0.402–0.764	50	18.2
0.15	0.400–0.744	50	20.8
0.20	0.399–0.732	50	21.7
0.25	0.393–0.723	50	18.2

3.4. Data Reduction

To obtain the mass flow rate of air entering the heat exchanger, during the experiments conducted at Victoria University, a special nozzle with an inner diameter of 300 mm was located at the inlet section of the test rig. By applying Bernoulli's equation, the air velocity in the nozzle can be obtained as Engineering ToolBox.com (2011):

$$V = C \sqrt{\frac{2\Delta p}{\rho}} \quad (3.1)$$

where Δp is the pressure drop in the nozzle, ρ is the air density and $C = 0.94$ is the correction factor Engineering ToolBox.com (2011).

The air density is calculated from the ideal gas law:

$$\rho = \frac{P}{RT} \quad (3.2)$$

where P is the atmospheric pressure, T is the ambient temperature and $R = 287 \text{ J/kgK}$ is the gas constant.

The mass flow rate through the nozzle was obtained as the product of the nozzle velocity (see Equation 3.1), air density and nozzle cross-sectional area:

$$\dot{m}_a = \rho V \frac{\pi d^2}{4} \quad (3.3)$$

where $d = 300 \text{ mm}$ is the nozzle diameter.

The heat rejection rate can be calculated as follows:

$$\dot{Q} = \dot{m}_w C_{pw} (T_{in,w} - T_{out,w}) \quad (3.4)$$

where \dot{m}_w represents the mass flow rate of water, C_{pw} the specific heat of water, $T_{in,w}$ the inlet water temperature and $T_{out,w}$ the outlet water temperature.

3.5. CFD Simulation

The commercial CFD software FLUENT[®] is used in this study to carry out the simulation in the heat exchanger. FLUENT[®] is a computer program for modelling fluid flow and heat and mass transfer in various geometries. It provides modelling for laminar and turbulent fluid flow problems. Steady state and transient analysis can also be performed. Using FLUENT[®], the velocity, temperature and pressure distribution in the flow field can be obtained. The usual programming of the FLUENT[®] software is not prepared for every need of the users. However, user-defined functions (UDFs) can be used to define boundary conditions, material properties and source terms according to the user's need using C programming language.

Figure 3.7 shows the schematic representation of the inputs required in FLUENT[®] to carry out the simulation. The first requirement of the simulation is to build the geometry and generate the mesh using ANSYS Workbench. Next, the boundary conditions and any UDFs need to be used should be defined for the model. Then, the FLUENT[®] software calculates for the solutions and the results of CFD calculation at the end of a computational simulation can be obtained.

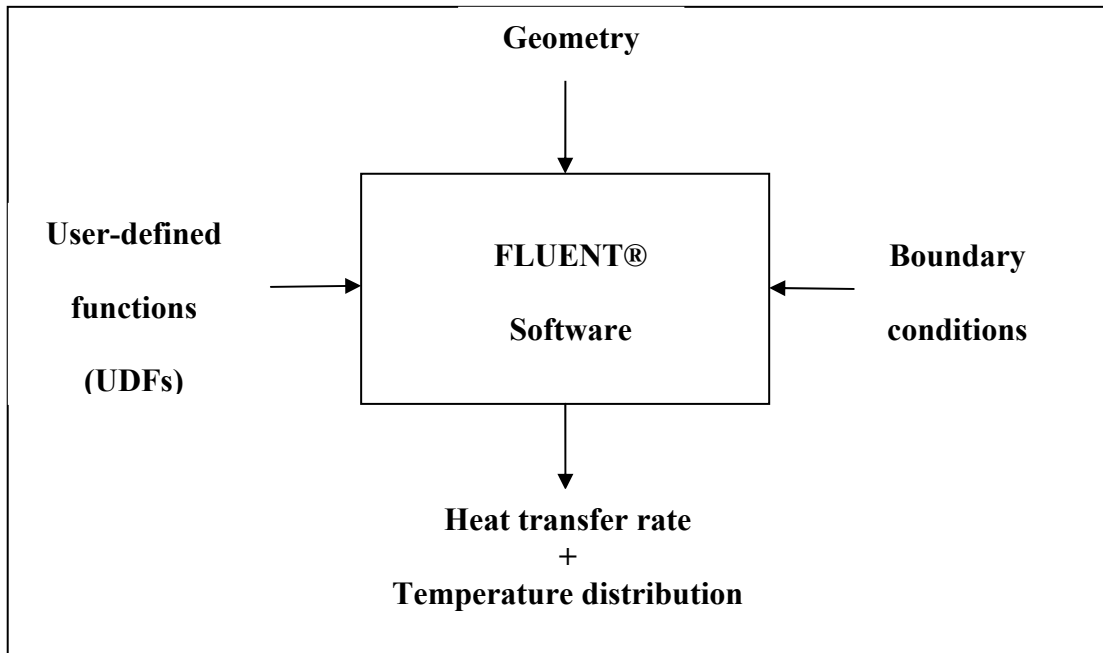


Figure 3.7: Schematic of the inputs required in FLUENT® and some outputs.

In this study, the polypropylene compact-plate heat exchanger is simulated numerically using FLUENT®. The 3D fluid-flow distribution and the heat transfer in the water-to-air heat exchanger are investigated.

3.5.1. The Governing Equations

3.5.1.1. The Continuity Equation

The mass continuity equation or mass conservation equation is (Bird et al., 2007):

$$\frac{\partial \rho}{\partial t} + \frac{\partial}{\partial x}(\rho u) + \frac{\partial}{\partial y}(\rho v) + \frac{\partial}{\partial z}(\rho w) = 0 \quad (3.5)$$

where t is the time, ρ is the density and u, v, w are the velocity components.

3.5.1.2. The Momentum Equation

The following equations represent the conservation of momentum (Bird et al., 2007):

$$\frac{\partial}{\partial t}(\rho u) + \frac{\partial}{\partial x}(\rho uu) + \frac{\partial}{\partial y}(\rho uv) + \frac{\partial}{\partial z}(\rho uw) = -\frac{\partial P}{\partial x} + \frac{\partial \tau_{xx}}{\partial x} + \frac{\partial \tau_{xy}}{\partial y} + \frac{\partial \tau_{xz}}{\partial z} + \rho g_x + F_x \quad (3.6)$$

$$\frac{\partial}{\partial t}(\rho v) + \frac{\partial}{\partial x}(\rho vu) + \frac{\partial}{\partial y}(\rho vv) + \frac{\partial}{\partial z}(\rho vw) = -\frac{\partial P}{\partial y} + \frac{\partial \tau_{yx}}{\partial x} + \frac{\partial \tau_{yy}}{\partial y} + \frac{\partial \tau_{yz}}{\partial z} + \rho g_y + F_y \quad (3.7)$$

$$\frac{\partial}{\partial t}(\rho w) + \frac{\partial}{\partial x}(\rho wu) + \frac{\partial}{\partial y}(\rho wv) + \frac{\partial}{\partial z}(\rho ww) = -\frac{\partial P}{\partial z} + \frac{\partial \tau_{zx}}{\partial x} + \frac{\partial \tau_{zy}}{\partial y} + \frac{\partial \tau_{zz}}{\partial z} + \rho g_z + F_z \quad (3.8)$$

where P is the static pressure, τ is the stress tensor and ρg and F are the gravitational body force and external body force, respectively.

3.5.1.3. The Energy Equation

The conservation equation of energy is (Fluent, 2010):

$$\begin{aligned} & \frac{\partial}{\partial t}(\rho E) + \frac{\partial}{\partial x}[u(\rho E)] + \frac{\partial}{\partial y}[v(\rho E)] + \frac{\partial}{\partial z}[w(\rho E)] \\ & = \frac{\partial}{\partial x}\left(k \frac{\partial T}{\partial x}\right) + \frac{\partial}{\partial y}\left(k \frac{\partial T}{\partial y}\right) + \frac{\partial}{\partial z}\left(k \frac{\partial T}{\partial z}\right) + \rho(vg_x + ug_y + wg_z) \end{aligned} \quad (3.9)$$

where $k \frac{\partial T}{\partial x}$ represent the energy transfer due to conduction. The cases simulated in

this chapter contain only one species and no source terms are used.

In Equation 3.9:

$$E = h - \frac{P}{\rho} + \frac{v^2}{2} \quad (3.10)$$

where h is the sensible enthalpy and can be expressed as:

$$h = \int_{T_{ref}}^T C_p dT \quad (3.11)$$

where T_{ref} is 298.73 K.

For the experimental conditions simulated here, the energy equation reduces to:

$$\begin{aligned} \frac{\partial}{\partial t}(\rho E) + \frac{\partial}{\partial x}[u(\rho E)] + \frac{\partial}{\partial y}[v(\rho E)] + \frac{\partial}{\partial z}[w(\rho E)] \\ = k \left(\frac{\partial^2 T}{\partial x^2} + \frac{\partial^2 T}{\partial y^2} + \frac{\partial^2 T}{\partial z^2} \right) + \rho(vg_x + ug_y + wg_z) \end{aligned} \quad (3.12)$$

3.5.2. Geometry Creation

Initially, the 3D geometry was created for the heat exchanger using ANSYS Design Modeller 12.0. Due to computer power limitations, conducting numerical study of the complete compact heat exchanger is complicated. As a result, the 3D flow through the single narrow water channel between two parallel airflow channels for only one-half of the domain shown in Figure 3.8 was simulated, because the flow was expected to be symmetrical about the centreline of the geometry. Due to the complexity of generating the flute walls that hold the two surfaces of the polypropylene board together, the simulation was carried out without them and the difference in heat transfer result is expected to be small. Figure 3.9 shows the current domain used in this study, the physical dimensions of the heat exchanger and the boundary conditions used to carry out the simulations. The domain is 609 mm in height, 304.5 mm wide and 3.8 mm deep.

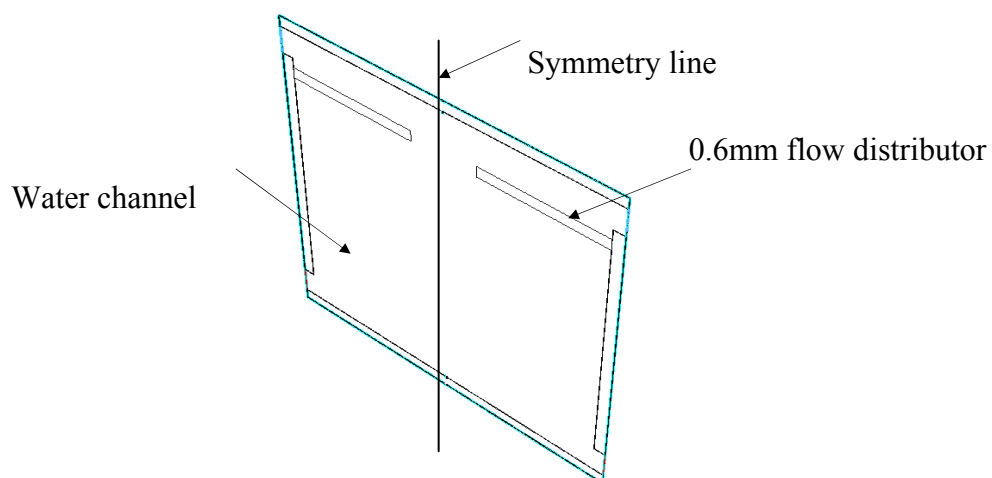


Figure 3.8: Plate heat exchange geometry.

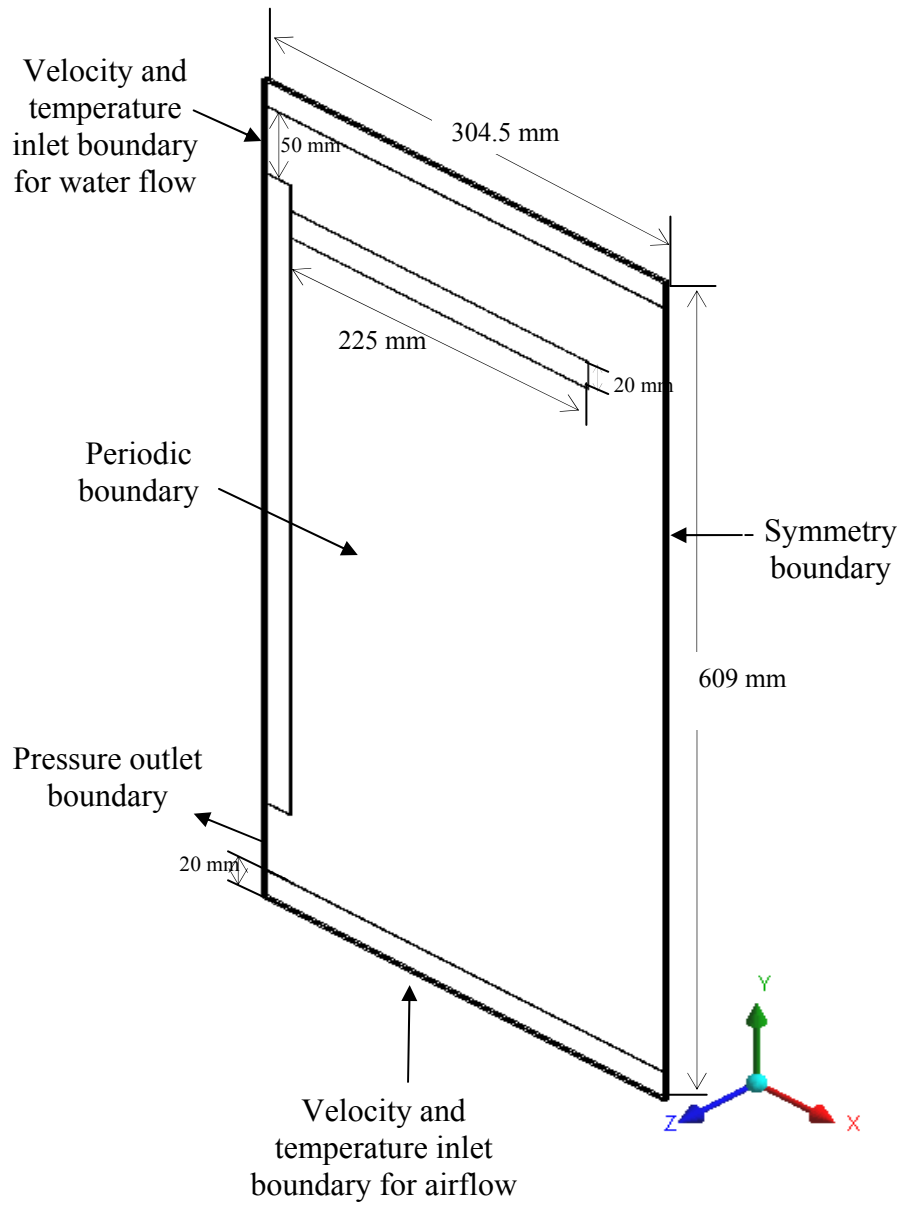


Figure 3.9: Domain dimensions and boundary conditions used in this study.

3.5.3. Boundary Conditions

Boundary conditions specify the flow and thermal variables on the boundaries of the physical domain. Figure 3.9 shows the boundary conditions utilised in this study, which are as follows.

3.5.3.1. Inlet Boundary Conditions

The velocity and temperature values are specified at the inlet of the water and air channels. The direction of the inlet velocity is normal to the surface. The inlet velocity was calculated from channel mass flow rate and channel inlet cross-sectional area.

3.5.3.2. Outlet Boundary Conditions

At the outlet, the pressure boundary condition is specified as a constant value equal to zero gauge pressure. This is the case for both the water and air outlet channels.

3.5.3.3. Wall Boundary Conditions

Wall boundary condition is used to bound fluid and solid regions. Since the wall zone here is a two-side wall, which is a wall that forms the interface between two regions such as the fluid/solid interface, FLUENT[®] enables the two sides of the wall to be

coupled, prompting the solver to calculate the heat transfer directly from the solution in the adjacent cells.

3.5.3.4. Periodic Boundary Conditions

The computational domain of the heat exchanger was reduced to two halved air channels and one water channel, and the flat boundaries of the outer half air channel were treated as periodic surfaces to represent the complete heat exchanger. The periodic boundary condition was not specified for the water channel because one of the walls in the water channel had a flow distributor. With this periodic boundary condition, only flows in one water channel and one full air channel are simulated. The total heat transfer from a heat exchanger with 250 channels of water and airflows can be obtained by timing this number of channels to the results obtained from one channel simulation using period boundary conditions. This periodic boundary condition has greatly reduced the computation cost in this simulation.

3.5.3.5. Symmetry Boundary Conditions

Symmetric boundary conditions were chosen for one-half of the heat exchanger. This was done because the geometry of the heat exchanger and the expected pattern of the flow and the thermal solution are symmetric (see Figure 3.8). When using this type of boundary condition in such regions, there is no need for additional boundaries. FLUENT[®] assumes zero flux of all quantities across asymmetric boundary. There is no convective flux across asymmetry plane, and the normal velocity component is zero.

3.5.4. Grid Independence and Meshing

Prior to analysing the heat exchanger model in the FLUENT[®] solver, it was necessary to create a mesh structure. The mesh structure specifies the resolution at which FLUENT[®] analyses the model. Therefore, a grid independence study was carried out to ensure the results accuracy. Figure 3.10 presents the variation of heat rejection rate against the grid numbers. As shown in Figure 3.10, at stage A the results vary with grid resolution; at stage B the results tend towards constant, so the grid at stage B shows grid independent. For final simulations, the mesh was created for the heat exchanger using quadrilateral mesh with around 500,000 cells to ensure the simulated results are grid independent.

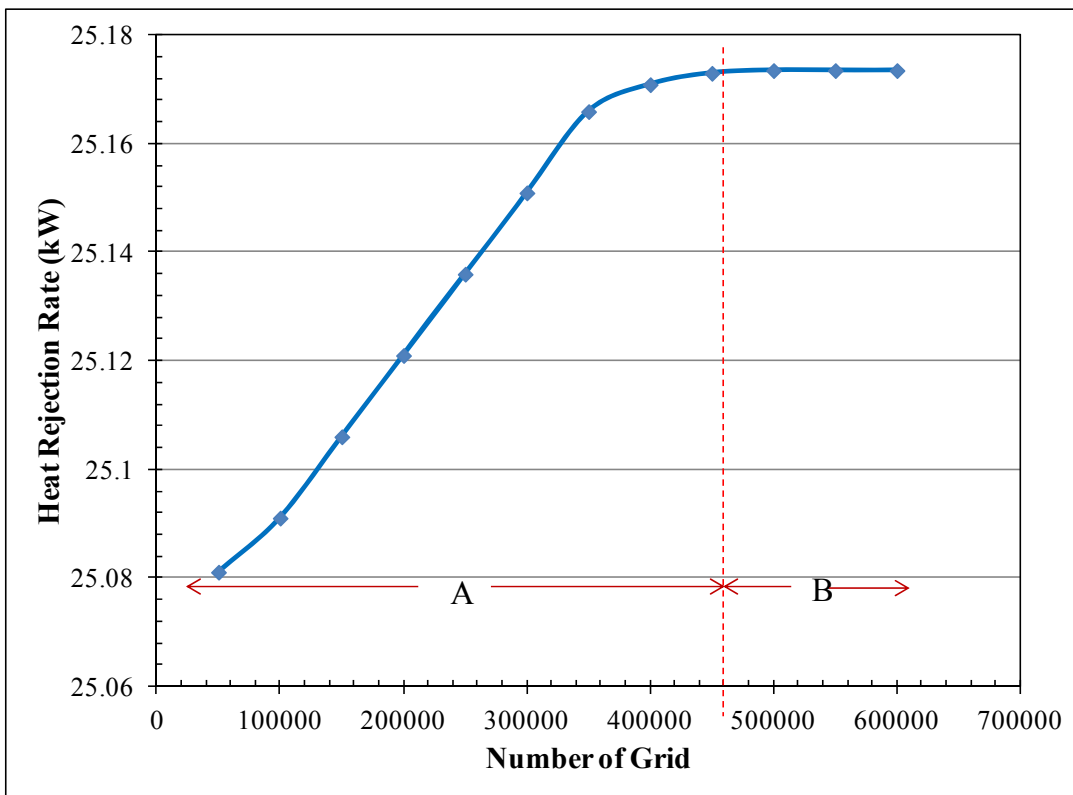


Figure 3.10: Grid independence test.

3.5.5. Working Fluid Properties

Water and air were taken as the working fluids. Viscosity, thermal conductivity and the density of water and air were taken as a function of temperature. Algebraic equations derived by the method of curve fitting are shown in Appendix B. These equations were programmed using UDFs and compiled in FLUENT[®] to compute the properties at each iteration of the solution process. Thus, when solving the energy equation, the properties changed as the temperature changed in the flow channels.

3.5.6. Solid Properties

A solid zone is a group of cells for which the heat conduction is solved. The only required inputs for the solid zone are the material properties of the solid, which are entered into the material conditions panel of the FLUENT[®]. In this study, the material used was Polypropylene and the properties are summarised as follows:

$$\text{Density } (\rho) = 950 \text{ Kg}/m^3$$

$$\text{Specific Heat } (C_p) = 1600 \text{ J}/(\text{KgK})$$

$$\text{Thermal Conductivity } (k) = 0.16 \text{ W}/(\text{mK})$$

3.5.7. Solver

The segregated solver was used to solve the governing equations for the conservation of mass, momentum and energy equations. The semi-implicit method for pressure-linked equations algorithm was used for the calculation of the pressure and the velocity, which were needed for the solution of the energy equation. The numerical domain consisted of 500,000 elements and a first-order upwind differencing scheme was used at all interior grid points. The convergence criteria are set 1×10^{-3} for continuity and x, y and z momentum, and 1×10^{-6} for the energy. The solution was converged and the overall heat balance throughout the domain was reached. The second-order upwind differencing scheme was tested and the difference between the results of first-order and second-order upwind differencing scheme were found to be very small (0.024%).

3.6. Results and Discussion

3.6.1. Experimental Results

Figure 3.11 shows the variation of the heat rejected by the Polypropylene compact heat exchanger, with the air mass flow rates at different flow rates of hot water carried out at equal inlet water temperature of 50°C. Figure 3.11 shows that, for each value of the water flow rate, the heat rejected by the heat exchanger increases with the increase of the air mass flow rate. It can also be seen from the figure that the heat rejection increases with increasing water flow rate. However, increasing the inlet temperature of the ambient air will cause a reduction in the heat rejected by the compact heat

exchanger. Further, it is shown that the Polypropylene compact heat exchanger rejects a higher rate of heat at higher water and air mass flow rates.

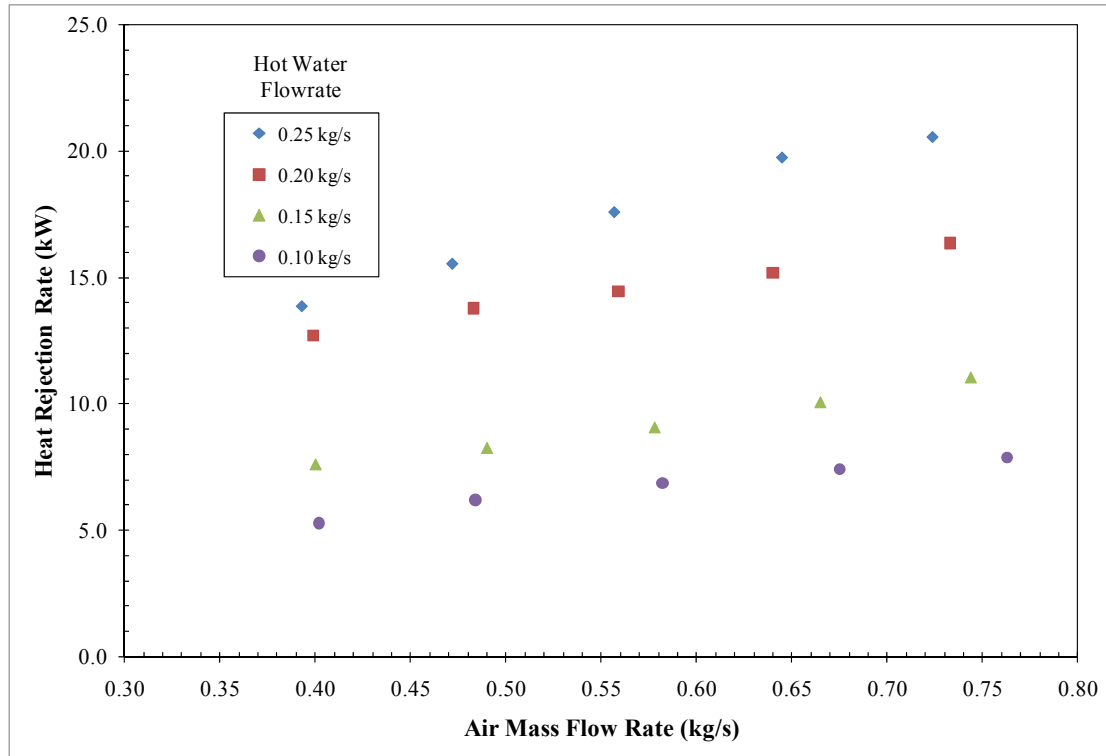


Figure 3.11: Comparison of the heat rejection rate at various air and water mass flow rates (results from Victoria University laboratory).

Due to the rejection of heat to the airside, the water temperature decreases as it flows through the plate heat exchanger. Figure 3.12 shows the experimental results from Yallourn power station of the inlet and outlet temperature of the water entering and leaving the compact heat exchanger. The experimental test was for the period 24 to 25 January 2011. As shown in Figure 3.12, the inlet temperature of the water varied between 37 and 41°C according to the ambient air temperature, whereas the outlet water temperature reached values between 17 and 25°C. The ambient air temperature, as

shown in the figure, varied between 14 and 22°C, which is quite close to the outlet water temperature, and this means that the compact heat exchanger performed well.

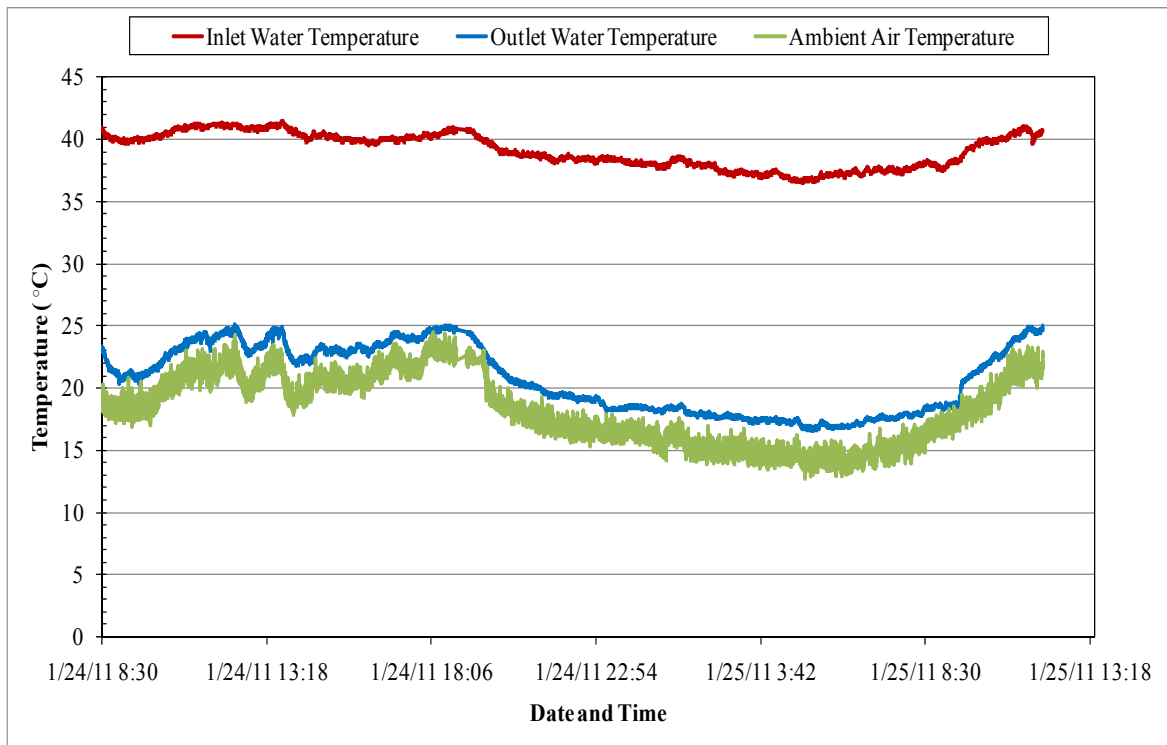


Figure 3.12: Temperature of water entering and leaving the compact heat exchanger and the ambient air temperature for the period 24 to 25 January 2011 (results from Yallourn power station).

The heat rejected by the compact heat exchanger corresponding to this test was calculated from the measured data and is shown in Figure 3.13. The heat rejection rate varied between 9.5 and 13.4 kW, with the variation of inlet water and air temperatures over the day at water flow rate around 0.15 kg/s and air mass flow rate around 1.38 kg/s. As shown in the figure, when the difference between the inlet and outlet water temperature is high, the compact heat exchanger rejects more heat.

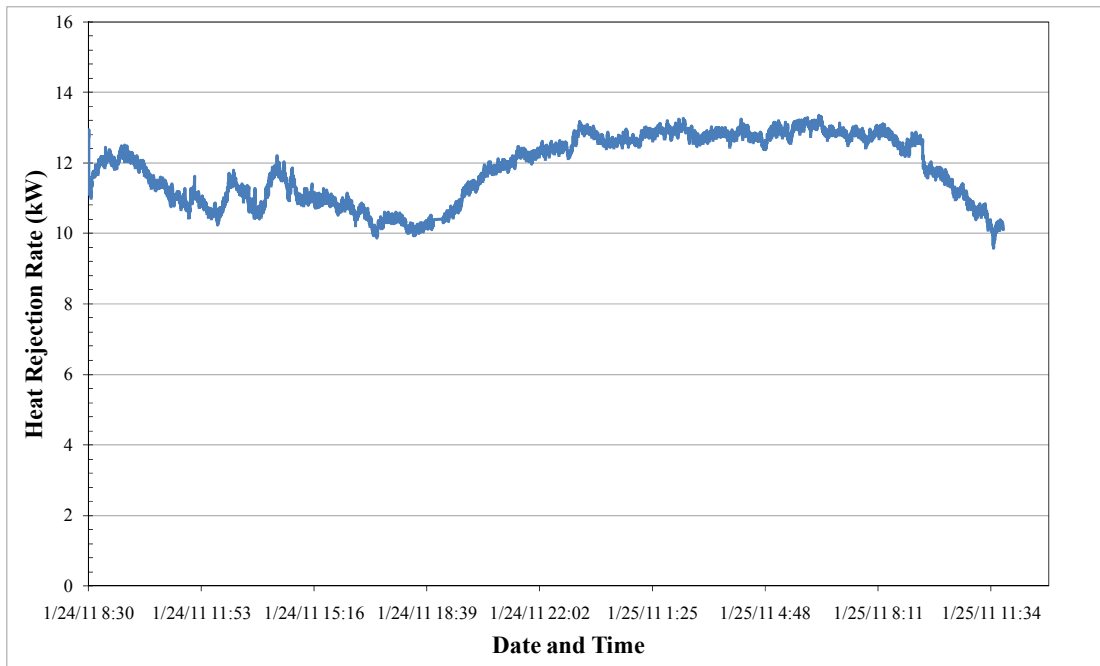


Figure 3.13: Heat rejected by the polypropylene compact heat exchanger for the period 24 to 25 January 2011.

Another test was carried out for the period 15 to 24 February 2011, and the results are shown in Figure 3.14. The inlet water temperature varied between 38 and 48°C, the outlet water temperature reached 14–28°C and the ambient air temperature varied between 12–23°C. Figure 3.15 shows the heat rejection rates related to this test. The water flow rate was around 0.18 kg/s and the mass flow rate of air was around 1.40 kg/s. The heat rejection rate has a magnitude of 10.5 to 19.2 kW.

It was observed that, for all tests carried out at Yallourn power station, the compact heat exchanger performed well and was able to reduce water temperature effectively.

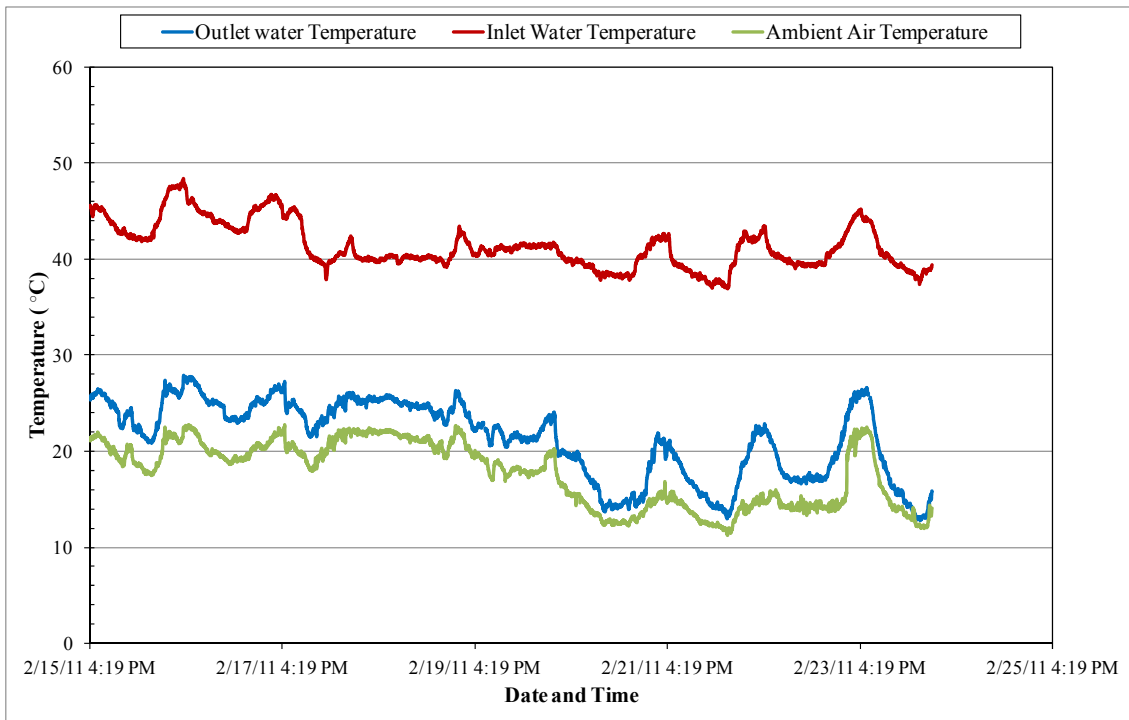


Figure 3.14: Temperature of water entering and leaving the compact heat exchanger and the ambient air temperature for the period 15 to 24 February 2011.

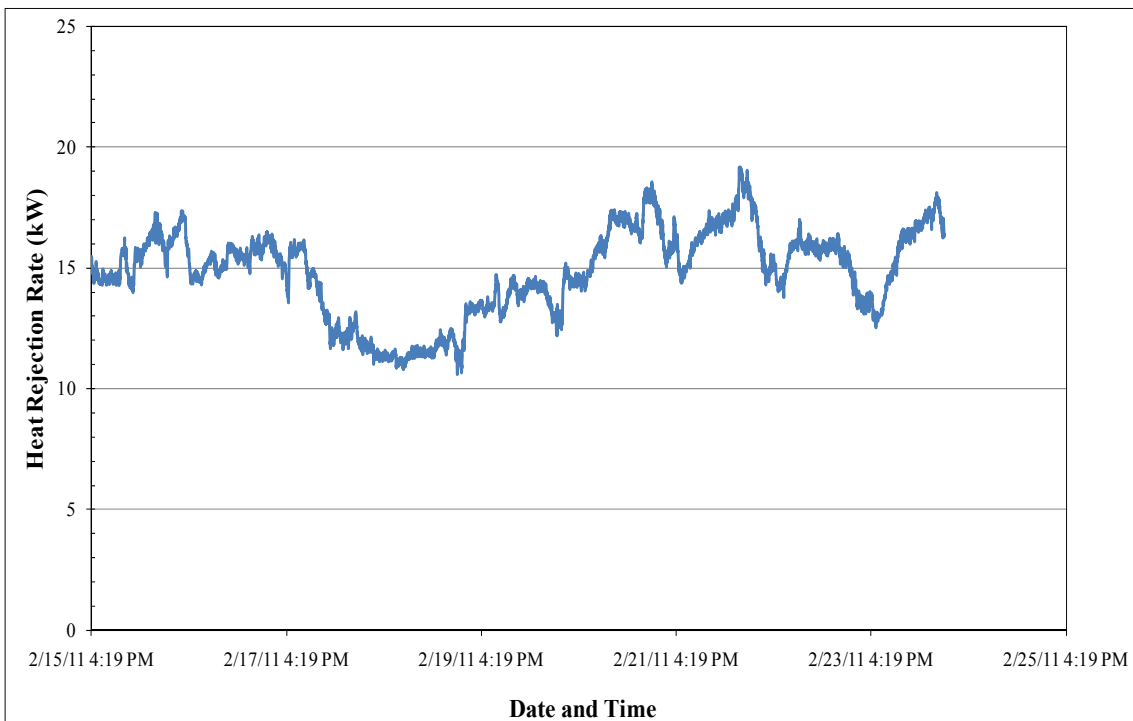


Figure 3.15: Heat rejected by the compact heat exchanger for the period 15 to 24 February 2011.

3.6.2. Simulation Results

3.6.2.1. Flow Visualisation

Flow distribution inside the plate heat exchanger's channel is shown in Figure 3.16 and Figure 3.17. In both these figures, flow distribution is depicted by path lines for water and air streams. The Reynolds number for the water flow is in alter of 50 and for the air flow is in alter of 600. As a result, the laminar model has been used in this simulation.

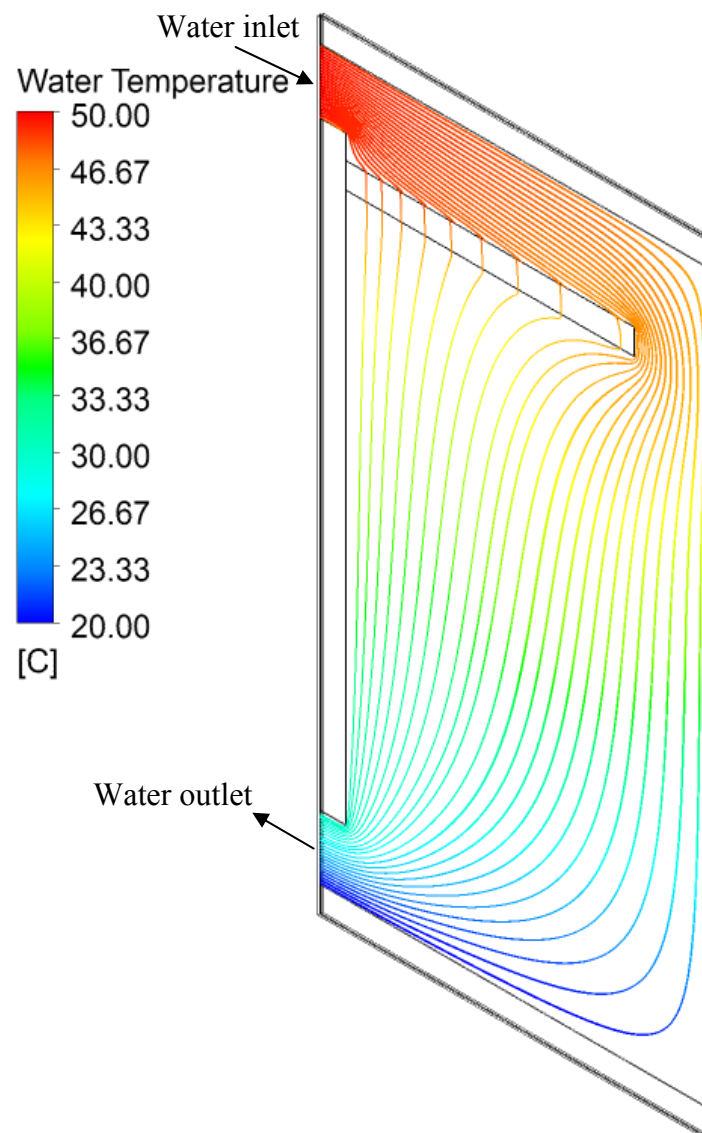


Figure 3.16: Flow visualisation inside the plate heat exchanger that indicates the decrease in temperature in the direction of flow.

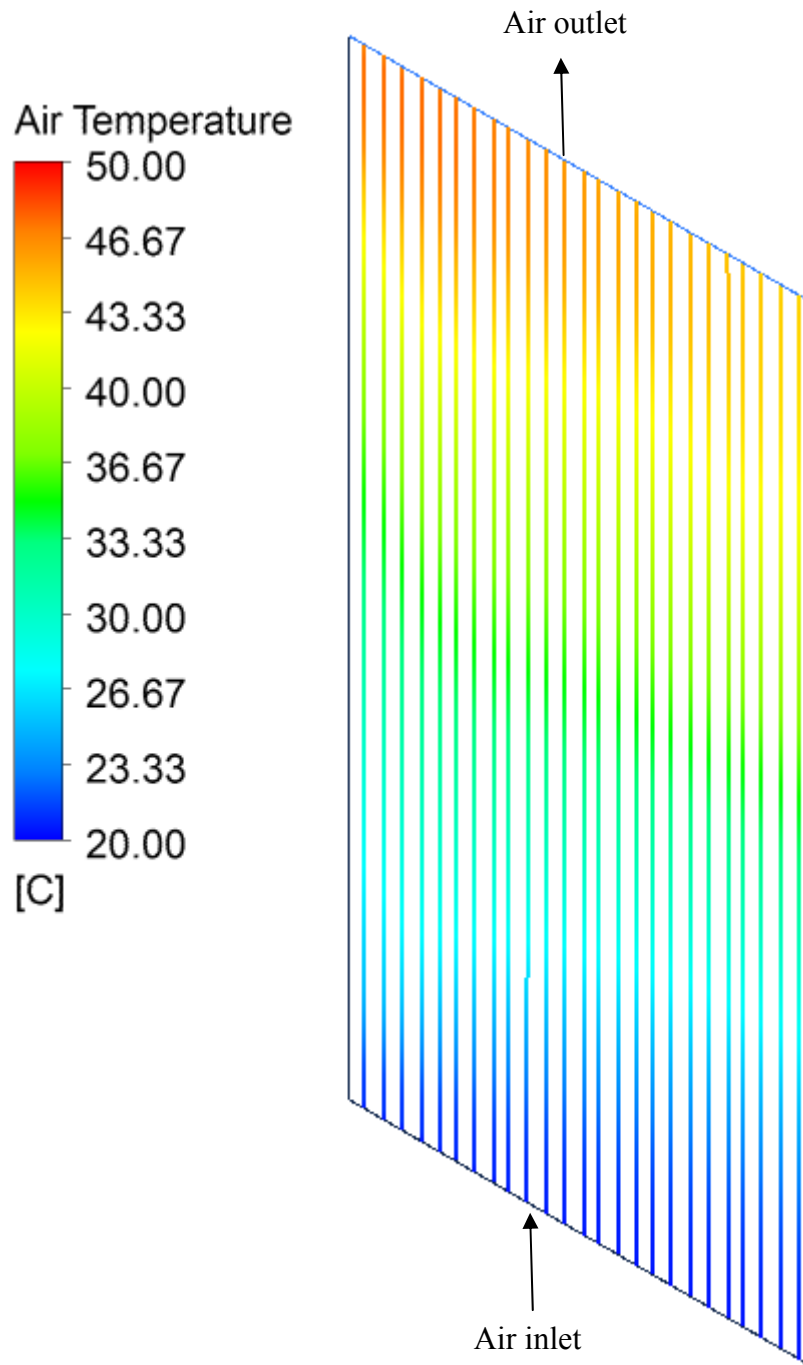


Figure 3.17: Flow visualisation inside the plate heat exchange for air channel that indicates the increase in temperature in the direction of flow.

3.6.2.2. Temperature Distribution

The temperature distribution inside the water channel is shown in Figure 3.18. The temperature distribution gradually varies from the top of the channel to the bottom, as clearly shown in the figure.

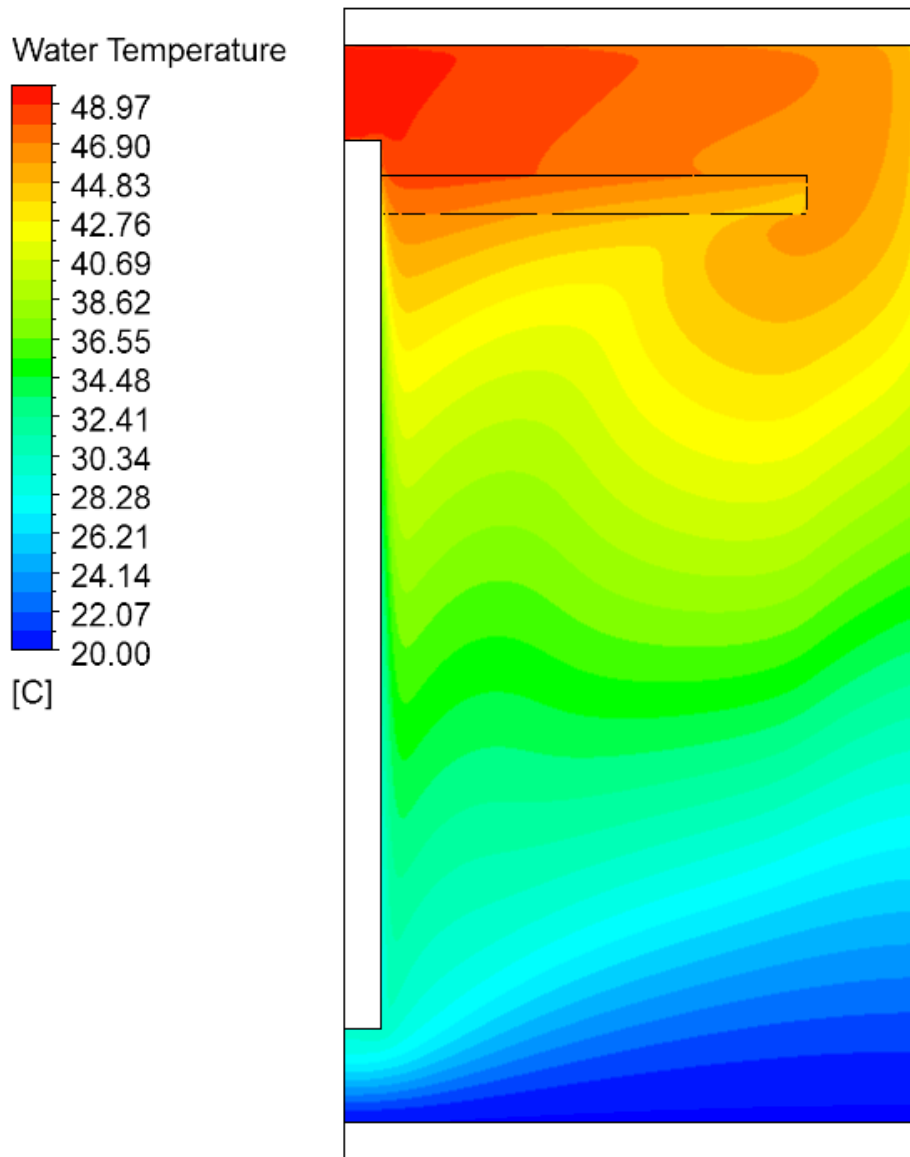


Figure 3.18: Temperature distribution inside the water channel.

The temperature variation over the plate surface of the plate heat exchanger by heat transferring from hot water to cold air is shown in Figure 3.19. In this figure, heat transfer range is identified by colour changes on the plate surface.

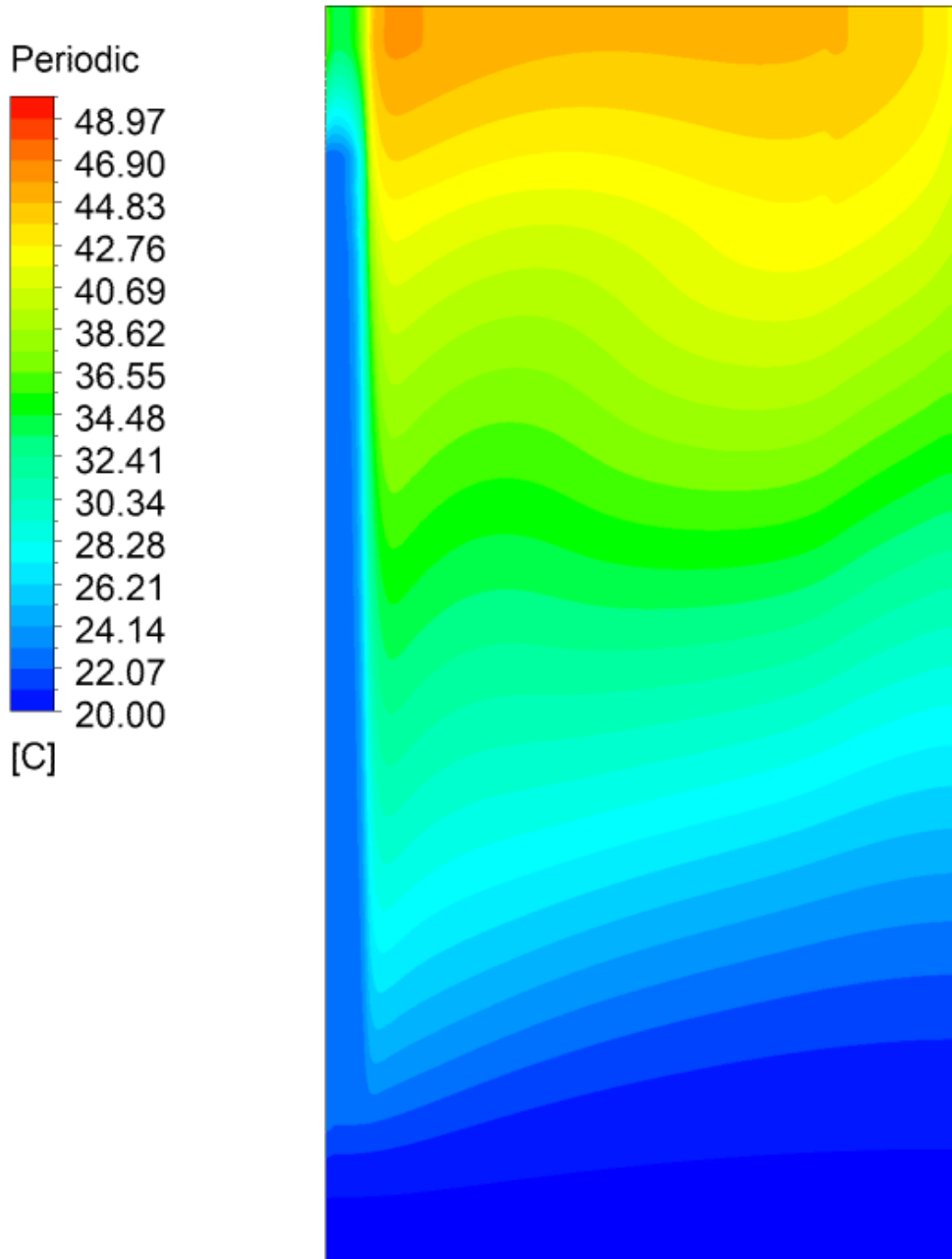


Figure 3.19: Temperature distribution over plate surface of the plate heat exchanger.

3.6.2.3. Velocity Distribution

Figure 3.20 represents the flow streamlines coloured by velocity magnitude inside the water channel. As shown in the figure, the water flow travels from the inlet to the internal water channel before turning down, to be distributed inside the channel.

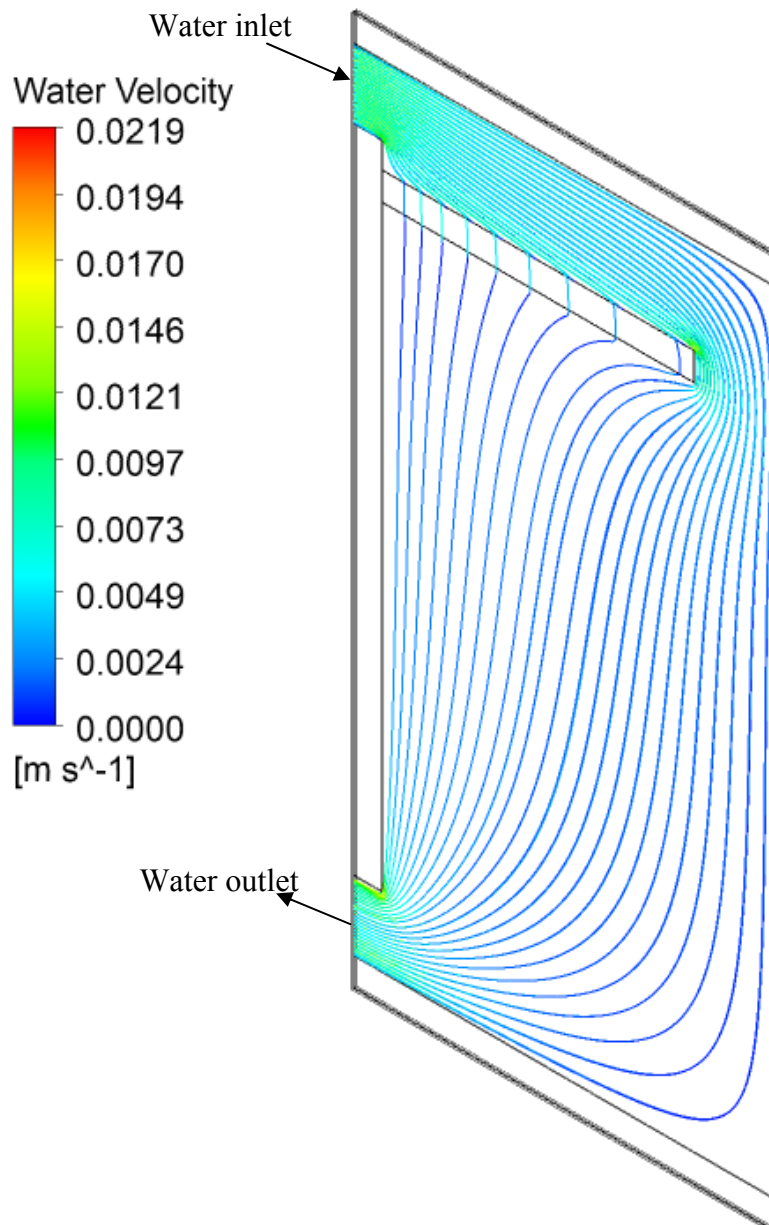


Figure 3.20: Velocity streamline inside the water channel. Water enters at the top left-hand corner and leaves at the bottom left-hand corner.

3.7. Validation of Simulation Results with Experimental Results

The heat rejection rates for the compact heat exchanger, calculated using both experimental and simulated data, were compared. Figure 3.21 shows comparison based on the data corresponding to hot water flow rate of 0.25 kg/s, air flow rate range from 0.393 to 0.724 kg/s and inlet water and air temperature of 51.8°C and 18.18°C, respectively. The figure shows that the heat rejection rate predicted by the CFD simulation is in agreement with the experimental results. Figures 3.22–3.23 give a comparison of the heat rejection rate obtained from the experiments and those predicted using CFD, based on the data shown in Appendix A. The results show a good agreement between the simulated and experimental data, as shown in Figures 3.22–3.23.

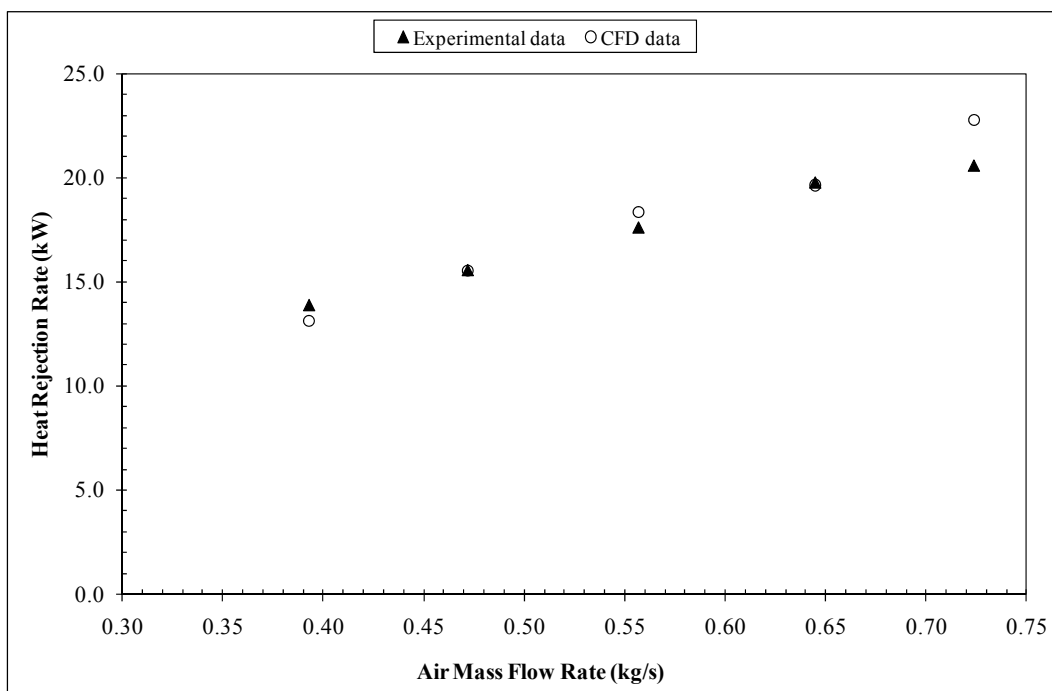


Figure 3.21: Comparison of the measured and simulated values of the heat rejection rates for the compact heat exchanger at water flow rate of 0.25 kg/s.

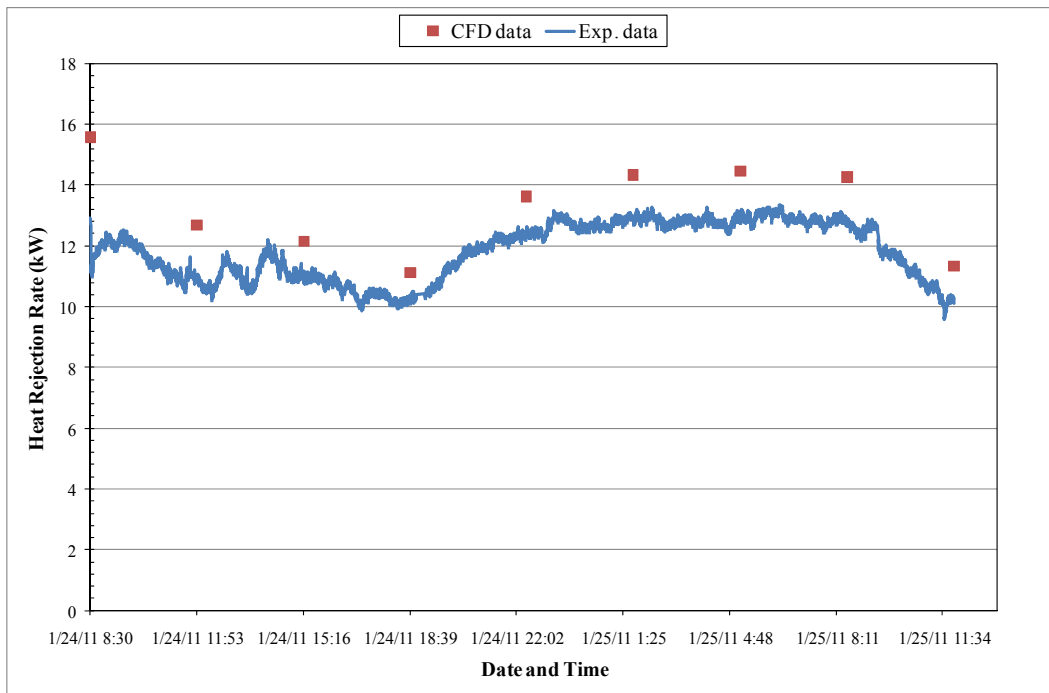


Figure 3.22: Comparison of the measured and simulated values of the heat rejection rates for the compact heat exchanger for the period 24 to 25 January 2011.

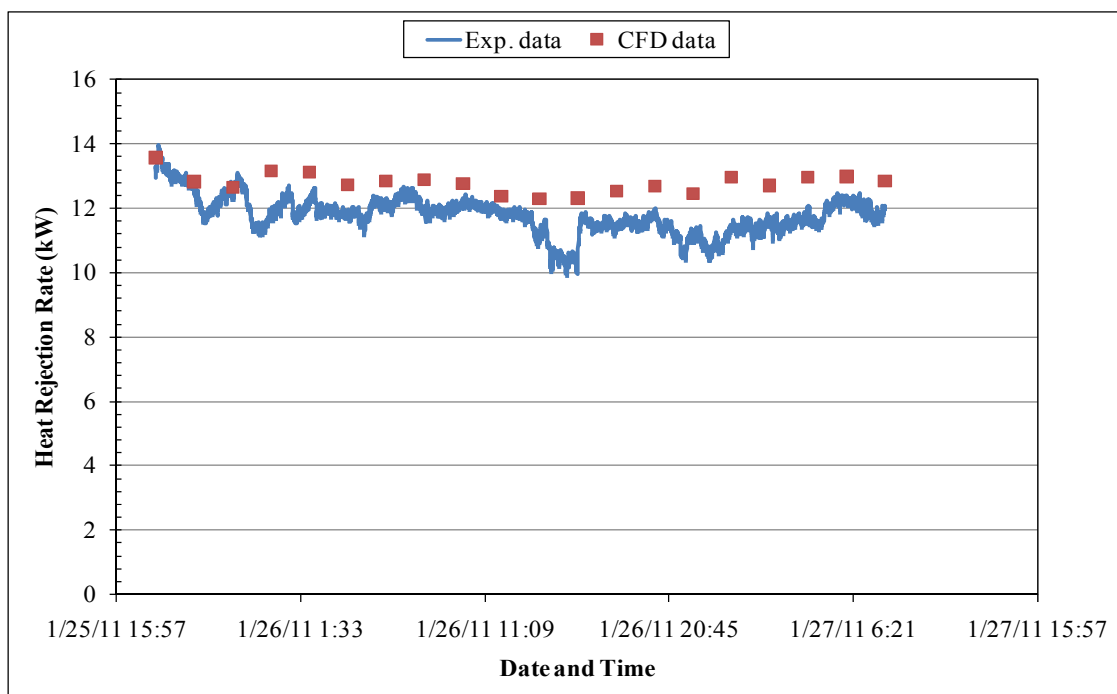


Figure 3.23: Comparison of the measured and simulated values of the heat rejection rates for the period 25 to 27 January 2011.

3.8. Comparison of the Heat Rejection Rate between Aluminium Alloy and Polypropylene Compact Heat Exchanger

Polypropylene compact heat exchangers offer many advantages over metal heat exchangers. They are less expensive and are easier to shape than metals. They are also corrosion and fouling resistant. However, their lower thermal conductivity compared to that of metal heat exchangers has prevented their extensive use.

CFD simulations were performed for a Polypropylene and an aluminium alloy compact heat exchanger using the same computational domain and boundary conditions as shown in Figure 3.9. The properties of aluminium are given as Fluent (2010):

$$\text{Density } (\rho) = 2719 \text{ Kg}/m^3$$

$$\text{Specific Heat } (C_p) = 871 \text{ J}/(\text{KgK})$$

$$\text{Thermal Conductivity } (k) = 202.4 \text{ W}/(\text{mK})$$

The heat transfer rates from aluminium alloy and Polypropylene heat exchangers for the same operation conditions were obtained, and these are shown in Table 3.2. It was found that the Polypropylene heat exchanger achieved 98% of the heat transfer rate achieved by the aluminium alloy heat exchanger. This is in spite of the fact that the thermal conductivity of aluminium is more than 1,000 times that of Polypropylene. Considering their lower cost, reduced need for maintenance and ease of use, Polypropylene compact heat exchangers are an excellent substitute for metal heat exchangers, in terms of performance and economy.

Table 3.2: Comparison of the heat rejection rate between Polypropylene and Aluminium Alloy heat exchanger.

Material	Thermal conductivity (W/mK)	Heat exchanger dimension (mm)	Operation conditions	Heat transfer rate (kW)
Polypropylene	0.16	950×609×609	$T_{w,in}=50^{\circ}\text{C}$, $T_{a,in}=20^{\circ}\text{C}$, $\dot{m}_{w,in}=0.25\text{ kg/s}$, $\dot{m}_{a,in}=1\text{ kg/s}$	25.17
Aluminium alloy	202.4	950×609×609	$T_{w,in}=50^{\circ}\text{C}$, $T_{a,in}=20^{\circ}\text{C}$, $\dot{m}_{w,in}=0.25\text{ kg/s}$, $\dot{m}_{a,in}=1\text{ kg/s}$	25.74

3.9. Transient Response of the Polypropylene Plate Compact Heat Exchanger to Inlet Temperature Change

In practice, there may be a sudden change in temperature from the condensate of the power plant to the Polypropylene compact heat exchanger, creating unsteady behaviour in the heat exchanger. Therefore, transient analysis helps us to predict the behaviour of the heat exchanger to a sudden change in the temperature of the working fluid and provides a guideline for power stations for responding to sudden changes in ambient conditions. In this simulation, the transient response of the heat exchanger to the inlet temperature change was carried out using the CFD software FLUENT®.

In transient simulation, FLUENT[®] discretises flow and heat transfer equations over a time step. To run the transient case, the steady state flow and heat transfer was first generated to provide the initial conditions for transient simulation. Then, the transient mode was activated and the time step size of 1 second was specified. The inlet water temperature was changed from 50°C to 40°C and the model was run until the solution approached the steady state behaviour (after 1,615 seconds), as shown in Figure 3.24. The inlet air temperature was also changed from 20°C to 30°C and the solution approached the steady state behaviour (after 1,403 seconds), as shown in Figure 3.25. This shows that when air cooled condensers are used for cooling power plants, the time lag for the heat exchangers to fully respond to changes to ambient air temperature would be around half an hour.

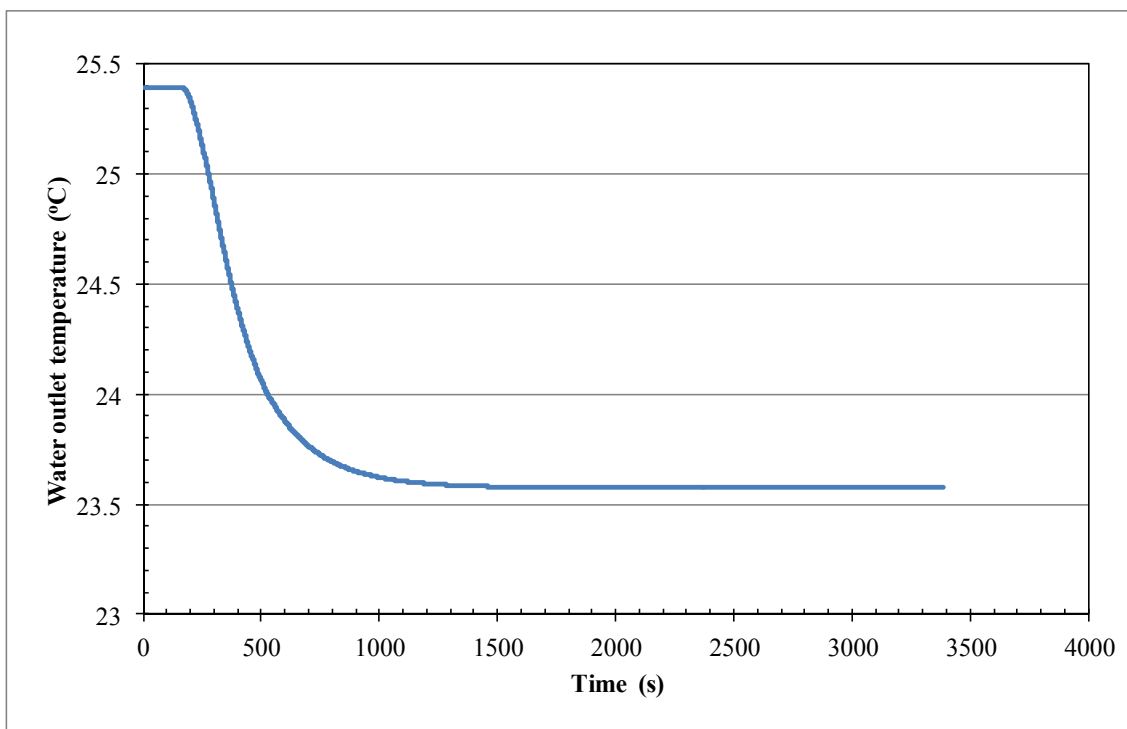


Figure 3.24: Transient response of water stream.

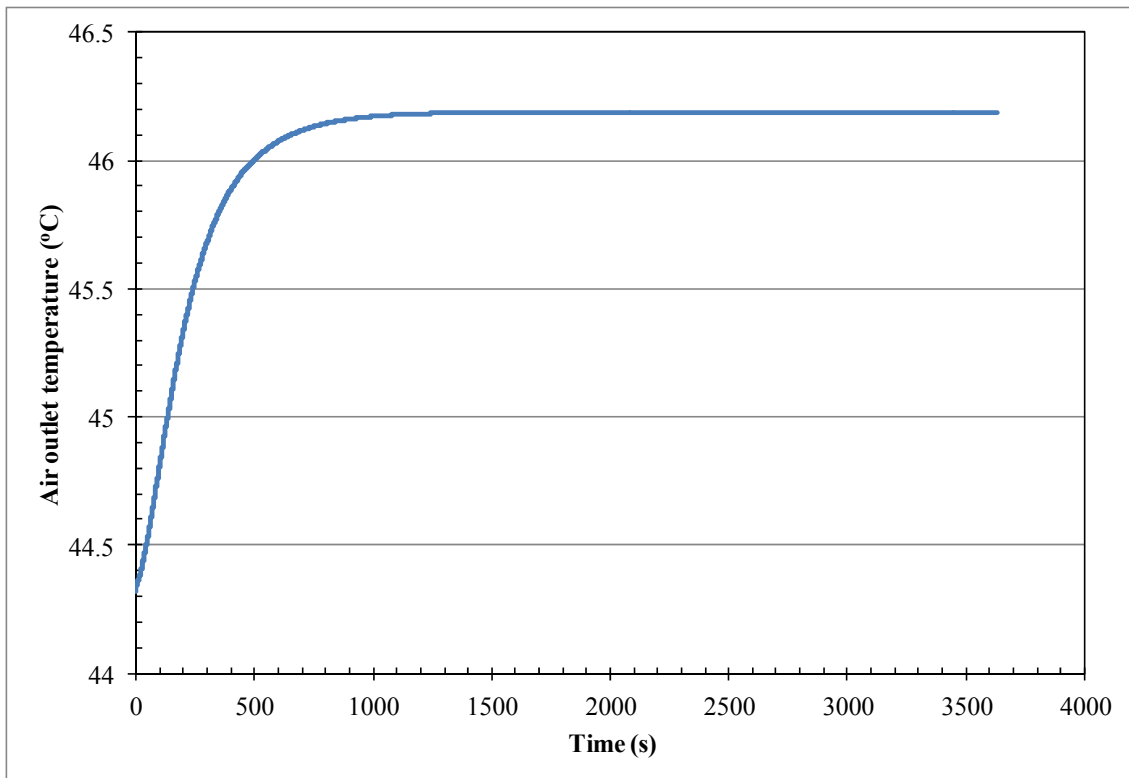


Figure 3.25: Transient response of air stream.

3.10. Conclusions

Experiments of heat transfer in a Polypropylene compact heat exchanger were conducted under various conditions for water-to-air heat exchange. The heat rejection rates of water-to-air in the Polypropylene compact heat exchanger were obtained. The results show that the heat rejection rate increases as the water and air mass flow rates increase. From all the tests conducted, it was concluded that the compact heat exchanger performs well and can reduce water temperature effectively. A 3D computational model was developed for the investigation of the fluid flow and the heat transfer in the compact heat exchanger. The simulation results of the heat rejection rates were obtained

and compared with the experimental results. It was found that they were in good agreement. Moreover, a comparison of the heat rejected by the Polypropylene and an aluminium alloy compact heat exchanger were performed using FLUENT[®] software and it was found that the Polypropylene compact heat exchanger achieved 98% of the heat transfer rate achieved by the aluminium alloy heat exchanger. The analysis of the performance of a Polypropylene compact heat exchanger model developed in this study shows that this model is an efficient tool and that it can be used in future applications.

This experiment studied heat transfer without taking into account condensation. As mentioned before, condensation is a very important phenomenon in many engineering operations and it is necessary that we increase our understanding of the physics of condensation in heat exchangers. Therefore, in the next two chapters the heat and mass transfer in a condensation heat exchanger is studied in more detail. In Chapter 4, a new mathematical model is derived for condensation heat exchangers and tube condensers. In Chapter 5, a simulation of a condensation heat exchanger is constructed using CFD software FLUENT[®].

CHAPTER 4: MATHEMATICAL MODEL OF CONDENSING HEAT EXCHANGER

4.1. Mathematical Model of Heat Exchanger with Condensation

The model studied in this work consists of two fluid streams separated by a solid wall. Cooling water flows vertically inside one of the channels, while a mixture of air and water vapour flows vertically in the other channel. The water vapour condenses on the cool wall and a liquid film forms that flows downwards under the influence of gravity. A schematic of a plate heat exchanger with condensation showing the important states is presented in Figure 4.1. The condenser is divided into a number of small elements of incremental length dx and each segment acts as a control volume for the air-vapour mixture (1), film condensation (2), wall material (3) and the cold-water stream (4), as shown in Figure 4.1.

The major assumptions that are used to derive the basic modelling equations may be summarised as:

- Negligible heat and mass transfer through the walls to the environment
- One dimensional flow
- Film condensation only occurs on the solid wall surface

- Uniform cross-sectional area of the heat exchanger

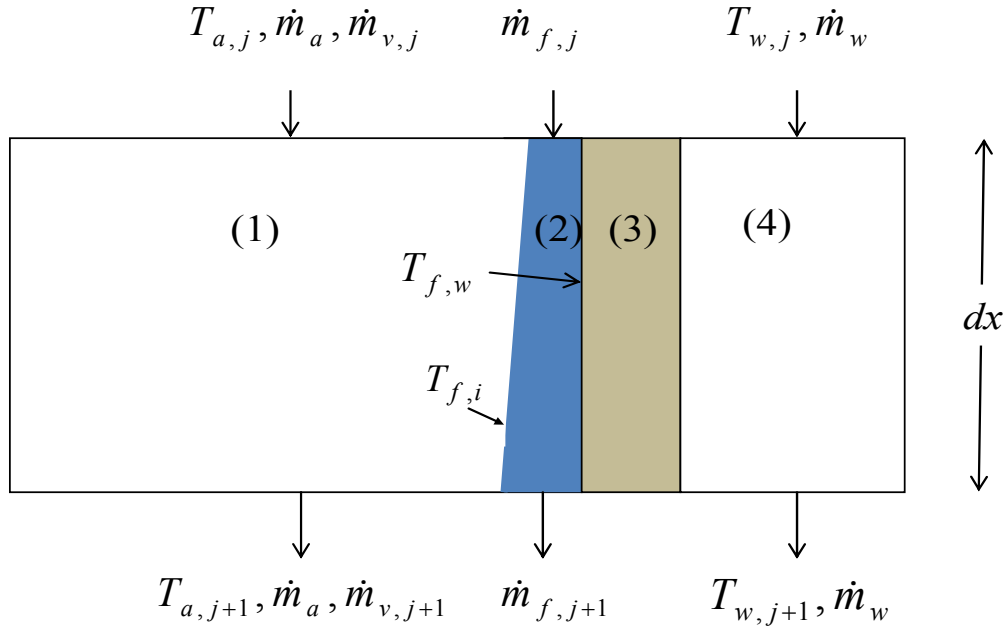


Figure 4.1: Schematic diagram of the small element in considering control volume analysis.

The temperature of the air-vapour mixture entering the element is designated by $T_{a,j}$, the inlet mass flow rate of water vapour by $\dot{m}_{v,j}$, the outlet temperature by $T_{a,j+1}$, an outlet mass flow rate of water vapour by $\dot{m}_{v,j+1}$ and the mass flow rate of dry air is \dot{m}_a . The mass flow rates of the condensate film entering and leaving the element are designated $\dot{m}_{f,j}$ and $\dot{m}_{f,j+1}$, and film thickness is δ . The temperature of the film/vapour interface is designated by $T_{f,i}$. A solid wall separates the condensate film and the coolant and the temperatures of the wall adjacent to each of the fluids are $T_{f,w}$ and $T_{w,w}$, respectively. The cooling water entering the element is $T_{w,j}$, and $T_{w,j+1}$ is the outlet temperature. The mass flow rate of the cooling water is \dot{m}_w .

4.1.1. Heat and Mass Transfer Analysis

4.1.1.1. Heat Balance on the Air-Vapour Mixture

For steady flows, the heat balance of the air-vapour mixture channel can be expressed as:

$$\dot{m}_a C_{pa} T_{a,j} + \dot{m}_{v,j} (h_{fg,0} + C_{pv} T_{a,j}) = \dot{m}_a C_{pa} T_{a,j+1} + \dot{m}_{v,j+1} (h_{fg,0} + C_{pv} T_{a,j+1}) + dx H_{av} (T_a - T_{f,i}) \quad (4.1)$$

where $h_{fg,0}$ is the latent heat of the water at $T = 0^\circ\text{C}$, which is the reference temperature for calculating the enthalpy. In the above equation, $h_{fg,0} + C_{pv} T_{a,j}$ is the specific enthalpy of the water vapour (Cengel and Boles 2008) and the temperature T_a is in Celsius. By re-arranging the terms, dividing both sides of the equation by dx , and taking the limit, Equation 4.1 can be expressed as:

$$-(\dot{m}_a C_{pa} + \dot{m}_v C_{pv}) \frac{dT_a}{dx} - (h_{fg,0} + C_{pv} T_a) \frac{d\dot{m}_v}{dx} = H_{av} (T_a - T_{f,i}) \quad (4.2)$$

The total heat transfer from the air-vapour mixture to the condensate film consists of the sensible heat Q_s and the latent heat Q_l ; that is:

$$\begin{aligned} Q &= Q_s + Q_l \\ &= dx H_a (T_a - T_{f,i}) + (\dot{m}_{v,j} - \dot{m}_{v,j+1}) h_v \\ &= dx H_{av} (T_a - T_{f,i}) \end{aligned} \quad (4.3)$$

After simplification, we obtain:

$$H_{av} = H_a - \frac{h_v}{(T_a - T_{f,i})} \frac{d\dot{m}_v}{dx} \quad (4.4)$$

where H_{av} is the overall HTC including both the sensible and latent heat, and h_v is the heat transported by the water vapour to the condensate film as water vapour is condensed into water liquid.

The rate of condensation can be calculated from the definition for mass transfer coefficient, which can be expressed as:

$$-d\dot{m}_v = (\dot{m}_{v,j} - \dot{m}_{v,j+1}) = dxK(C_v - C_{v,i}) \quad (4.5)$$

where K is the mass transfer coefficient of the water vapour, C_v is the average concentration of water vapour in the air-vapour mixture and $C_{v,i}$ is the water-vapour concentration at the interface between the mixture and the condensation, which depends on interface temperature $T_{f,i}$. By using the bulk density ρ as the representative density across the mixture channel, the above equation can be written as:

$$\frac{d\dot{m}_v}{dx} = -K\rho(Y_v - Y_{v,i}) \quad (4.6)$$

where Y_v is the mass fraction of the water vapour in the air-vapour mixture, and is related to the specific humidity, ϖ , by:

$$Y_v = \frac{\dot{m}_v}{\dot{m}} = \frac{\dot{m}_v}{\dot{m}_a + \dot{m}_v} = 1 - \frac{1}{1 + \varpi} \quad (4.7)$$

and \dot{m} is the total mass flow rate of the air-vapour mixture. We assume that the air, the water vapour and their mixture are all ideal gases and ideal gas law can be applied to determine their respective densities.

4.1.1.2. Force and Momentum Balance on the Condensate Film

By considering the balance between the weight of the fluid element, the buoyancy force and the viscous shear force in the small region 2, as shown in Figure 4.1, the velocity gradient of the condensate in the film can be derived as:

$$\frac{du}{dy} = \frac{(\rho_l - \rho_g)g}{\mu_l}(\delta - y) + \frac{\tau_g}{\mu_l} \quad (4.8)$$

where ρ_l is the density of the condensate, ρ_g is the density of the air-vapour mixture at the interface, μ_l is the dynamic viscosity of the condensate and τ_g is the shear stress at the interface between the air-vapour mixture and the condensate film. Here we have assumed that the condensate film is very thin and the direction of the shear stress is the same as that of the buoyancy force. Nusselt's theory neglects interfacial shear. The velocity distribution in the condensate film can then be derived as:

$$u = \frac{(\rho_l - \rho_g)g}{\mu_l} \left(\delta y - \frac{1}{2} y^2 \right) + \frac{\tau_g}{\mu_l} y \quad (4.9)$$

Here we have assumed that the velocity of the condensate is zero at the inner surface of the condenser wall. The mass flow rate increase in the condensate film because of water vapour condensing from the air-vapour mixture can be calculated from:

$$\frac{d\dot{m}_v}{dx} = - \left(\frac{\rho_l(\rho_l - \rho_g)g\delta^2}{\mu_l} + \frac{\rho_l\tau_g\delta}{\mu_l} \right) \frac{d\delta}{dx} \quad (4.10)$$

Combining Equations 4.6 and 4.10 enables the condensate film thickness δ to be determined.

The heat transfer balance in the condensate film can be calculated after the manner of Nusselt (1916); that is:

$$H_{av}(T_a - T_{f,i}) = k_f \frac{(T_{f,i} - T_{f,w})}{\delta} + \frac{d(\dot{m}_f h_f)}{dx} \quad (4.11)$$

$$T_{f,i} = T_{f,w} \quad \text{if } \delta = 0$$

where h_f is the specific enthalpy of the condensate. The last term in the above equation takes into account the energy change of the condensate in the small element dx , as shown in Figure 4.1. This change is due to the change in \dot{m}_f and the change of the condensate temperature. This term has been neglected in previous studies Kuhn (1995) and is included in this work to form part of the differential and algebraic equations.

4.1.1.3. Heat Transfer at the Solid Wall

Under the assumption that the temperature in the condensate varies linearly across the film, the heat conduction at the interface between the solid wall and the condensate film can be calculated as $k_f(T_{f,i} - T_{f,w})/\delta$. This heat conduction through the condensate film and that through the solid wall are equal to each other. Hence:

$$\frac{k_f(T_{f,i} - T_{f,w})}{\delta} = \frac{k_s(T_{f,w} - T_{w,w})}{\delta_s} \quad (4.12)$$

where k_s and k_f are the thermal conductivities of the solid wall and the condensate film, respectively.

4.1.1.4. Heat Transfer in the Cooling Channel

The heat transfer from the solid wall to the stream of cooling channel should be balanced by the heat transfer in the coolant. Hence:

$$\frac{k_s(T_{f,w} - T_{w,w})}{\delta_s} = H_w(T_{w,w} - T_w) \quad (4.13)$$

where H_w is the convective HTC of the water in the coolant channel. A thermal energy balance on the cooling water shown in Figure 4.1 results in the following expression:

$$C_{pw} \dot{m}_w \frac{dT_w}{dx} = H_w (T_{w,w} - T_w) \quad (4.14)$$

That is, the heat transfer into the coolant causes the water temperature to change. In deriving Equation 4.14, we have assumed that the outer wall of the cooling channel is well insulated and there is no heat loss from this outer wall.

The above equations are derived for a plate heat exchanger with condensation of co-current flows. For heat exchangers of counter flows, these equations remain valid, but the mass flow rate of the cooling water assumes a negative value. In this case, we are assuming that the cooling water in Figure 4.1 flows upwards, which is in the opposite direction to that of the air-vapour mixture.

4.2. Mathematical Model of Tube Condenser

A mathematical model was developed to study the condensation of water vapour in the tube condenser, in which the air-vapour mixture is flowing downward inside a vertical tube (the inner and outer radii of the tube are r_i and r_o), while cooling water is flowing counter-currently up through the annulus, as shown in Figure 4.2.

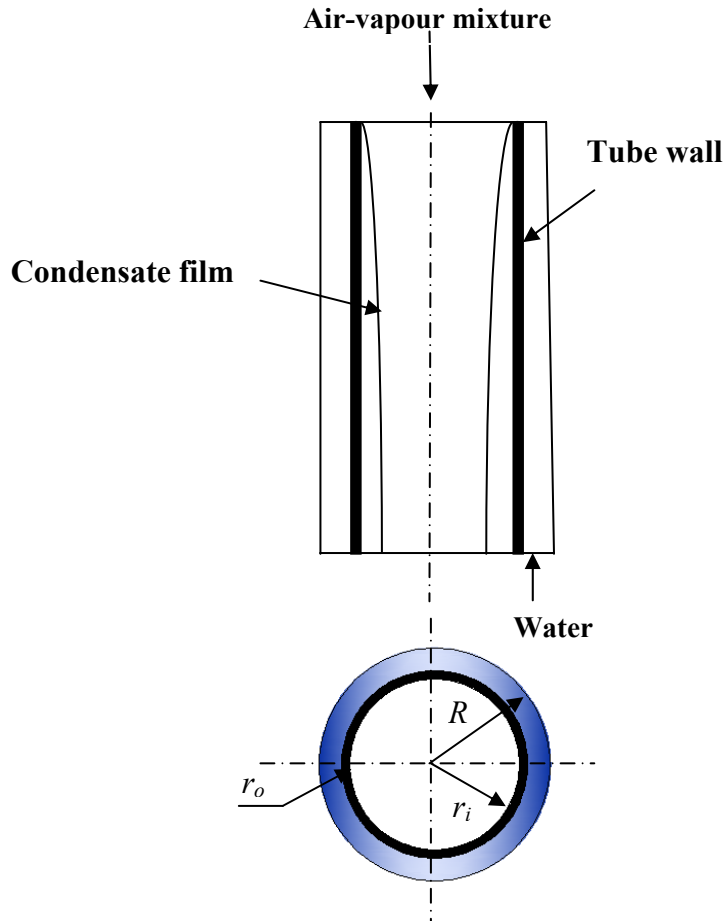


Figure 4.2: Schematic diagram of a tube condenser.

The systems of equations can be derived similarly as above and are as follows. The heat balance of the air-vapour mixture for tube condenser can be expressed as:

$$-(\dot{m}_a C_{pa} + C_{pv} \dot{m}_v) \frac{dT_a}{dx} - (h_{fg,0} + C_{pv} T_a) \frac{d\dot{m}_v}{dx} = 2\pi(r_i - \delta) H_{av} (T_a - T_{f,i}) \quad (4.15)$$

The overall HTC, H_{av} , including the sensible and latent heat can be obtained by:

$$H_{av} = H_a - \frac{h_v}{2\pi(r_i - \delta)(T_a - T_{f,i})} \frac{d\dot{m}_v}{dx} \quad (4.16)$$

The rate of condensation can be calculated from the definition for mass transfer coefficient, which can be expressed as:

$$\frac{d\dot{m}_v}{dx} = -2\pi(r_i - \delta)K\rho(Y_v - Y_{v,i}) \quad (4.17)$$

The mass flow rate increase in the condensate film because of water vapour condensing from the air-vapour mixture can be calculated from:

$$\frac{d\dot{m}_v}{dx} = -2\pi\rho_l \left[\frac{(\rho_l - \rho_g)g}{\mu_l} (r_i\delta^2 - \frac{5}{6}\delta^3) + \frac{\tau_g}{\mu_l} (r_i\delta - \delta^2) \right] \frac{d\delta}{dx} \quad (4.18)$$

The heat balance on the condensate film can be calculated as:

$$H_{av}(T_a - T_{f,i}) = \frac{k_f(T_{f,i} - T_{f,w})}{(r_i - \delta)\ln[r_i / (r_i - \delta)]} + \frac{1}{2\pi(r_i - \delta)} \frac{d(\dot{m}_f h_f)}{dx} \quad (4.19)$$

$T_{f,i} = T_{f,w}$ if $\delta = 0$

The heat transfer through the solid wall can be simplified to:

$$\frac{k_f(T_{f,i} - T_{f,w})}{\ln[r_i / (r_i - \delta)]} = \frac{k_s(T_{f,w} - T_{w,w})}{\ln(r_o / r_i)} \quad (4.20)$$

The heat transfer from the solid wall to the stream of cooling tube should be balanced by the heat transfer in the coolant. Hence:

$$\frac{k_s (T_{f,w} - T_{w,w})}{r_o \ln(r_o / r_i)} = H_w (T_{w,w} - T_w) \quad (4.21)$$

The thermal energy balance on the cooling water results in the following expression:

$$C_{pw} \dot{m}_w \frac{dT_w}{dx} = 2\pi r_o H_w (T_{w,w} - T_w) \quad (4.22)$$

Here, we have assumed that cooling water flowing between the pipe and an outer cylinder and the out cylinder is insulated.

4.3. Models and Formulations of Heat and Mass Transfer

The HTC, H_a and H_w , for the air-vapour mixture and water flows can be obtained from the correlations for Nusselt number in channel flows:

$$Nu = \frac{Hd}{k} = f(Re_d, Pr) \quad (4.23)$$

where Pr is the Prandtl number $\left(Pr = \frac{C_p \mu}{k} \right)$ and:

$$Re_d = \frac{\rho U d}{\mu}$$

where d is the hydraulic diameter of the channel for air-vapour mixture or the water channel in the case of the plate condenser. In the case of the tube condenser, d can be the diameter of the inner pipe for air-vapour mixture or hydraulic diameter for the coolant flowing between the two cylinders. The mass transfer coefficient, K , is obtained by using correlation for Sherwood number:

$$Sh = \frac{Kd}{D} = f(Re_d, Sc) \quad (4.24)$$

Here Sc is the Schmidt number and D is the molecular diffusivity that can be calculated as a function of temperature and pressure, as recommended by Dharma Rao et al. (2008):

$$D = \frac{1.87 \times 10^{-10} \times T^{2.072}}{P} \quad (4.25)$$

Here P is the total pressure in the air-vapour mixture. The saturation vapour pressure of water is a function of temperature and can be determined from the expression given by Dharma Rao et al. (2008), namely the Antoine relation:

$$P_v = \exp(77.3450 + 0.0057T - 7235/T) / T^{8.2} \quad (4.26)$$

where T is in Kelvin. The specific humidity of air-vapour mixture ϖ can be calculated as:

$$\varpi = \frac{m_v}{m_a} = \frac{0.622P_v}{P - P_v} \quad (4.27)$$

For film condensation, the suction effect, developing flow, roughness effect and properties variation are considered. These are discussed below.

4.3.2. Suction Effect Consideration

At high mass fractions of water vapour in the mixture, it is important to consider the suction effect on heat and mass transfer, which arises because of steep temperature and concentration gradients near the interface. Consequently, the correlations to be employed for heat and mass transfer calculation must consider this (Bird, Stewart and Lightfoot, 2007). Thus, Kays and Moffat (1975) obtained correlation for suction effect as follows:

$$\frac{St}{St_o} = \frac{\ln(1+B_h)}{B_h} \quad (4.28)$$

where St/St_o is the ratio of Stanton number with suction to that without suction.

$B_h = \dot{m}_v'' / GSt$ is called the Spalding factor. Equation 4.28 can be simplified and

rewritten as:

$$Nu_x = \left[\exp\left(\frac{\dot{m}_v'' RePr}{G_{mix} Nu_{o,x}}\right) - 1 \right]^{-1} \left(\frac{G_{mix}}{\dot{m}_v'' RePr} \right)^{-1} \quad (4.29)$$

where \dot{m}_v'' is the actual condensate mass flux at the interface between the air-vapour mixture and the condensate film and G_{mix} is the mass flux of the mixture. Using the analogy between the heat and mass transfer, the Sherwood number is expressed as:

$$Sh_x = \left[\exp\left(\frac{\dot{m}_v'' ReSc}{G_{mix} Sh_{o,x}}\right) - 1 \right]^{-1} \left(\frac{G_{mix}}{\dot{m}_v'' ReSc}\right)^{-1} \quad (4.30)$$

After taking into account the suction effect on the rate of mass transfer at the gas and condensate film interface, the mass flux at the interface can be calculated according to Bucci et al. (2008):

$$\dot{m}_v'' = \rho K \ln(1 + B_m) \quad (4.31)$$

where:

$$B_m = \frac{Y_{v,i} - Y_{v,b}}{1 - Y_{v,i}} \quad (4.32)$$

Here, $Y_{v,i}$ is the mass fraction of water vapour at the gas-liquid interface and $Y_{v,b}$ is the bulk mass fraction of water vapour in the air-vapour mixture. Equations 4.31 and 4.32 are more general than Equation 4.6 since they account for suction effect.

4.3.3. Developing Flow Consideration

As most of the heat transfer takes place in the first part of the condenser, it may be important to consider the developing flow effects in the heat and mass transfer model. In Equations 4.29 and 4.30, $Nu_{o,x}$ and $Sh_{o,x}$ denote the respective local Nusselt and Sherwood numbers after taking into account the developing flow in the thermal entrance region, as suggested by Reynolds, Swearngen and McEligot (1969):

$$Nu_{o,x} = Nu_o \left[1 + \frac{0.8(1 + 7 \times 10^4 Re^{-3/2})}{(x + x_0)/d} \right] \quad (4.33)$$

Using the heat and mass transfer analogy, the Sherwood number including the effect from the thermal entrance region can be written as:

$$Sh_{o,x} = Sh_o \left[1 + \frac{0.8(1 + 7 \times 10^4 Re^{-3/2})}{(x + x_0)/d} \right] \quad (4.34)$$

where x_0 is an initial entrance length.

The Nusselt and Sherwood numbers for fully developed flows, without accounting for the suction effect, can be calculated according to Holman (1992):

$$Nu_o = 1.04 \times 0.0395 Re^{0.75} Pr^{1/3} \quad (4.35)$$

$$Sh_o = 1.04 \times 0.0395 Re^{0.75} Sc^{1/3} \quad (4.36)$$

The subscript o represents fully developed flows. The above equations without the factor 1.04 are those for constant wall temperature. For constant heat flux at the wall, the factor should be included. In this model, this factor is included even though it is close to unity.

4.3.4. Roughness Effect Consideration

As condensation proceeds along the condenser, the flow of the condensate changes from laminar to turbulent flow, and the condensate film surface becomes rough and wavy. This roughness effect is modelled using the correlations suggested by Norris (1970) for the heat transfer over rough surfaces:

$$Nu_{o,r} = Nu_{o,s} \left(\frac{f_r}{f_s} \right)^{nh} \quad (4.37)$$

Using the heat and mass transfer analogy, the Sherwood number is given by:

$$Sh_{o,r} = Sh_{o,s} \left(\frac{f_r}{f_s} \right)^{nm} \quad (4.38)$$

where the subscripts r and s refer to the tube rough and smooth conditions, $nh = 0.68 \text{Pr}^{0.215}$ and $nm = 0.68 \text{Sc}^{0.215}$, and f_r/f_s represents the ratio of the Fanning friction factor for a rough wall to that for a smooth wall. For a smooth wall, the friction factor is calculated from:

$$f_s = 0.316 \times Re^{-0.25} \quad (4.39)$$

For a rough wall, the friction factor is given by Haaland (1983) as:

$$\frac{1}{f_r^{1/2}} = -1.8 \log_{10} \left[\frac{6.9}{Re} + \left(\frac{\varepsilon/d}{3.7} \right)^{1.11} \right] \quad (4.40)$$

where Re is the Reynolds number for the air-vapour mixture flow. The friction factor, f_r , increases as the surface roughness increases. An assumption of roughness height ε being equal to 0.5δ is chosen, as suggested by Siddique et al. (1994). In the model used here, we apply the roughness corrections to the condensate film starting from $x = 0$ and assume that all the flows are turbulent. The interfacial shear stress is calculated as:

$$\tau_g = f \rho_g \frac{(U - u_{fb})^2}{2} \quad (4.41)$$

where U is the bulk velocity of the air-vapour mixture, u_{fb} is the mean velocity of the water liquid in the condensate film and ρ_g is the density of the air-vapour mixture.

4.3.5. Thermophysical Properties

An important step in the calculation is the definition of physical properties of the fluids. The thermal conductivity, density, viscosity and specific heat for the gas

mixture, condensate and the coolant are required for the calculation. Given the large temperature variation that can be expected in the condensation of water vapour in the presence of non-condensable gas, the assumption of constant fluid properties may give rise to errors, because the fluid properties vary with temperature. These variations of fluid properties then cause a variation of velocity and temperature throughout the boundary layer or over the flow cross section of the duct or tube. In this research, the physical properties for liquid water, dry air and water vapour are obtained by using the curve fittings listed in Appendix B as a function of temperature.

4.3.6. Buoyancy Effect

Many experimental studies of condensation from gas-vapour mixtures are based on water flowing counter-currently upward as a coolant in the condensers. It has been found experimentally that the temperature increase of the coolant may be small but the wall temperature of the inner pipe can be high. This could be the result of low HTC on the cooling side. In this case, the heat transfer in the coolant channel is affected by buoyancy. The buoyancy effect is confined within an enclosed space and can be modelled as suggested by Kays, Crawford and Weigand (2005) as:

$$Nu_w = 0.046Ra^{1/3} \quad (4.42)$$

where Ra is the Rayleigh number and can be calculated as:

$$Ra = GrPr = \frac{g \beta \rho^2 C_p \delta_o^3}{\mu k} (T_{w,w} - T_w) \quad (4.43)$$

and δ_o is the channel width of the coolant flow. The combined HTC in the cooling flow is then calculated as a combination of the forced and natural convection:

$$Nu_{combined} = (Nu_{forced}^n \pm Nu_{natural}^n)^{1/n} \quad (4.44)$$

with $n = 3$, as recommended by Churchill (1977), for vertical surfaces. The plus sign is invoked when the forced and natural convections are assisting one another, and the minus sign is used when opposing flows are caused by forced convective and natural convective. The models using Equations 4.42–4.44 assume that the coolant stays as liquid phase. In some applications, the temperature in the coolant reaches high enough that boiling occurs. In these cases, different models should be used to model the heat transfer in the coolant.

4.4. Numerical Solution Procedures

The full system of seven differential and algebraic equations describing the heat and mass transfer that occurs in condensation from air-vapour mixture in the plate heat exchanger is given by Equations 4.2, 4.6, 4.10, 4.11, 4.12, 4.13 and 4.14. For the tube condenser, the system is given by Equations 4.15, 4.17, 4.18, 4.19, 4.20, 4.21 and 4.22. These equations can be used to solve for the seven unknowns, T_a , \dot{m}_v , δ , $T_{f,i}$, $T_{f,w}$, $T_{w,w}$ and T_w . The differential equations were discretised using the first-order-forward Euler method, and the calculations were performed using the fourth-order Runge-Kutta method to solve the differential and algebraic equations to obtain the mixture temperature, water temperature, wall temperatures, condensation rate and

heat flux. The boundary conditions are: the inlet water-vapour temperature, inlet water-vapour mass flow rate, inlet cooling water temperature, cooling water mass flow rate, air mass flow rate and inlet pressure. A computer program was written in MATLAB[®] to solve these equations.

In this research, the numerical solutions were performed for vapour condensation in plate heat exchanger and tube condenser systems to compare the predictions with available experimental results from the literature. All the experimental results to be discussed later applied to counter flows between the coolant and the air-vapour mixture, and therefore the mass flow rate for the coolant \dot{m}_w was taken as negative to apply the differential equations presented above.

In solving the differential equations, the location of the air-vapour mixture inlet was taken as $x = 0$ and that of the exits was taken as $x = L$. The x_0 in Equations 4.33 and 4.34 was taken as $0.5d$ to avoid divergence. A marching method was used, starting from $x = 0$. We assumed that at $x = 0$, the thickness of the condensate film $\delta = 0$, and this results in $T_{fi} = T_{fw}$. When $\delta = 0$ at $x = 0$, Equations 4.10 and 4.18 cannot be used to solve for the film thickness at $x = dx$. To overcome this difficulty, Equations 4.10 and 4.18 were integrated and an algebraic equation was solved for calculating the film thickness at $x = dx$. At $x > dx$, Equations 4.10 and 4.18 were used. These equations are easier to solve than the integrated algebraic equation.

For the counter-flow condensers considered here, boundary conditions at both $x = 0$ (for the air-vapour mixture) and $x = L$ (for coolant) are given. Because of this, a straightforward marching method cannot be used. Instead, a shooting scheme in

combination with the marching method was used. At $x = 0$, the exit temperature of the coolant, $T_{w,L}$, was estimated to initiate the solution procedure and the solutions were marched to $x = L$. The predicted $T_{w,N}$ was compared with the boundary condition T_w at $x=L$. If the relative error between the predicted $T_{w,N}$ and T_w at $x=L$ (a boundary condition) was larger than 10^{-7} , a newly estimated $T_{w,I}$ was used and the solution was repeated. The convergence of the solutions was established by comparing the predicted total condensation rates from using two discretisations with $N = 1,000$ and $N=10,000$, respectively. It was found that the difference was less than 0.01%. In the results presented in this work, only the results from $N = 10,000$ are given.

In solving the differential and algebraic equations, the physical properties such as specific heat, dynamic viscosity, density and diffusivity for water, dry air and water vapour were all allowed to vary with temperature and were calculated from the correlations given in Appendix B using the local mean temperature at each x_j . The thermal conductivity and dynamic viscosity of the air-vapour mixture were calculated according to Bird, Stewart and Lightfoot (2007), and the specific heat of the air-vapour mixture was calculated using the mass-weighted average (see Appendix B).

In solving for the air-vapour mixture temperature T_a , the energy transported by the water vapour into the condensate film, h_v , needs to be calculated. In the literature, several methods of calculating this energy are available. One is:

$$h_v = h_{fg,i} \quad (4.45)$$

where $h_{fg,i}$ is the latent heat of vapourisation at the temperature $T_{f,i}$. This assumes that the energy transported by the water vapour to the condensate film is that due to the condensation of saturated water vapour into saturated liquid. The second method is given by Baehr and Stephan (2006):

$$h_v = C_{pv} (T_a - T_{f,i}) + h_{gh,i} + 0.68C_{pL} (T_{f,i} - T_{f,w}) \quad (4.46)$$

where C_{pv} is the specific heat of water vapour and C_{pL} is the specific heat of liquid water. In Equation 4.46, the first term on the right hand side is that due to superheating and the third term is that due to sub-cooling.

By examining Figure 4.1, it can be seen that, as the water vapour is transported from the air-vapour mixture to the condensate film, the vapour carries with it the energy that includes the latent heat and the sensible heat of the liquid water as it crosses the interface (because of the mass transfer). One way to represent this is:

$$h_v = h_{fg,0} + C_{pv} T_{f,i} \quad (4.47)$$

where $h_{fg,0}$ is the latent heat of the water at $T = 0^\circ\text{C}$, which is the reference temperature for calculating the enthalpy. However, it was found from numerical results that Equations 4.46 and 4.47 can produce temperature jumps near the air-vapour inlet for some situations (which we think is physically unrealistic) and a more appropriate representation of this energy can be expressed as:

$$h_v = h_{fg,0} + C_{pv} T_a \quad (4.48)$$

This shows that all the energy from the water vapour in the bulk of the air-vapour mixture is transported into the condensate as the water vapour is condensed, while Equation 4.46 shows that some of the energy ($C_{pv}(T_a - T_{f,i})$) is left behind in the air-vapour mixture. Further, the enthalpy value calculated from Equation 4.48 is very close to the enthalpy of the superheated steam as given on EngineeringToolBox.com (2010). In the results presented later, only results using Equation 4.48 are considered. One consequence of Equation 4.48 is that, when it is combined with Equations 4.2 and 4.4, it shows that the energy balance for the air-vapour mixture involves only the sensible heat; the latent heat is released at the interface when the phase change occurs.

In solving Equation 4.11 for the energy balance in the condensate film, the average temperature across the film is required. This was calculated by assuming that the temperature varies linearly across the film, as shown by Bromley (1952).

4.5. Results and Discussion

4.5.1. Comparison of Model Predictions for Condensation in Plate Heat Exchanger with Existing Experimental Results

Below, the present theoretical work for condensation in plate heat exchanger is validated with the experimental data of Ambrosini et al. (2008), who conducted experiments in a 2 m-long square cross-sectional plane channel ($0.34\text{m} \times 0.34\text{m}$) to study the heat and mass transfer in the condensation of water vapour from humid air. They obtained experimental data from five tests at various inlet conditions for heat fluxes along the channel, the total condensation rate and the outlet water temperature. These data were related to five operating conditions characterised by a nominal value of the secondary coolant temperature close to 30°C , a steam generator power of 10 kW and mixture velocities from 1.5 to 3.5 m/s, as shown in Table 4.1. Numerical results were obtained from the present work for heat flux, condensation rate and outlet water temperature $T_{w,out}$ for the same conditions of inlet water temperature $T_{w,in}$, inlet mixture velocity V , inlet air temperature T_a , and relative humidity of the air at the inlet ϕ as those of Ambrosini et al. (2008). The heat fluxes, condensation rate and outlet water temperature computed from the present model are shown in Figures 4.3, 4.4 and 4.5, respectively, which show satisfactory agreement with the experimental data of Ambrosini et al. (2008).

Table 4.1: Experimental conditions from Ambrosini et al. (2008).

Test	$T_{w,in} [^{\circ}C]$	$V_{mix} [m / s]$	ϕ	$T_{a,in}$
1	31.24	1.46	100	82.66
2	31.10	2.02	100	80.61
3	31.07	2.52	97.83	79.13
4	30.90	3.01	87.35	78.73
5	30.71	3.59	96.55	75.02

Figure 4.3 shows the comparison between the heat flux estimated by the theoretical model $Q=H_{av}(T_a-T_{f,i})$ and the experimental data of Ambrosini et al. (2008). Agreement between the model predictions and the experimental data is quite good. The predicted heat flux shows a sharp decrease at $x = 0$ and this sharp increase occurs over a shorter distance than that in the experimental data. This means that Equations 4.33 and 4.34 may not fully allow for the effects resulting from the developing flow in the entrance region of the mixture channel.

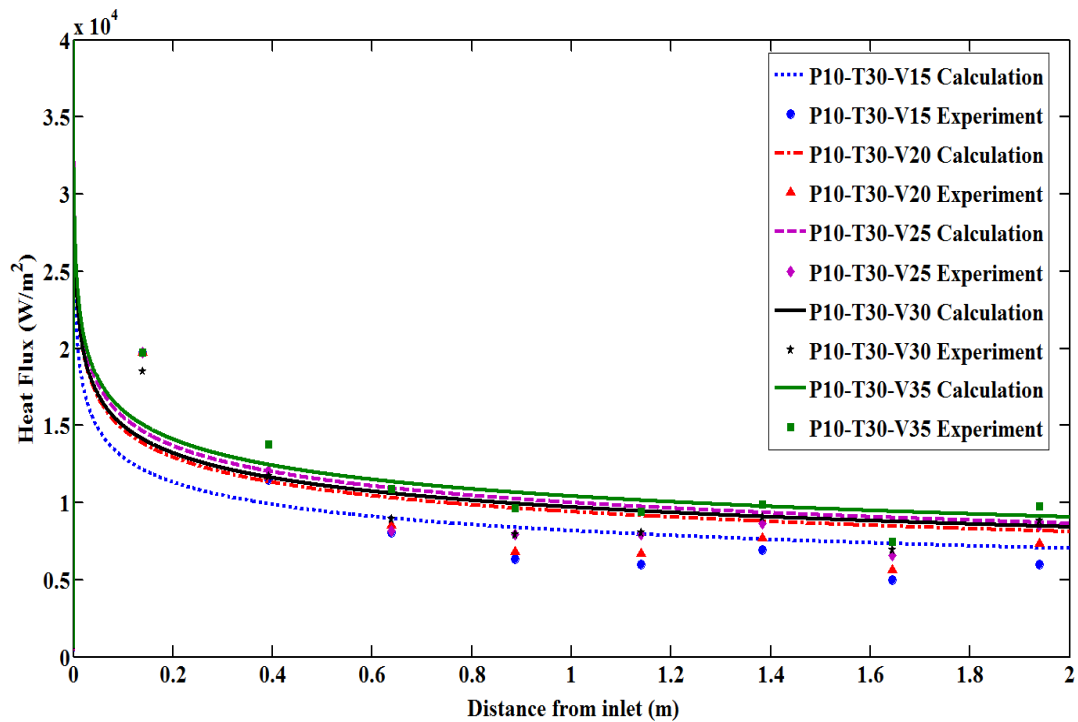


Figure 4.3: Comparison of the predicted and experimental heat flux for all the tests of Ambrosini et al. (2008).

The overall condensation rates computed from the present model for the different experimental conditions, as listed in Table 4.1, are shown in Figure 4.4. The predicted overall condensation rates were calculated by summing $-dm_v$ along the channel and these can also be calculated by the inlet and outlet mass flow rates of the water vapour in the air-vapour mixture channel. The results show a good agreement between the calculated and experimental data, with the maximum relative error being less than 9% between the predictions and the experimental results.

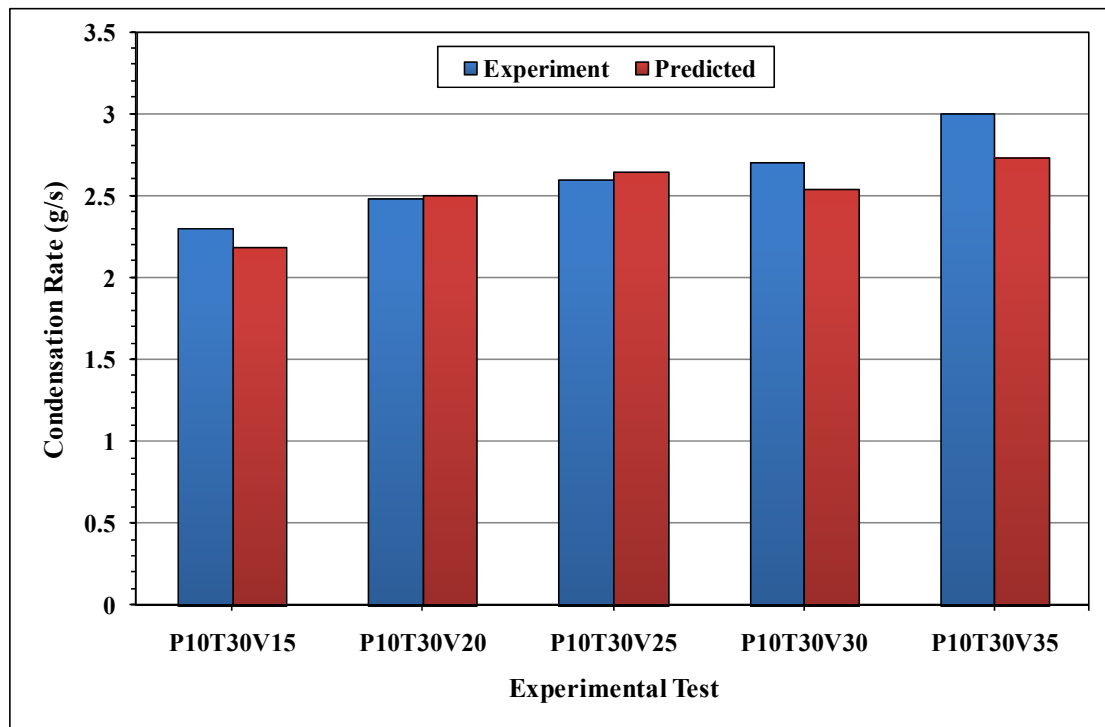


Figure 4.4: Comparison of the predicted and experimental values of condensation rate for all the tests of Ambrosini et al. (2008).

Figure 4.5 shows the comparison between the predicted outlet water temperature and the experimental data of Ambrosini et al. (2008). It can be seen from the figure that the predicted and experimental results are in very good agreement.

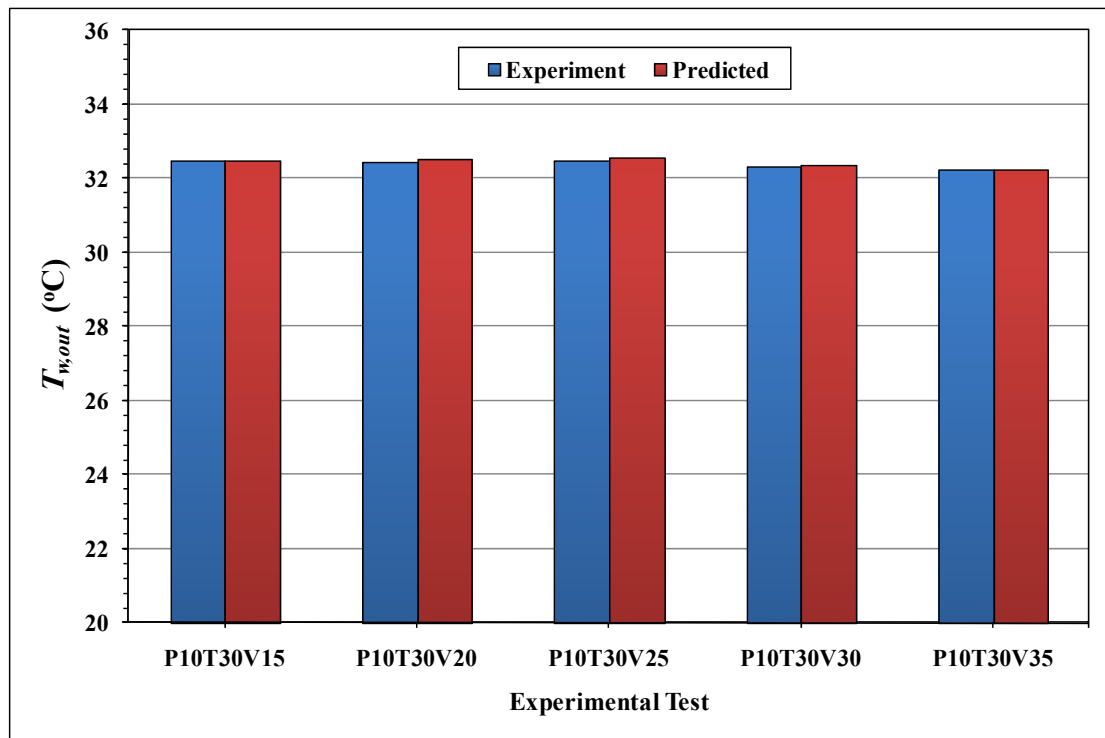


Figure 4.5: Comparison of the predicted and experimental values of outlet water temperature $T_{w,out}$ for all the tests of Ambrosini et al. (2008).

4.5.2. Comparison of Model Predictions for Condensation in Tube with Existing Experimental Results

The present theoretical work is validated against the experimental data of Siddique (1992), Kuhn (1995) and Tanrikut and Yesin (1998). The test sections of all these experiments were circular, vertical, metallic tubes, surrounded by annular jackets through which a liquid coolant (liquid water) flowed. The gas-vapour mixture flowed downward in the tube, while the coolant in the jacket flowed upward. Each of these experimental studies includes a large number of tests, and several representative tests of a wide range of conditions were selected from each experimental study, as summarized in Table 4.2.

Table 4.2: Experimental runs used for comparison with predictions.

Reference	Run number	$T_{w,in} [^{\circ}C]$	$T_{mixt,in} [^{\circ}C]$	$u_{mixt} [m/s]$	$w_{a,in}$	Pressure [kPa]
Siddique (1992)	1	11	100	2.509	0.087	107.4
	6	10.2	100	2.561	0.332	132.7
	7	7	120	1.378	0.080	208.6
	11	7.9	120	1.388	0.33	259.6
	13	12.7	140	0.695	0.11	389.2
	17	7.7	139.9	0.694	0.34	474.5
	26	8	119.9	3.054	0.22	221.2
Kuhn (1995)	2.1-12	26.9	133.4	4.77	0.34	408.4
	2.2-1	27.9	134.6	11	0.01	132.8
	2.2-8	25.6	129.1	14	0.146	115.7
	3.1-2	29.9	140.3	8.64	0.01	205.9
	3.3-4	28.8	144	4.66	0.1	418.1
	3.5-4	22.7	132	6	0.35	400.5
	4.5-3	23	123	4	0.38	306.2
	4.5-5	22.7	140.3	2.54	0.38	503.4
Tanrikut and Yesin (1998)	2.3.1	16	160.9	18.22	0.098	296.9
	3.3.1	14.4	171.7	20.46	0.189	290.1
	3.4.1	14.4	163.4	18.30	0.193	390
	4.3.1	14.6	158.9	23.07	0.279	316
	5.4.1	14.4	152.7	17.04	0.369	394

The experiments of Siddique (1992) were conducted using air-steam mixture with inlet temperatures of 100, 120 and 140°C, respectively, inlet air mass fractions from 8 to 35%, and inlet mixture pressure from 0.11 MPa to 0.48 MPa. Siddique measured the respective temperatures of the cooling water, the gas-vapour mixture on the centreline and the inside and outside walls of the tube at nine stations spaced 30.5 cm apart along the length of the condenser ($L = 2.54\text{ m}$). To measure the bulk temperature of the coolant in the annulus, Siddique (1992) used small air bubbles to mix with the coolant to achieve a uniform temperature profile across the coolant channel.

The experiments of Kuhn (1995) were conducted for pure steam, steam-air mixture and steam-helium mixture. In this thesis, we compare the data from Kuhn only for the steam-air mixture experiments. In Kuhn, the coolant bulk temperature was not directly measured, rather it was estimated by measuring the temperatures at the inner and outer walls of the annulus and by calculating the temperature difference ratio (defined as a shape factor) numerically. Kuhn also investigated the effect of turbulent condensate film on the heat transfer by injecting liquid water using film distributors near the mixture inlet.

The experimental results of Tanrikut and Yesin (1998) were obtained for the condensation in the presence of air for the pressure range of 1.8–5.5 bars, $Re_v = 45,000\text{--}94,000$ and non-condensable gas mass fraction $X = 0$ to 52%. They found that inlet superheating of the steam has little effect on the heat flux and that the presence of air has a large effect on reducing the heat transfer in comparison with the condensation of pure vapour ($X = 0$).

In all three experiments (Kuhn 1995; Siddique 1992; Tanrikut and Yesin 1998), the local heat flux was estimated using:

$$q'' = \frac{\dot{m}_c C_p}{\pi d} \frac{dT_c}{dL}(x) \quad (4.49)$$

where T_c is the measured or estimated bulk temperature of the coolant, and the gradient dT_c/dL was estimated from a curve fit as a function of condenser length. The condensation rates were then estimated using:

$$\dot{m}_{cond} = \frac{\dot{Q}}{h_{fg}} \quad (4.50)$$

Here \dot{m}_{cond} is the total condensation rate (or the total condensation rate as collected), \dot{Q} is the total heat transfer rate across the condenser wall, and h_{fg} is the latent heat of condensation and was calculated using the averaged wall temperature of the condenser. In using Equation 4.50 to calculate the total condensation rate, the contribution of the sensible heat transfer in \dot{Q} was neglected.

4.5.2.1. Condensation Rate

The overall condensation rates computed from the present model for the different experiments, as listed in Table 4.2, are shown in Figures 4.6, 4.7 and 4.8, respectively. The predicted overall condensation rates were calculated by summing $-dm_v$ along the condenser tube and these can be calculated by using the inlet and outlet mass flow rates of the water vapour in the air-vapour mixture tube. As a result, the predicted condensation rates are the true condensation and are due to the mass transfer across the boundary layers in the channel only. This is in contrast to the condensation rates

from the three experiments given in Table 4.2, which were estimated from the overall heat transfer rates.

It can be seen from Figures 4.6, 4.7 and 4.8 that the predicted and experimental results obtained from different sources are in excellent agreement, with the maximum relative error being less than 6% between the predictions and the experimental results of Siddique (1992). For Kuhn (1995), the maximum relative error is less than 8.5%, and for Tanrikut and Yesin (1998), it is less than 4%. The results in Figures 4.6 to 4.8 also support the assumption made in deriving the condensation rates in the experiments that the sensible heat transfer is small in comparison to the latent heat transfer.

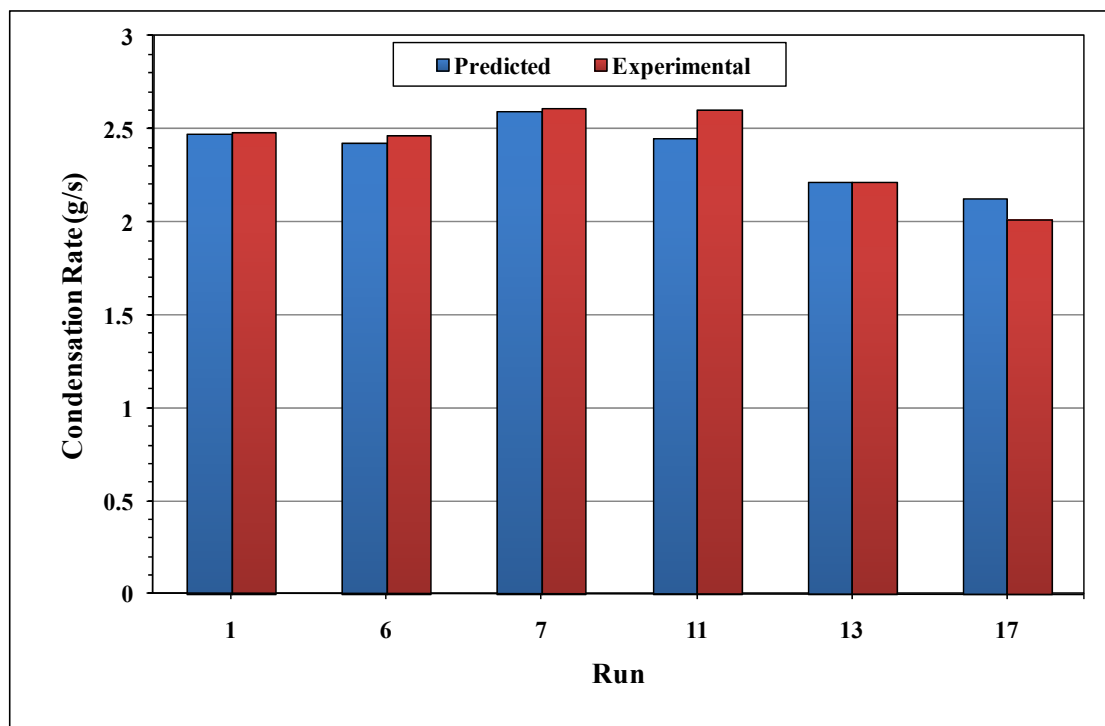


Figure 4.6: Comparison of the predicted condensation rates with the experimental results of Siddique (1992), runs 1, 6, 7, 11, 13 and 17.

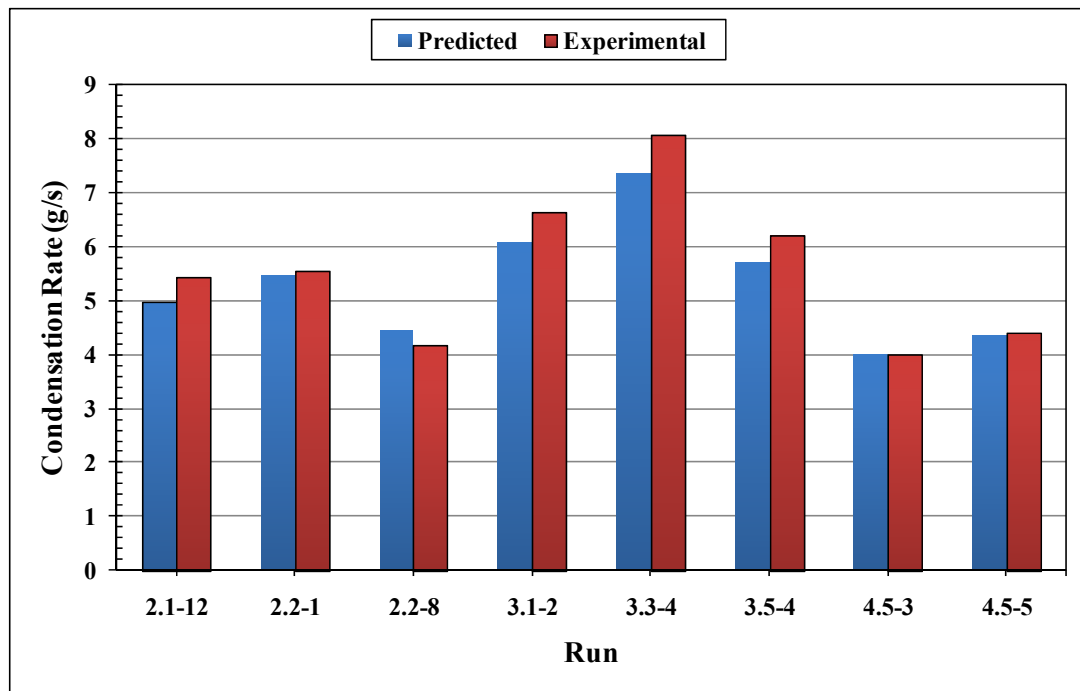


Figure 4.7: Comparison of the predicted condensation rates with the experimental results of Kuhn (1995), runs 2.1-12, 2.2-1, 2.2-8, 3.1-2, 3.3-4, 3.5-4, 4.5-3 and 4.5-5.

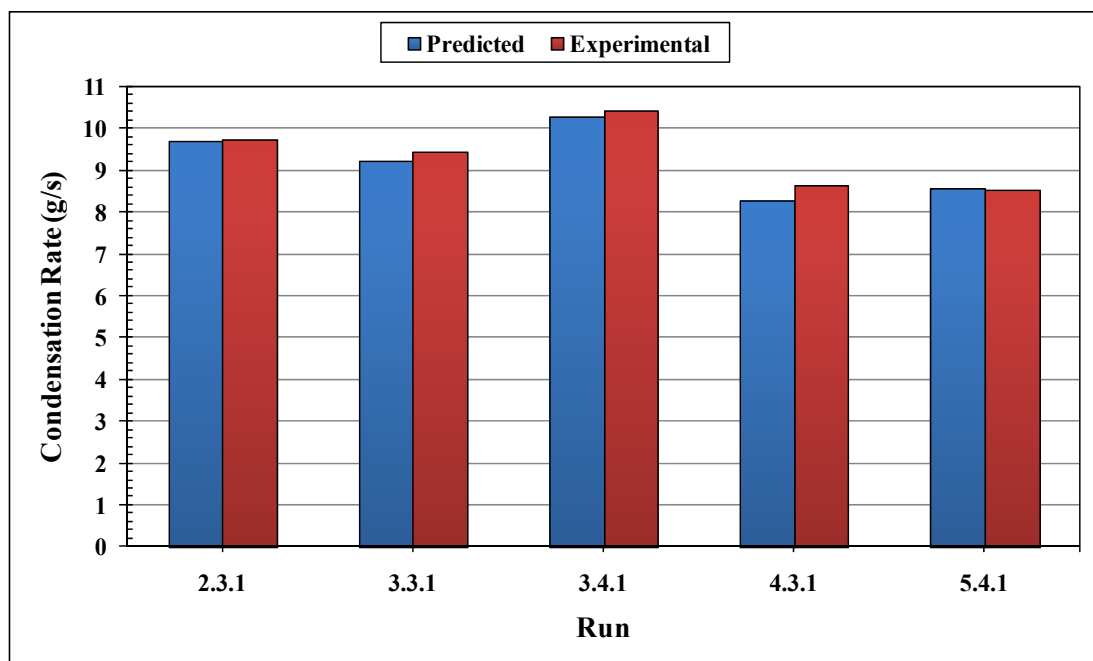


Figure 4.8: Comparison of the predicted condensation rates with the experimental results of Tanrikut and Yesin (1998), runs 2.3.1, 3.3.1, 3.4.1, 4.3.1 and 5.4.1.

Figures 4.6, 4.7 and 4.8 show that the errors between the predicted condensation rates and those from the experiments are random and no consistent trend can be detected. It is expected that a low mass fraction of water vapour in the air-vapour mixture would result in larger errors since the contribution from the sensible heat transfer to the overall heat transfer would be higher.

4.5.2.2. Temperature

Predicted axial variations of the temperatures for air-vapour mixture, inside and outside condenser walls, and cooling water temperatures are compared with the experimental data of Siddique (1992) and are shown in Figures 4.9, 4.10, 4.11 and 4.12. These Figures show that the predicted temperatures agree very well with the experimental data for all three runs. In the experimental results of Siddique, although both the inner and outer wall temperatures were measured, only results for inner wall temperature were presented in Siddique. Siddique measured the inner wall temperature by using thermocouples inserted in drilled holes, and the physical locations of the thermocouples were less than 0.2 mm from the inner surface of the condenser.

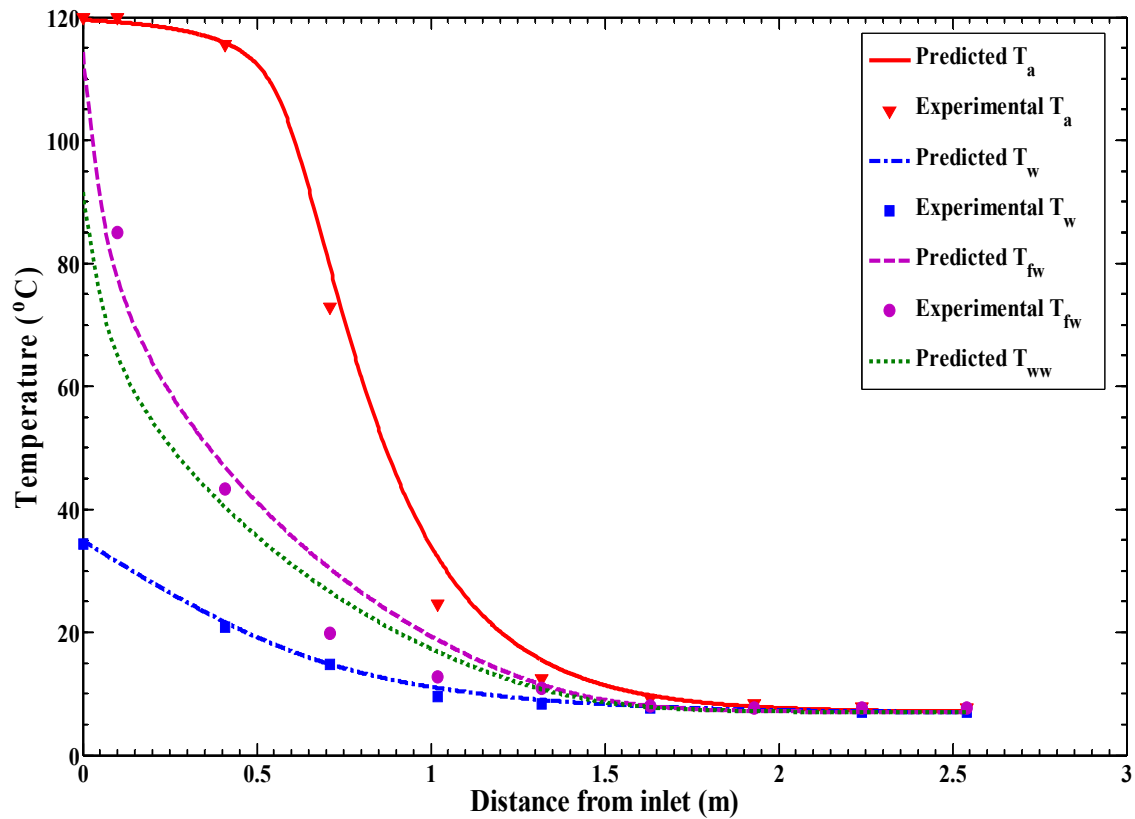


Figure 4.9: Comparison of the predicted temperatures of cooling water, wall and air-vapour mixture with the experimental results of Siddique (1992), run 7.

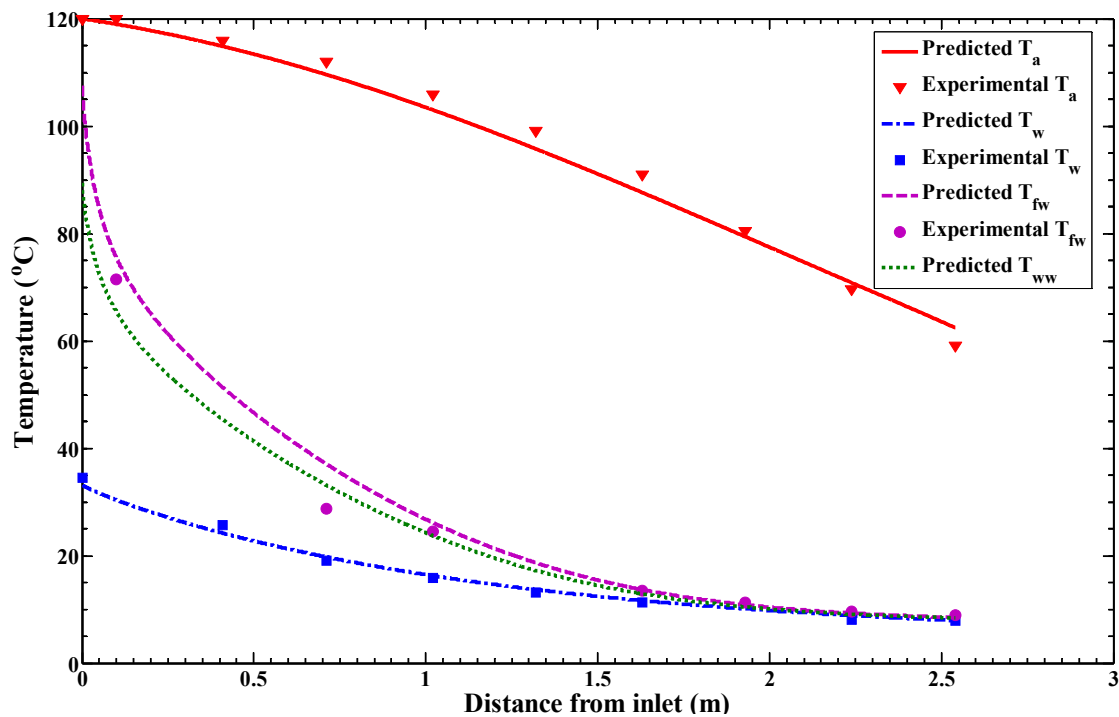


Figure 4.10: Comparison of the predicted temperatures of cooling water, wall and air-vapour mixture with those measured by Siddique (1992), run 11.

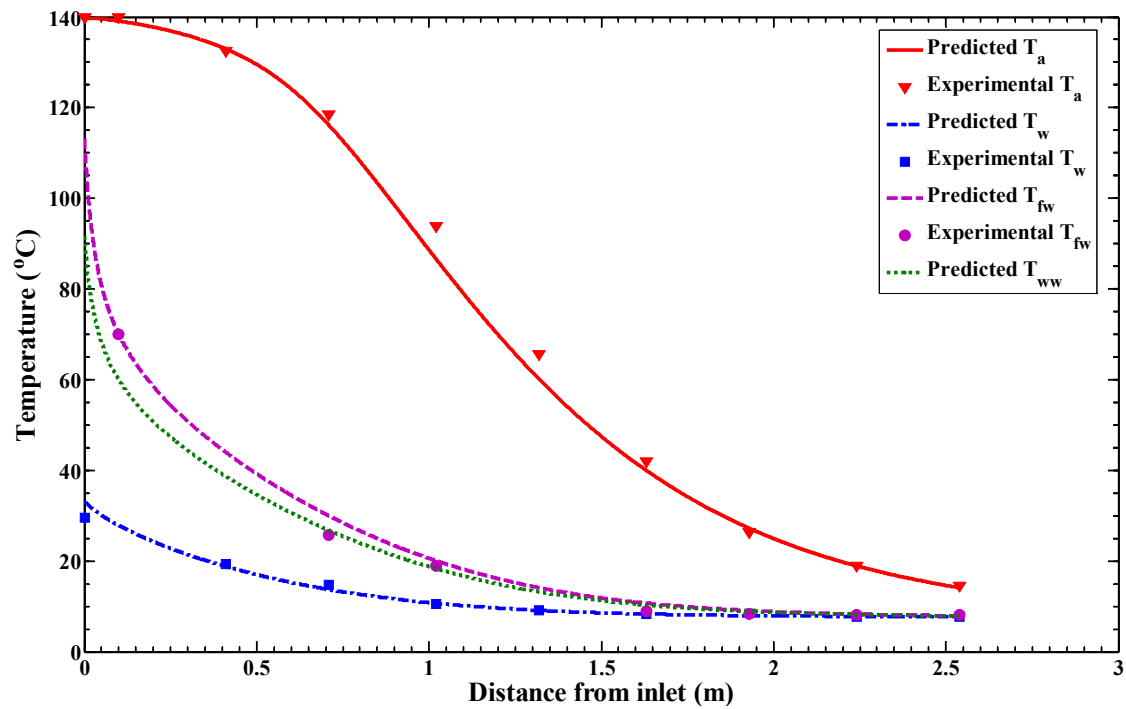


Figure 4.11: Comparison of the predicted temperatures of cooling water, water and air-vapour mixture with those measured by Siddique (1992), run 17.

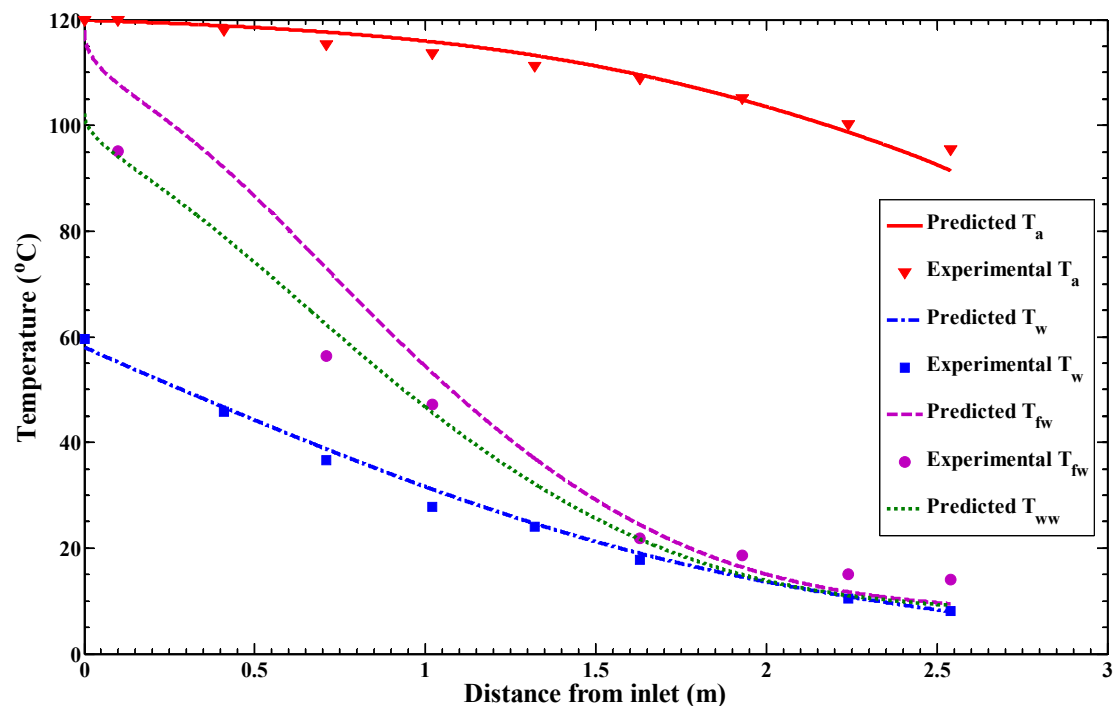


Figure 4.12: Comparison of the predicted temperatures of cooling water, water and air-vapour mixture with those measured by Siddique (1992), run 26.

Figures 4.9 to 4.12 show that the predicted centreline temperature of the air-vapour mixture and the coolant bulk temperature agree very well with the experimental data of Siddique (1992). The inner wall temperature measured by Siddique in general falls between the predicted T_{fw} and T_{ww} , as would be expected. This is remarkable given that the wall temperature falls sharply from the air-vapour mixture inlet to the coolant inlet.

Figures 4.9 to 4.12 show that the wall temperatures in the experiments of Siddique (1992) are far from constant and that they are very different from the temperatures of the coolant. This shows that, in modelling vapour condensation in the presence of non-condensable gas, the wall temperature cannot in general be assumed as constant. Due to this large difference between the wall temperature and the bulk temperature of the coolant, it is expected that buoyancy effects in the coolant channel are large and their effect on the convective heat transfer needs to be taken into account to achieve good agreement between the predictions and experimental results. The Reynolds, Rayleigh, and Grashof numbers are calculated and they are in general above 600, 3×10^6 , and 4×10^5 , respectively.

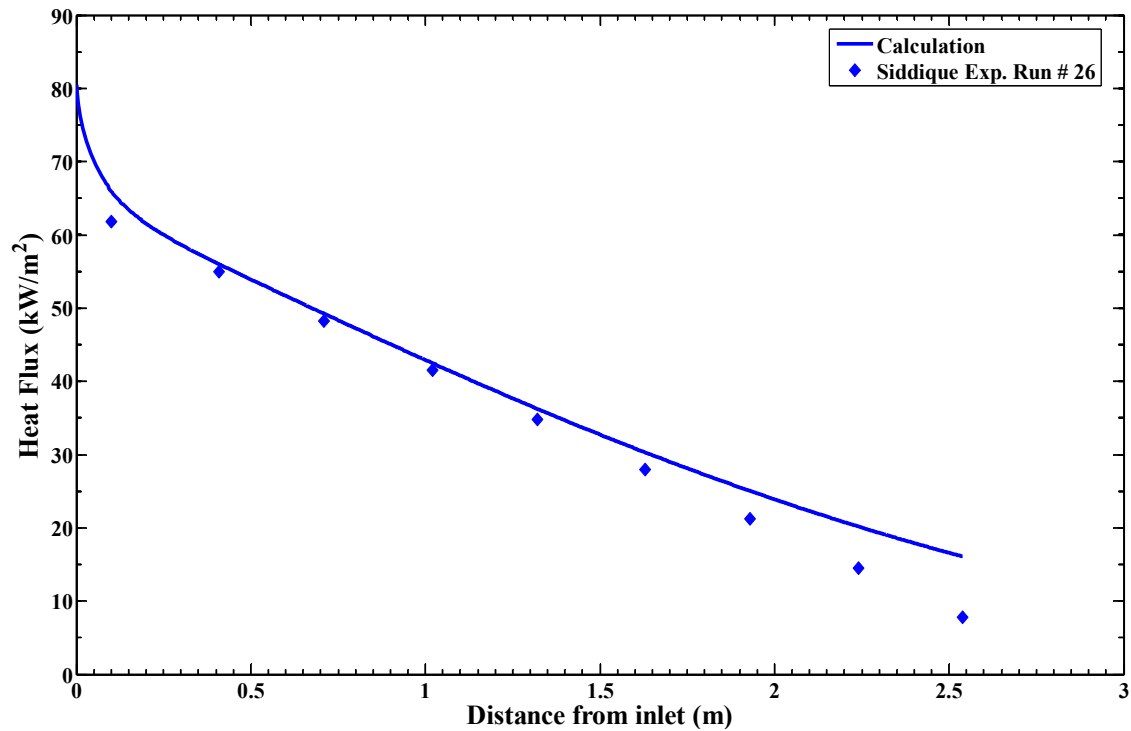


Figure 4.13: Comparison of the predicted heat flux with the experimental results of Siddique (1992), run 26.

Figure 4.13 shows the comparison between the heat flux estimated by the theoretical model and that from the experimental data of Siddique (1992) (run 26). The predicted heat flux was obtained using Equation 4.49. Instead of using differentiation of a curve fit from the predicted T_w , finite differences were used to approximate dT_w/dL using T_w obtained from the numerical solutions. Figure 4.13 shows that the agreement between the model predictions and the experimental data is very good, given the fact that the experimental data were obtained by the differentiation of a curve fit. This close agreement in the heat flux is a reflection of the remarkable agreement in the coolant bulk temperatures between the predictions and the experimental results. The predicted heat flux shows a sharp decrease at $x = 0$. This is because we have included the effect from the thermal entrance region in our model (see Equations 4.33 and 4.34). This sharp decrease in the heat flux near $x = 0$ is not shown in the experimental data. This

is because, to capture this sharp decrease in the heat flux experimentally, many more experimental points need to be measured near the inlet of the air-vapour mixture.

Figures 4.14 to 4.17 show the comparison of the predictions and the experimental results of Kuhn (1995) for the temperatures of cooling water, air-vapour mixture and the inner and outer walls. The condenser tube in the experiments of Kuhn (1995) was 2.418 m long, but the experimental results were presented only for distances up to 1.5 m from the inlet of the air-vapour mixture. It can be seen from these figures that the predicted temperatures of the cooling water agree very well with the experimental results, the predicted wall temperatures of the inner and outer surfaces agree with the experimental results reasonably well, and the predicted centreline temperatures for the air-vapour mixture are in general less than the experimental results. Overall, it can be seen from the figures that the model predictions and the experimental data are in good agreement.

Figures 4.14 to 4.17 again show that the difference between the wall temperature and the bulk temperature of the coolant is large for all the experimental data of Kuhn (1995). This large difference is due to the large thermal resistance to the heat transfer from the cooling channel. The Rayleigh numbers calculated using Equation 4.43 for the experimental data shown in Figures 4.13–4.16 are in general above 3×10^6 . This shows that the flow induced by the buoyancy effect in the cooling channel is fully turbulent (Kays et al. 2005) and greatly enhances or dominates the heat transfer in the coolant channel, as can be seen from Equation 4.44. Figures 4.14 to 4.17 also show the results without including the buoyancy effect in the cooling channel. The figures show that the differences in the predicted coolant bulk temperatures and the mixture

bulk temperatures with and without buoyancy effects are small. The differences in predicted wall temperatures can be more than 20% (relative to the coolant temperature), and the results that include the buoyancy effect agree with the experimental results much better than those that do not include the buoyancy effect.

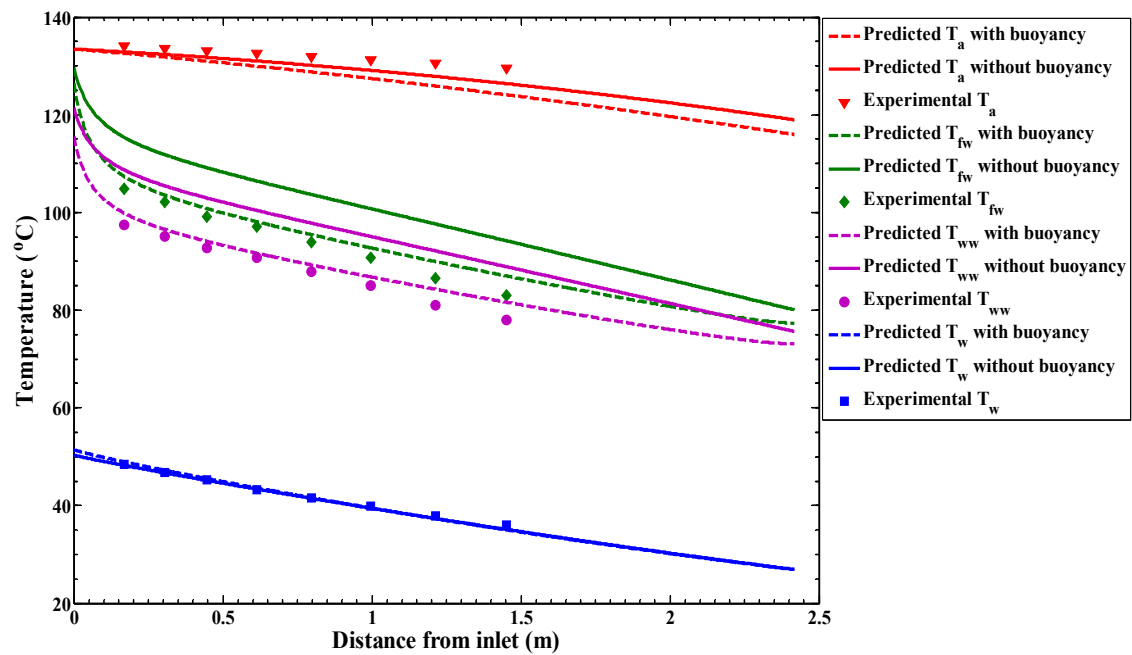


Figure 4.14: Comparison of the predicted temperatures of cooling water, air-vapour mixture, inner wall and outer wall with the experimental results of Kuhn (1995), run 2.1-12.

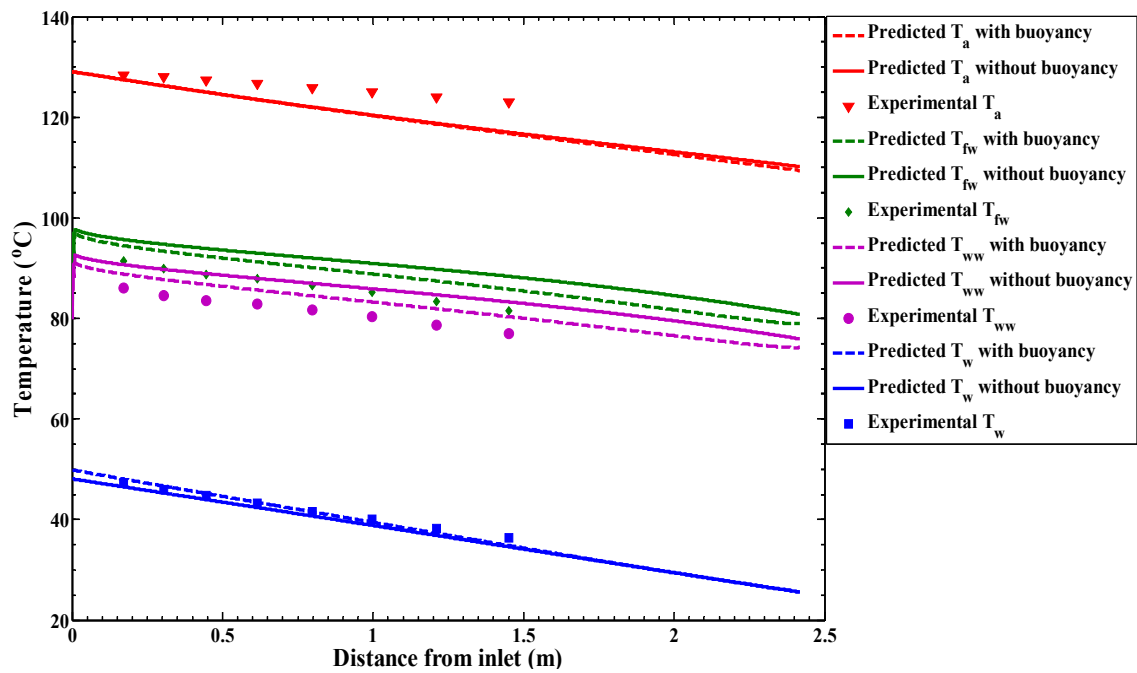


Figure 4.15: Comparison of the predicted temperatures of cooling water, air-vapour mixture, inner wall and outer wall with the experimental results of Kuhn (1995), run 2.2-8.

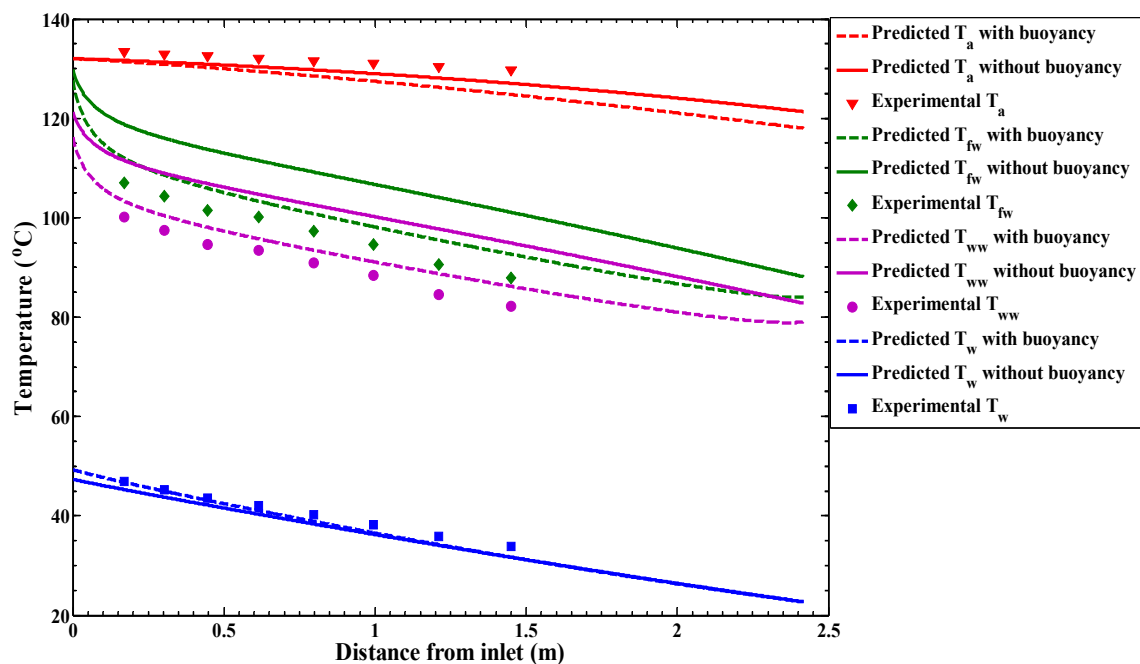


Figure 4.16: Comparison of the predicted temperatures of cooling water, air-vapour mixture, inner wall and outer wall with the experimental results of Kuhn (1995), run 3.5-4.

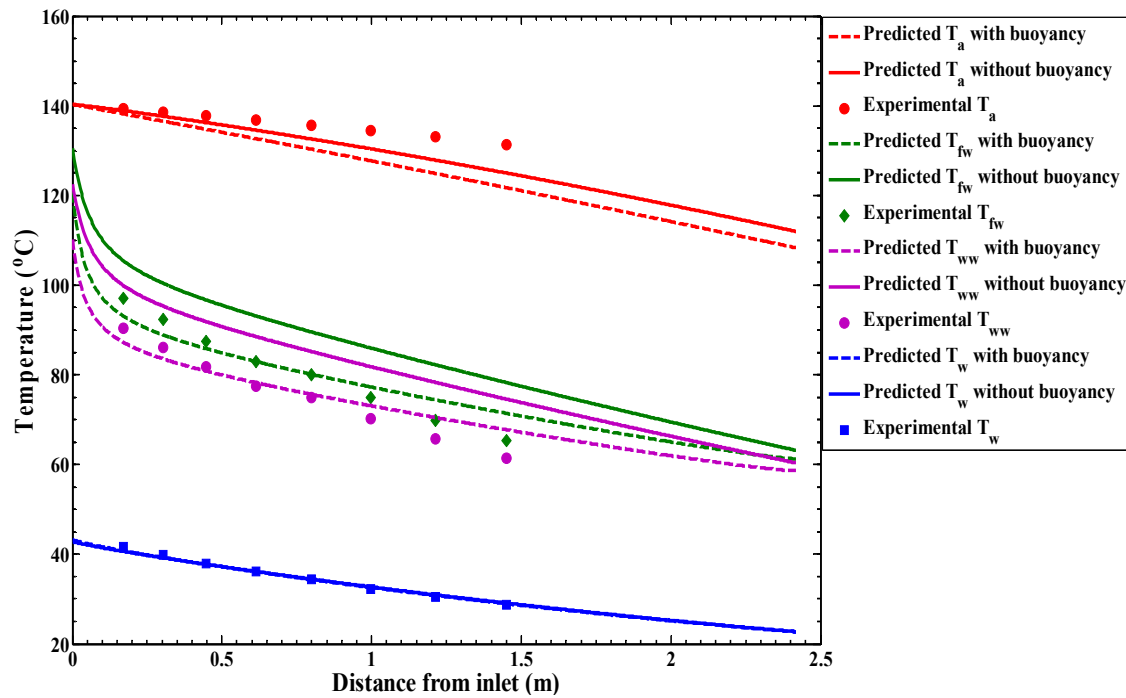


Figure 4.17: Comparison of the predicted temperatures of cooling water, mixture, inner wall and outer wall with the experimental results of Kuhn (1995), run 4.5-5.

Figure 4.18 shows the comparison of the predicted heat flux with the experimental results of Kuhn (1995) for the test 2.1-12. The figure shows that the predictions agree with the experimental data very well. Again, the very close agreement in the heat flux as shown in Figure 4.18 is a reflection of the remarkable agreement in the coolant bulk temperature between the predictions and the experimental results.

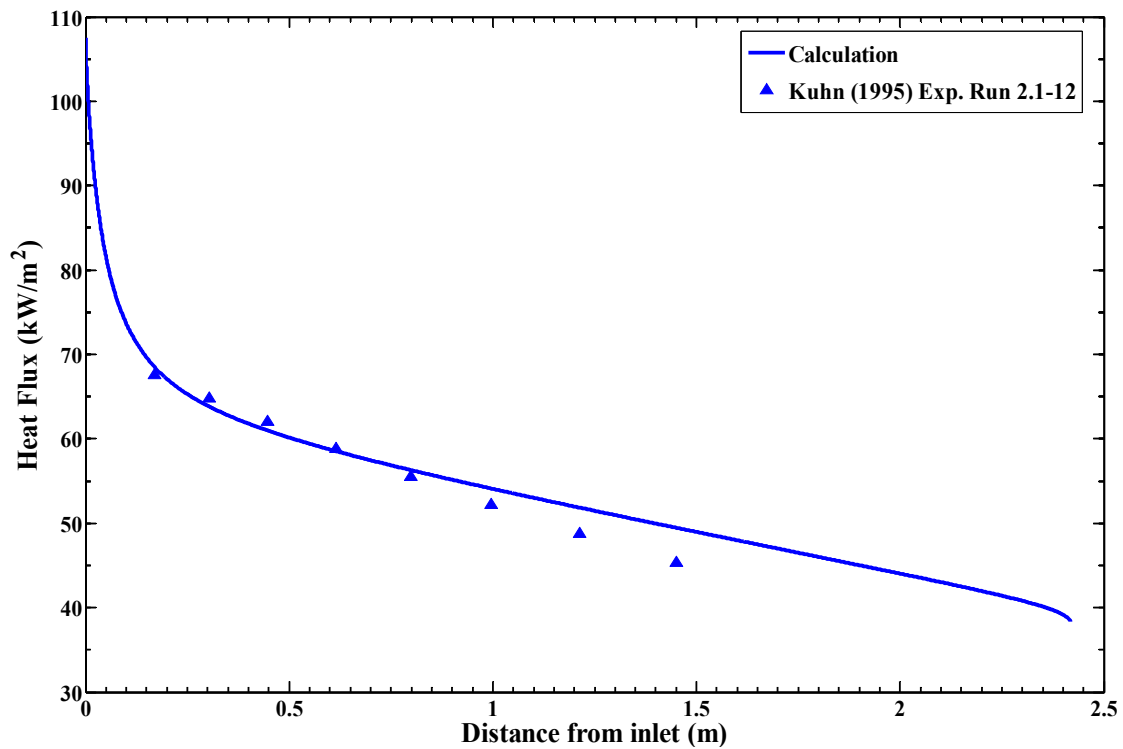


Figure 4.18: Comparison of predicted heat flux with the experiment results of Kuhn (1995), run 2.1-12.

Figures 4.19 to 4.22 show the comparison of the model predictions with the experimental results of Tanrikut and Yesin (1998) for the bulk temperatures of the air-vapour mixture, the temperatures of the inner and outer surfaces of the condenser wall and the bulk temperature of the cooling water. The figures show that the agreement between the predicted bulk coolant temperatures and that of the experiments are from good to reasonable, with the experimental results exhibiting a large degree of scatter.

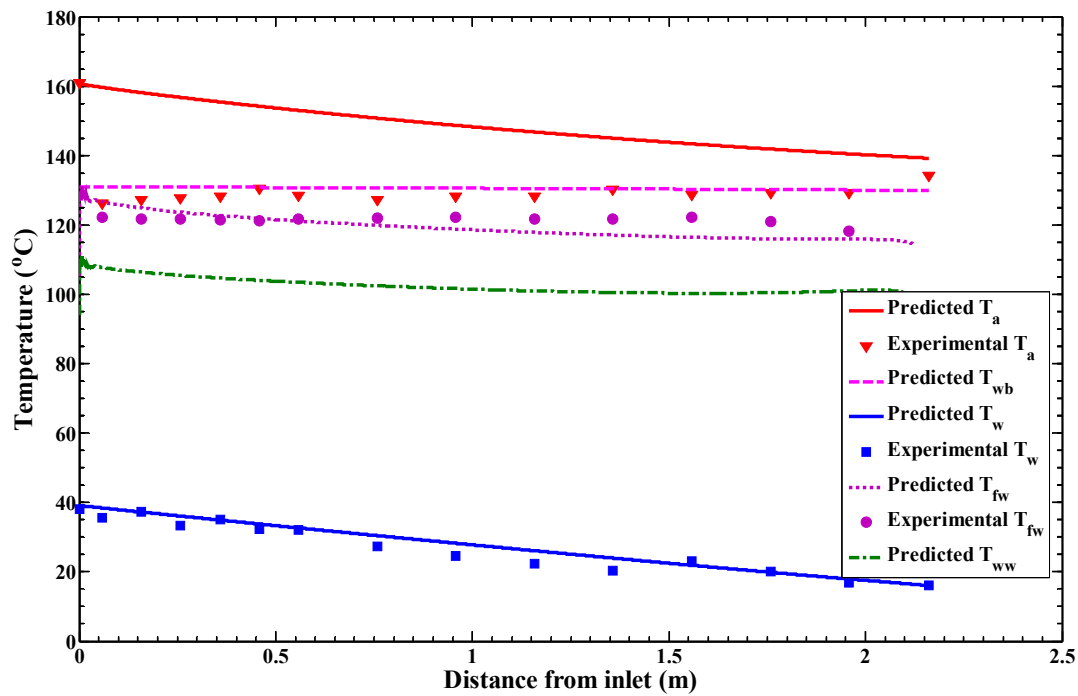


Figure 4.19: Comparison of the predicted temperatures of cooling water, wall and air-vapour mixture with the experimental results of Tanrikut and Yesin (1998), run 2.3.1.

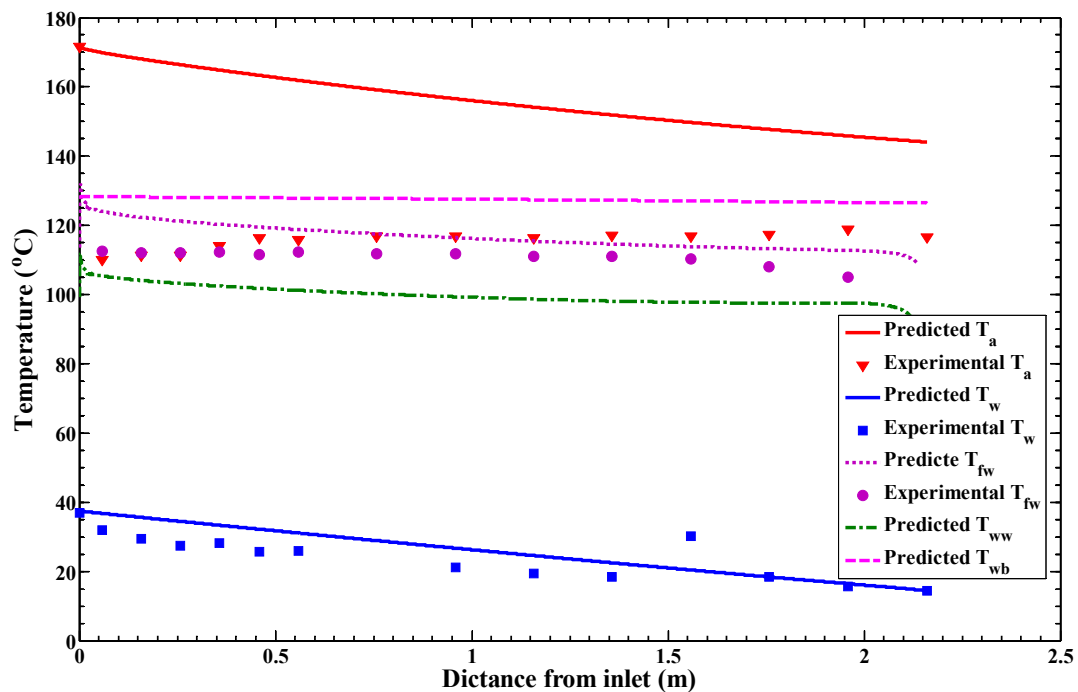


Figure 4.20: Comparison of the predicted temperatures of cooling water, wall and air vapour mixture with the experimental results of Tanrikut and Yesin (1998), run 3.3.1.

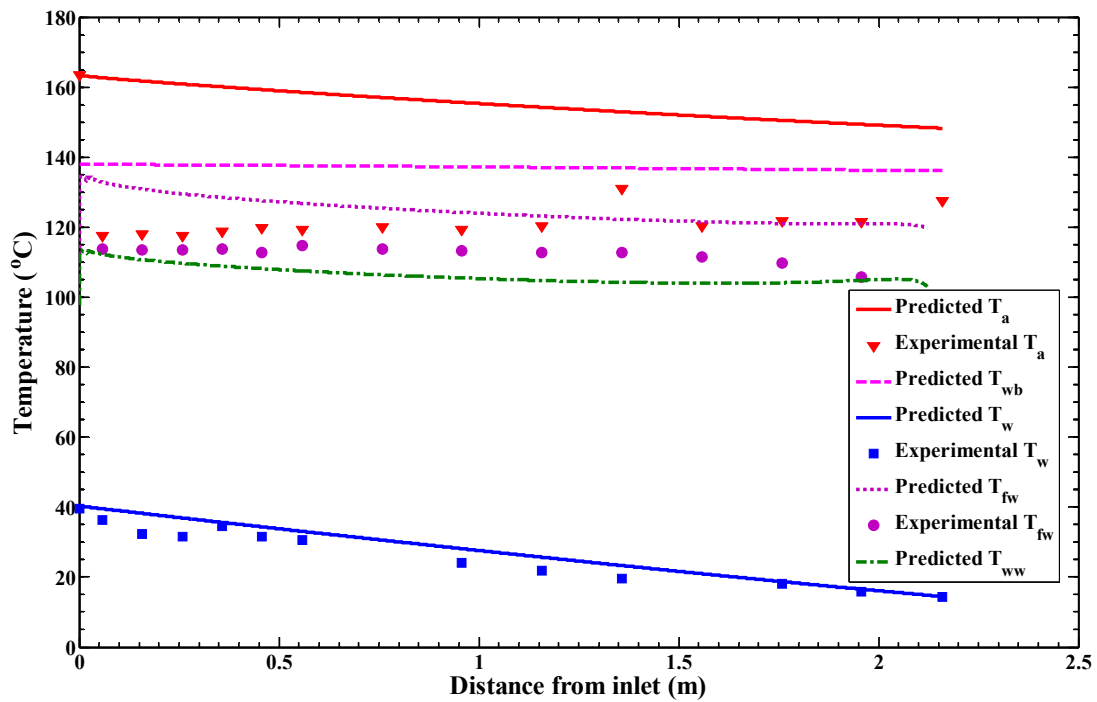


Figure 4.21: Comparison of the predicted temperatures of cooling water, wall and air-vapour mixture with the experimental results of Tanrikut and Yesin (1998), run 3.4.1.

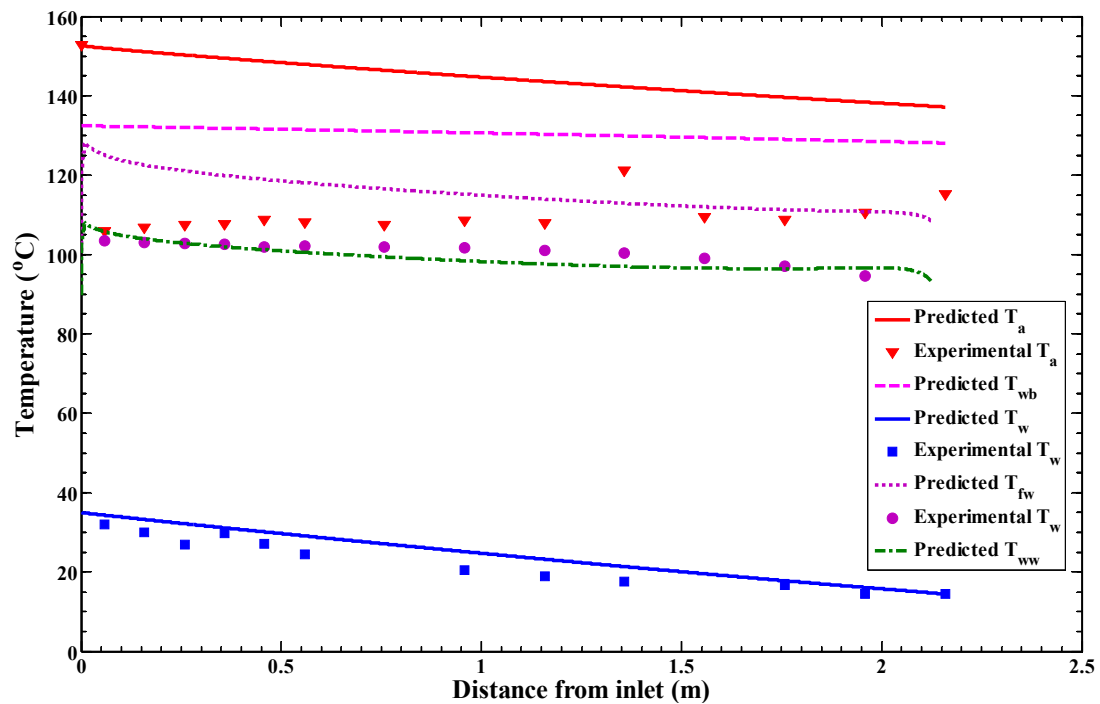


Figure 4.22: Comparison of the predicted temperatures of cooling water, wall and air-vapour mixture with the experimental results of Tanrikut and Yesin (1998), run 5.4.1.

Tanrikut and Yesin (1998) measured the inner wall temperatures using thermocouples embedded in the solid wall. The tips of the thermocouples were about 0.5 mm from the inner surface of the inside tube. Figures 4.19 to 4.22 show that, in general, the measured wall temperatures fall between T_{fw} and T_{ww} , as expected, except those shown in Figure 4.19, which are slightly above T_{fw} .

However, Figures 4.19 to 4.22 show that the agreement in the bulk temperature of the air-vapour mixture between the predictions and the experimental results of Tanrikut and Yesin (1998) is poor, with the experimental results being well below the predicted results. According to Tanrikut and Yesin (2005), their central temperatures along the condenser tube were predicted from the Gibbs-Dalton law by using calculated local air mass fraction from the energy balance because the measured central temperatures were lower than those that were predicted. They suggested that this could be attributed to the sub-cooling of the centreline, possibly due to the detachment of liquid droplets from the condensate film towards the centreline of the tube as reported in Tanrikut and Yesin (1998). Tanrikut and Yesin (1998) also found that the predicted central temperatures inside the condenser tube using the Gibbs-Dalton law were in general less than the estimated saturation temperatures.

By assuming that the tips of the thermocouples in the centreline of the condenser tube are covered by liquid water, it is possible that the measured centreline temperatures are closer to the wet bulb temperature than the dry bulb temperature. Following Bird et al. (2007), it can be shown that the following relationship exists between the wet bulb temperature and the dry bulb temperature:

$$\frac{T_{\infty} - T_{wb}}{\ln(1 + B_m)} = \left(\frac{Pr}{Sc}\right)^{1-n} \frac{h_g}{C_p} \quad (4.51)$$

where T_{∞} is the dry bulb temperature (T_a); T_{wb} is the wet bulb temperature, $n = 1/3$; h_g is the specific enthalpy carried by the water when it is evaporates at the wet bulb temperature; and:

$$B_m = \frac{Y_0 - Y_{\infty}}{1 - Y_0} \quad (4.52)$$

Here Y_0 is the mass fraction of the water vapour at the interface and Y_{∞} is the mass fraction of the water vapour at the far field. Equation 4.52 is similar to Equation 4.32. The values for Pr and Sc are taken as 0.74 and 0.58, as suggested by Bird et al. (2007). In Figures 4.19 to 4.22, the predicted wet bulb temperatures are shown. These figures show that, for run 2.3.1 of Tanrikut and Yesin (1998), the predicted wet bulb temperatures using Equation 4.51 agree reasonably well with the estimated centreline temperatures from the experiments.

4.6. Discussion and Conclusions

A mathematical model was developed to study the condensation of water vapour in the presence of non-condensable gas in plate heat exchanger and tube condensers, in which the vapour mixture flows downward and the cold water flows upward. The model includes the heat and mass transfer in the mixture channel, the heat transfer in the condensate film, condenser wall and the coolant channel. Previous models mainly

include the mixture channel and the condensate film. The model developed is general and can be used to predict the heat and mass transfers for both co-current and counter-flow condensers. A numerical scheme is presented to solve the differential and algebraic equations. In this work, only results for the vapour mixture flowing downward and the cold water flowing upward are compared with the experimental data because most of the experimental data available in the literature are for counter-flow condensers.

The predictions from the model are compared with the experimental results of Ambrosini et al. (2008) for condensation in plate heat exchanger. Agreement between the model predictions and the experimental data is good for condensation rate, heat flux and water outlet temperature. Further, the predictions from the model are compared with the experimental results of Siddique (1992), Kuhn (1995) and Tanrikut and Yesin (1998), all of who conducted their experiments in cylindrical condensers. It was found that the predicted condensation rates and the bulk temperatures of the coolant agree very well with the experimental results obtained by all three groups of researchers. The predicted wall temperatures of the condenser agree reasonably well with the experimental results, and the predicted bulk temperatures of the air-vapour mixture agree very well with the experimental results of Siddique (1992), reasonably well with the experimental results of Kuhn (1995) and poorly with the experimental results of Tanrikut and Yesin (1998).

Tanrikut and Yesin (1998) presented the estimated centreline temperature for the air-vapour mixture because they found that their measured temperature was not only below that estimated from Gibbs-Dalton law but also below the saturation

temperature. By assuming that the thermocouples were covered by liquid water in the experiments of Tanrikut and Yesin (1998), it is possible that the temperatures measured by Tanrikut and Yesin (1998) are close to the wet bulb temperature. A relationship between the dry bulb temperature and the wet bulb temperature (see Equation 4.51) was derived and used to estimate the wet bulb temperature using the predicted bulk temperature of the air-vapour mixture and the mass fraction of the water vapour. It was found that for only one set of the experimental results (run 2.3.1) did the predicted wet bulb temperature agree reasonably well with the estimated centreline temperature of Tanrikut and Yesin (1998).

The model predictions and all the experimental results presented here show that the wall temperature of the condenser can be much higher than the bulk temperature of the coolant. This shows that it is very difficult to select a constant wall temperature (or constant heat flux) in modelling condensation from heat and mass transfer in the mixture channel alone, and the condenser (including the gas-vapour mixture channel, the condenser wall and the coolant channel) needs to be modelled as a whole system. Further, because of the large temperature difference between the condenser wall and the coolant, it was found that the buoyancy effect on heat transfer in the coolant channel is in general large and cannot be neglected. This buoyancy effect on enhancing the heat transfer in the coolant channel was included in the present model, and found to be an important phenomenon in governing the performance of condensers.

Chapter 5: CFD Simulation of Condensing Heat Exchanger

In this chapter, the numerical simulations of the condensation heat exchanger, using the CFD software FLUENT[®], are carried out. A comparison of the simulation results with existing experimental data to validate the model is presented.

5.1. Governing Equations and Turbulence Modelling

The governing equations of mass, momentum and energy are given in Chapter 3. The turbulence and species equations are as follows.

5.1.1. Turbulence Equations

The governing equations for the turbulent kinetic energy k and the dissipation rate ε in the renormalisation-group (RNG) $k - \varepsilon$ model are:

$$\frac{\partial}{\partial t}(\rho k) + \frac{\partial}{\partial x_i}(\rho k u_i) = \frac{\partial}{\partial x_j} \left(\alpha_k \mu_{eff} \frac{\partial k}{\partial x_j} \right) + G_k + G_b - \rho \varepsilon + S_k \quad (5.1)$$

$$\begin{aligned} \frac{\partial}{\partial t}(\rho \varepsilon) + \frac{\partial}{\partial x_i}(\rho \varepsilon u_i) = & \frac{\partial}{\partial x_j} \left(\alpha_\varepsilon \mu_{eff} \frac{\partial \varepsilon}{\partial x_j} \right) + C_{1\varepsilon} \frac{\varepsilon}{k} (G_k + C_{3\varepsilon} G_b) \\ & - C_{2\varepsilon} \rho \frac{\varepsilon^2}{k} + S_\varepsilon \end{aligned} \quad (5.2)$$

In these equations, μ_{eff} is the effective viscosity and G_k represents the generation of turbulent kinetic energy due to the mean velocity gradients. G_b is the generation of turbulence kinetic energy due to buoyancy. $C_{1\varepsilon}$, $C_{2\varepsilon}$, and $C_{3\varepsilon}$ are constants. The quantities α_k and α_ε are the inverse effective Prandtl numbers for k and ε , respectively. S_k and S_ε are user-defined source terms.

5.1.2. Species Transport Equations

The conservation of species i can be given as:

$$\frac{\partial}{\partial t}(\rho Y_i) + \nabla \cdot (\rho \bar{v} Y_i) = -\nabla \cdot \bar{J}_i + R_i + S_i \quad (5.3)$$

where Y_i is the mass fraction of the species i , R_i is the net rate of production of species i , S_i is the source term for component i , and \bar{J}_i is the diffusion flux of species i in turbulent flow and can be calculated as:

$$\bar{J}_i = -\left(\rho D_{i,m} + \frac{\mu_t}{Sc_t} \right) \nabla Y_i - D_{T,i} \frac{\nabla T}{T} \quad (5.4)$$

where $D_{i,m}$ is the mass diffusion coefficient for species i in the mixture, μ_t is the turbulent viscosity, Sc_t is the turbulent Schmidt number and $D_{T,i}$ is the thermal diffusion coefficient.

5.2. Simulation of Condensation

5.2.1. The Experiments of Ambrosini et al. (2008) and the Benchmark Tests

In this study, the experimental data obtained by Ambrosini et al. (2008) are used to validate the predictions from simulations using the CFD package FLUENT[®]. The experiments were conducted in the CONAN facility at the Università di Pisa, Italy.

As shown in Figure 5.1, the experimental facility includes a primary loop circulating an air-steam mixture in a 0.34 m × 0.34 m plane channel that has a length of 2 m and a secondary loop in which cooling water flows in a 0.005 m × 0.35 m plane channel that is also 2 m long. A tertiary loop injects cold water from a large reservoir into a mixing vessel that maintains the cooling water in the secondary loop at a constant temperature. The air-steam mixture and the cooling water are separated by an aluminium plate of 45 mm thickness (thermal conductivity 117 W/mK).

Table 5.1 shows the experimental conditions of the five tests carried out by Ambrosini et al. (2008). These data relate to the following operating conditions: the nominal temperature of the cooling water was approximately 30°C, the steam generator had a power of 10 kW and mixture velocities were between 1.5 and 3.5 m/s.

The benchmark exercises had an active part in the Severe Accident Research network (SARnet) in Europe. The exercises were proposed to compare different CFD models in predicting heat and mass transfer during condensation.

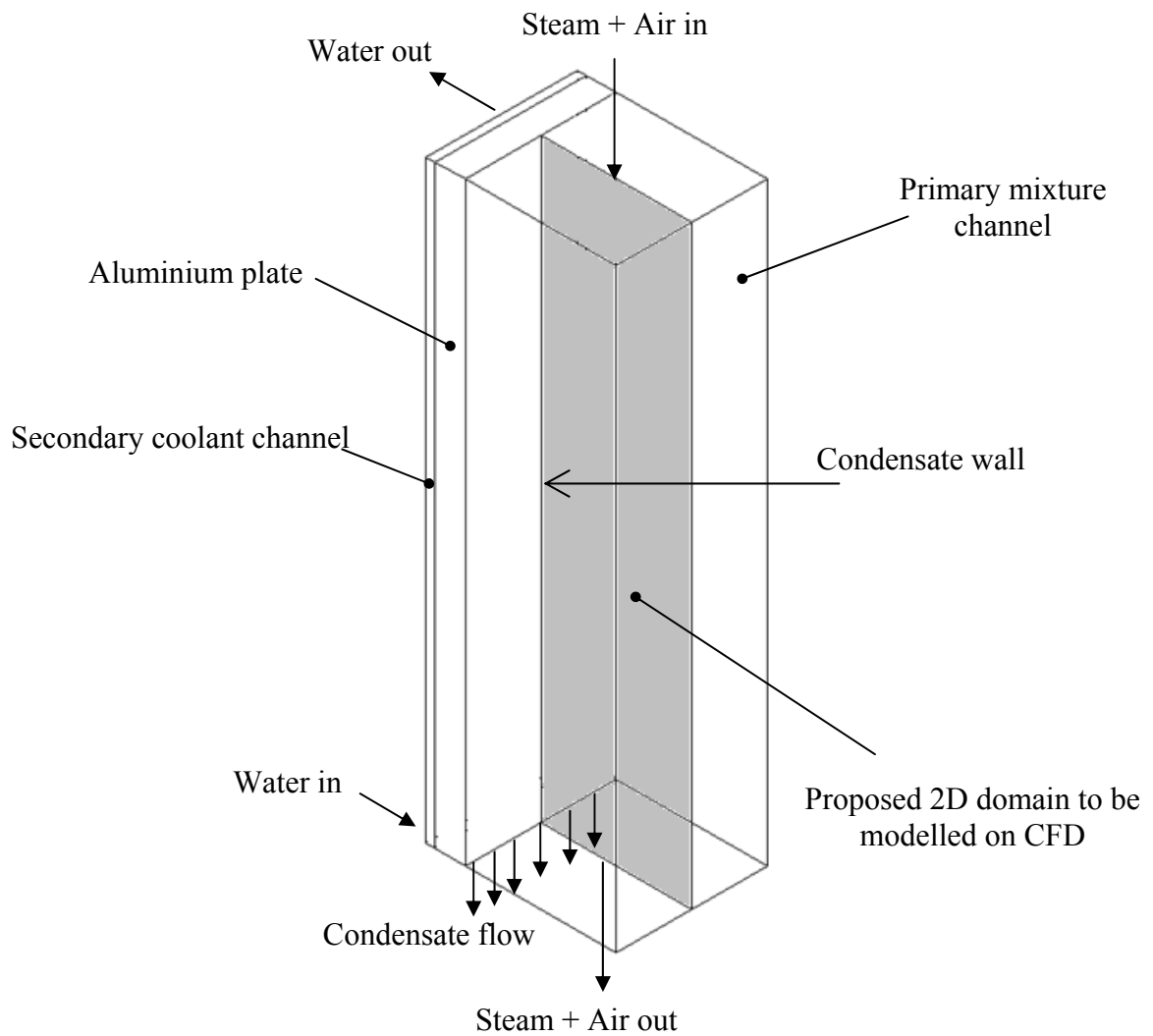


Figure 5.1: Experimental test section (Ambrosini et al. 2008).

Table 5.1. Experimental conditions of tests 1–5 conducted by Ambrosini et al. (2008).

Test	$T_{w,in}$ [°C]	\dot{m}_w [kg / s]	$T_{a,in}$	V_{mixt} [m / s]	ϕ	HTC [W / m ² K]
1	31.24	1.22	82.66	1.46	100	1581.65
2	31.10	1.22	80.61	2.02	100	1581.11
3	31.07	1.22	79.13	2.52	97.83	1580.95
4	30.90	1.22	78.73	3.01	87.35	1579.70
5	30.71	1.22	75.02	3.59	96.55	1578.80

In the Benchmark tests (Ambrosini et al. 2008), a 2D domain representing the centre plane of the mixture channel was suggested. The Benchmark tests were conducted in two steps: 1) adopting a conjugated heat transfer approach, including heat conduction in the heated plate and the energy transport in the air-steam channel; and 2) imposing an equivalent heat transfer conductance between the cooled surface and the secondary fluid, obtained as the reciprocal of the series of the heat transfer resistances of the plate and of the secondary fluid. Ambrosini et al. (2008) found that (to varying extents) most of the CFD models adopted were in reasonable agreement with the results obtained based on well-known correlations. Further, most codes provided a reasonable prediction of the expected behaviour, and there was a general tendency to underestimate entrance effects. The reason for this is still under consideration but it could result from the 3D nature of the flow and boundary conditions. Ambrosini et al. recommend further efforts be made to develop accurate but economical techniques for predicting near-wall behaviour without losing important quantitative information.

5.2.1.1. Step 0

In step 0, the heat and mass transfer from flows in the air-steam mixture channel were simulated using CFD. The coolant and the aluminium plate were replaced by a constant wall temperature. A 2D model similar to that formulated by Ambrosini et al. (2008) was created using ANSYS Workbench 12.0 to simulate condensation on an isothermal flat plate. The system is 2 m long and 0.34 m wide. Figure 5.2 shows the computational domain and the grid.

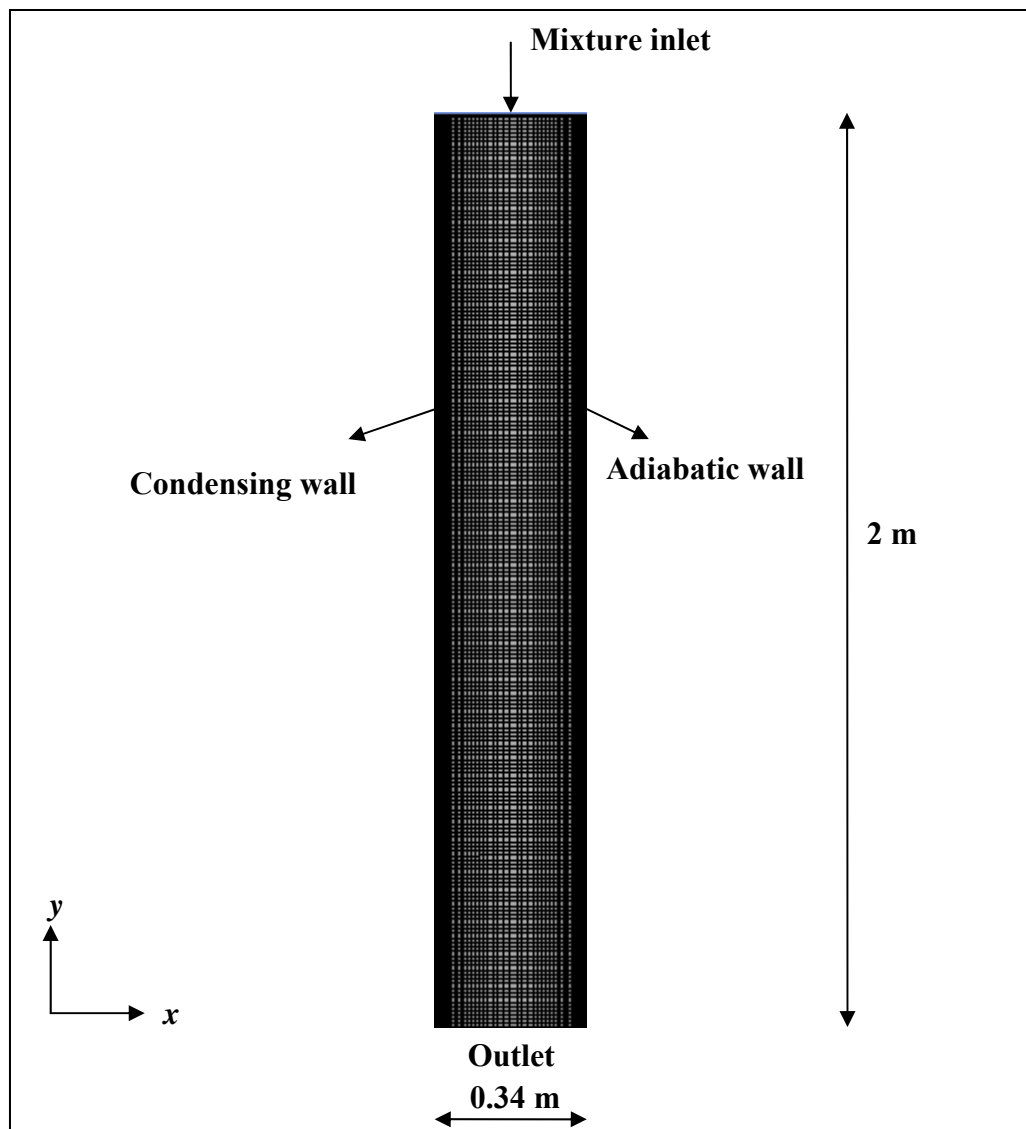


Figure 5.2: Computational domain and grid for steps 0 and 1.

A grid independent solution had to be insured first. For this reason, the mesh was checked at two different locations $y=1$ m, $x=0.001$ m and $y=1$ m, $x=0.0005$ m. The temperature at these locations is presented against the grid numbers, as shown in Figure 5.3. From Figure 5.3, we can see that the variation of temperature against grid resolution is constant, so the solution is grid independent. A structured rectangular grid of 10,100 elements was used to discretise the governing equations. To resolve the solution fields near the surface of the plate accurately, the mesh was refined at the surface.

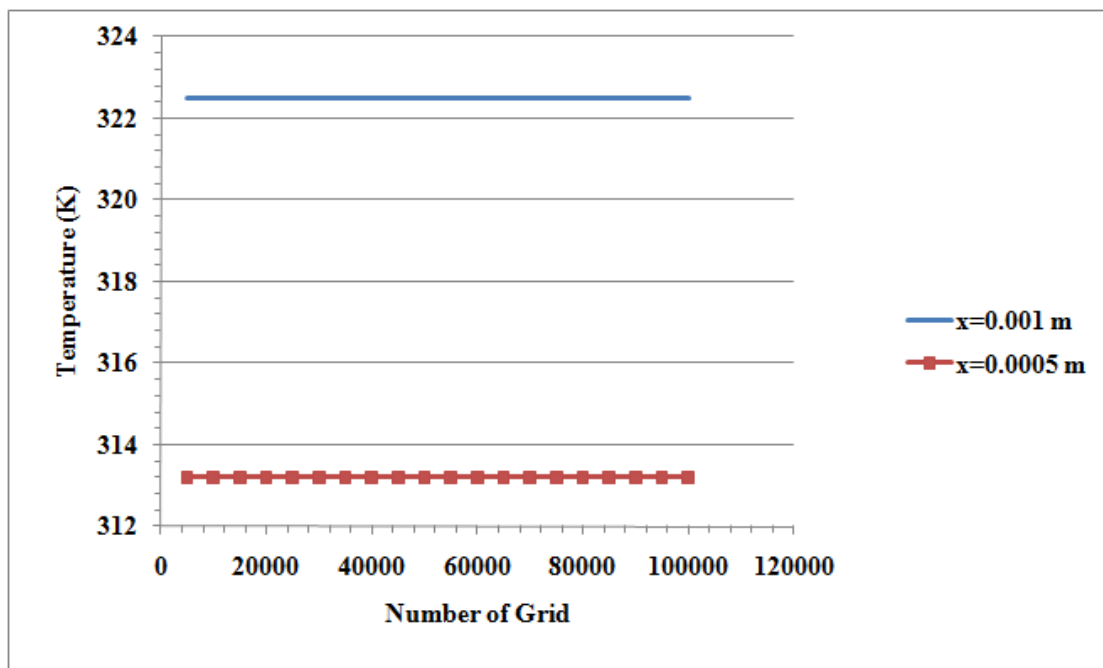


Figure 5.3: Grid independence test.

The same discretisation was used for both steps 0 and 1 in the present work. In step 0, the adequacy of the turbulence models adopted and the numerical grids were assessed by comparing predicted heat and mass transfer rates with those obtained from existing correlations, namely:

$$Nu_x = 0.0296Re_x^{0.8} Pr^{0.33} \quad (5.5)$$

$$Sh_x = 0.0296Re_x^{0.8} Sc^{0.33} \quad (5.6)$$

Here:

$$Re = \frac{\rho Vx}{\mu}, Sc = \frac{\mu}{\rho D}, Pr = \frac{C_p \mu}{k}$$

where x is the distance from the entrance of the air-steam mixture, μ is the dynamic viscosity of the mixture and C_p is the specific heat of the mixture. In performing the CFD simulations in step 0, the air and water vapour were introduced at the mixture inlet, as shown in Figure 5.2. This was achieved in FLUENT[®] by invoking the conservation of species. The physical properties of each component in the mixture were allowed to vary with temperature and the air-steam mixture was assumed to behave as an ideal gas. At the mixture inlet, the velocity, temperature and relative humidity of the mixture were set to those values given in Table 5.1. The pressure was assumed to be the ambient atmospheric pressure and the constant wall temperature was assumed as the average of the water inlet and outlet temperature, as suggested by Ambrosini et al. (2008). Other boundary conditions include a pressure outlet for the air-steam mixture at the outlet, and the wall facing the condensing wall was adiabatic (see Figure 5.2).

In this work, we assumed that water vapour condenses only at the surface of the aluminium plate and the mass condensation rate \dot{m}_{cond} is controlled by the diffusion of water vapour from the bulk stream to the condensing surface according to:

$$\dot{m}_{cond} = \rho D \frac{1}{1 - Y_v} \frac{\partial Y_v}{\partial x} \quad (5.7)$$

The diffusion coefficient of water vapour in air was calculated according to Li et al. (2010):

$$D = (2.775 \times 10^{-6} + 4.479 \times 10^{-8} T + 1.656 \times 10^{-10} T^2) P / 100 \quad (5.8)$$

The mass fraction of water vapour was calculated by:

$$Y_v = \frac{\omega}{1 + \omega} \quad (5.9)$$

where ω is the specific humidity of air-vapour mixture and can be calculated from the expression:

$$\omega = \frac{0.622 P_v}{P - P_v} \quad (5.10)$$

where P_v is the saturation vapour pressure of water as a function of temperature and can be determined by Li et al. (2010):

$$P_v = 1000 \times \exp(-0.4702 + 0.06991T - 2.249 \times 10^{-4} T^2 + 3.563 \times 10^{-7} T^3) \quad (5.11)$$

In this study, the heat flux from the gas mixture to the condensate film expressed as:

$$q'' = Q_l + Q_s = \dot{m}_{cond} h_{fg} + k \frac{dT}{dx} \quad (5.12)$$

where h_{fg} is the latent heat of condensation and is expressed as:

$$h_{fg} = 1000 \times (3601 - 6.865T + 0.01491T^2 - 1.652 \times 10^{-5}T^3) \quad (5.13)$$

The above relationships were used in the CFD simulation and these were implemented using UDFs in FLUENT[®].

Figure 5.5 shows the predicted Nusselt number from the CFD simulations in step 0 and the results are compared with the correlations given by Equation 5.5 and the CFD results from UJV (Nuclear Research Institute) (Ambrosini et al. 2008), who was one of the participants that simulated step 0 by using a realisable $k - \varepsilon$ model with enhanced wall treatment. Results shown in Figures 5.4 and 5.5 for pure heat transfer and heat and mass transfer cases were obtained under the following conditions:

- Inlet temperature 363.15 K
- Wall temperature 303.15K
- Inlet velocities: 3 and 6 m/s
- 2D problem
- Rectangular computational grid

The values of the inlet velocity were selected to allow for the analysis of the computed data at sufficiently large Reynolds numbers, to ensure that the forced convection correlations were applicable in at least the last part of the channel. The RNG $k - \varepsilon$ model with an enhanced wall treatment was used as one of the simplest options for turbulence available in FLUENT[®].

It can be seen from Figure 5.4 that the agreement between the CFD predictions and the correlation (see Equation 5.5) is good at high Reynolds numbers. The present CFD simulations agree almost perfectly with those obtained by UJV. At low Reynolds numbers, the CFD results are higher than those given in Equation 5.5. This could be because the correlation (see Equation 5.5) is for fully developed flows, while the CFD results simulate the flow development of the air-steam mixture at the entrance region. Figure 5.5 shows the predicted Sherwood number from the CFD simulations in step 0 and the results are compared with the correlations given in Equation 5.6 and those from UJV. Again, agreement between the predictions and the correlation (see Equation 5.6) is reasonable at high Reynolds numbers, but poor at low Reynolds numbers. The present CFD results agree with those of UJV and a negligibly small difference exists at low Reynolds numbers. However, Figure 5.5 shows that the discrepancy between the present CFD results and the correlation (see Equation 5.5) is larger than the results for the Nusselt number shown in Figure 5.4. The results shown in Figures 5.4 and 5.5 are consistent with those given in Ambrosini et al. (2008). This reveals that the turbulence models and the grid resolutions used in predicting the heat and mass transfer in step 0 are adequate.

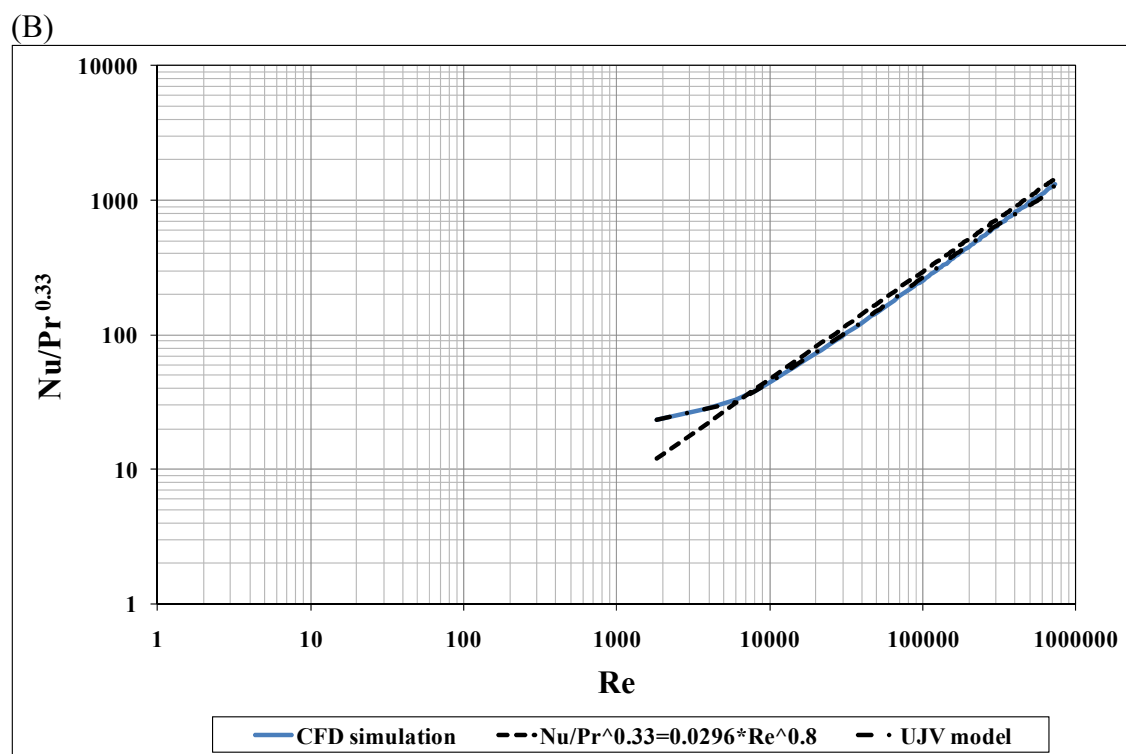
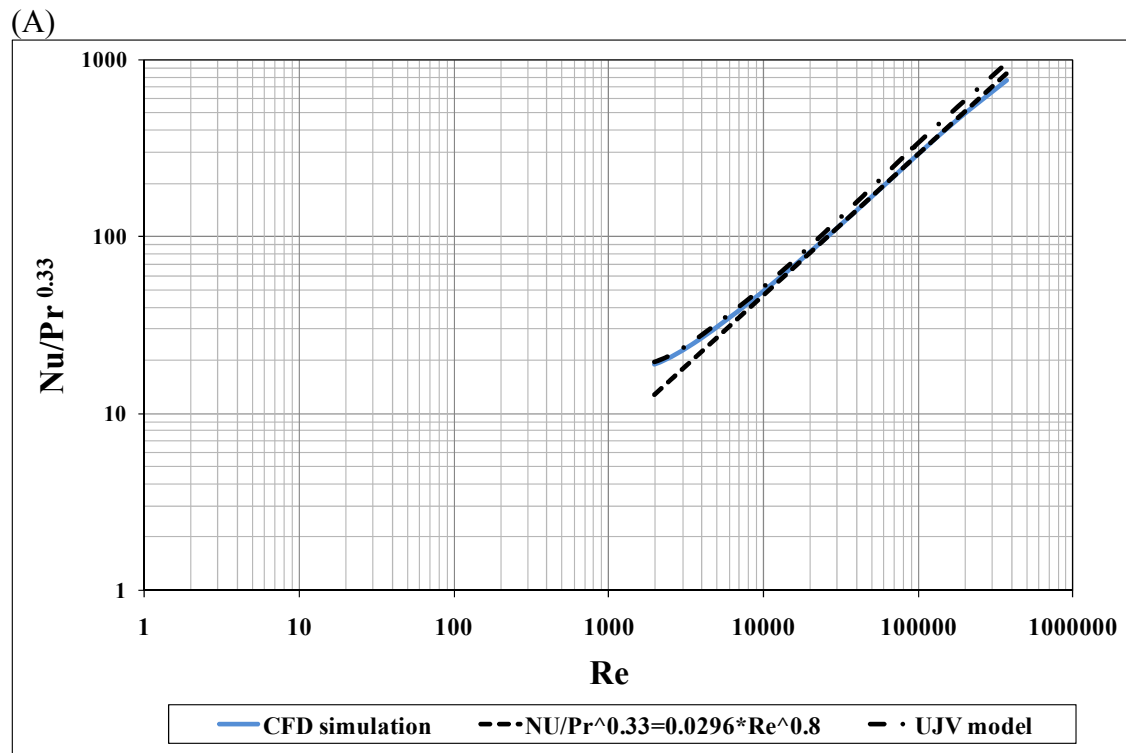


Figure 5.4: Results obtained for two heat transfer cases in step 0: (A) T30-V3, (B) T30-V6.

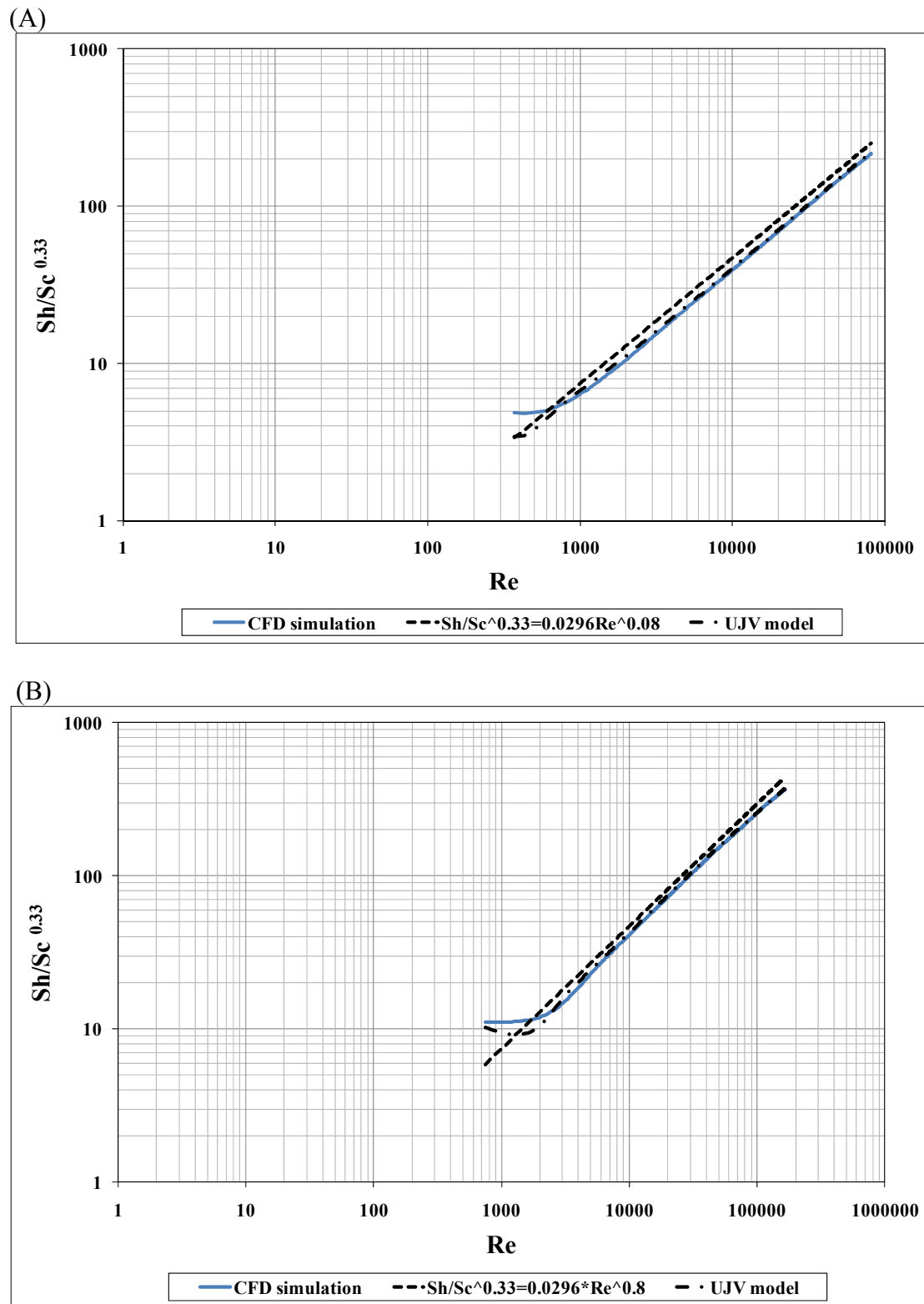


Figure 5.5: Results obtained for two heat and mass transfer cases in step 0: (a)

T30-V3, (b) T30-V6.

5.2.1.2. Step 1

In this step, the same geometry and grid were used as in step 0 except that, at the condensing wall, the constant temperature boundary condition was replaced by a constant HTC. The HTC values used in the simulations are those given in Ambrosini et al. (2008) (see Table 5.1).

In this simulation, the effect of the condensate film on the heat and mass transfer was neglected; that is, we assumed that the thickness of the condensate film was zero. In reality, this film thickness increases with the distance from the mixture entrance and it is in general very small. It is expected that the error introduced by this assumption is small. To include the effects of the condensate film requires that a multi-phase and multi-species model be formulated and this will be investigated in the future.

In specifying a HTC at the condensing wall, the heat flux is calculated by:

$$q'' = H (T_w - T_c) \quad (5.14)$$

where H is the overall HTC including the aluminium plate and the HTC on the wall exposed to the coolant. T_w is the temperature of the condensing wall in contact with the air-steam mixture and T_c is the temperature of the coolant. Equations 5.12 and 5.14 allow the temperature of the wall adjacent to the air-steam mixture to be determined and the heat flux from the mixture to the wall to be balanced with the heat flux from the aluminium plate to the coolant. As in step 0, the heat flux was calculated using Equation 5.12.

Figures 5.6 and 5.7 show the comparisons between the CFD predictions and the experimental data of Ambrosini et al. (2008) of the heat flux at the condensing surface and the condensation rate under various experimental conditions.

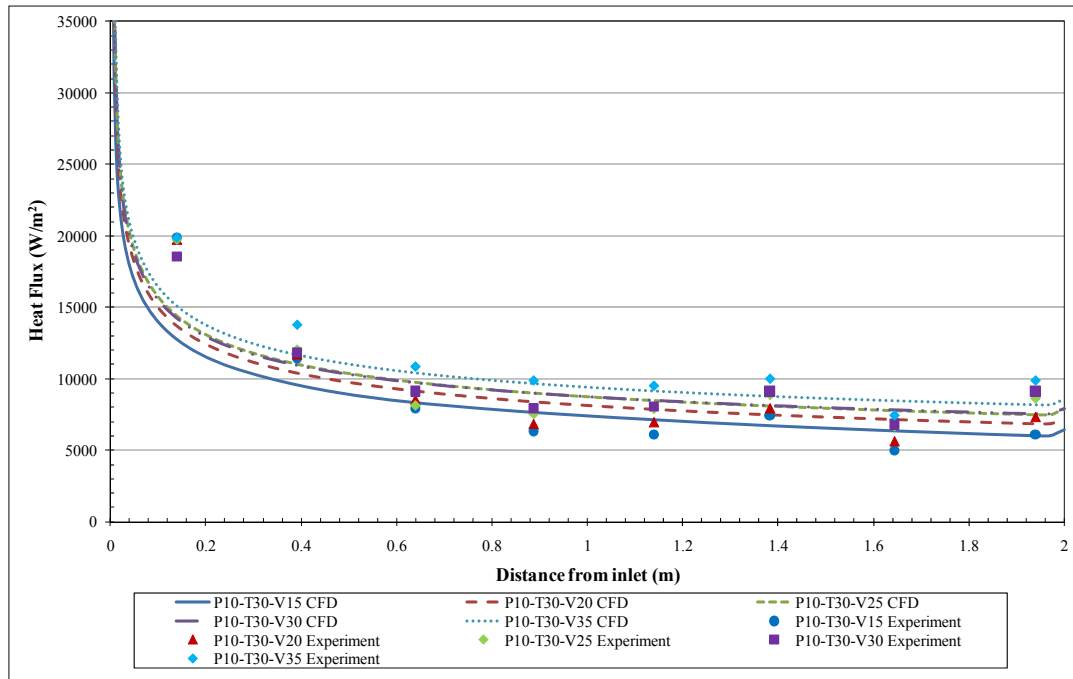


Figure 5.6: Comparison of calculated and experimental values of heat flux.

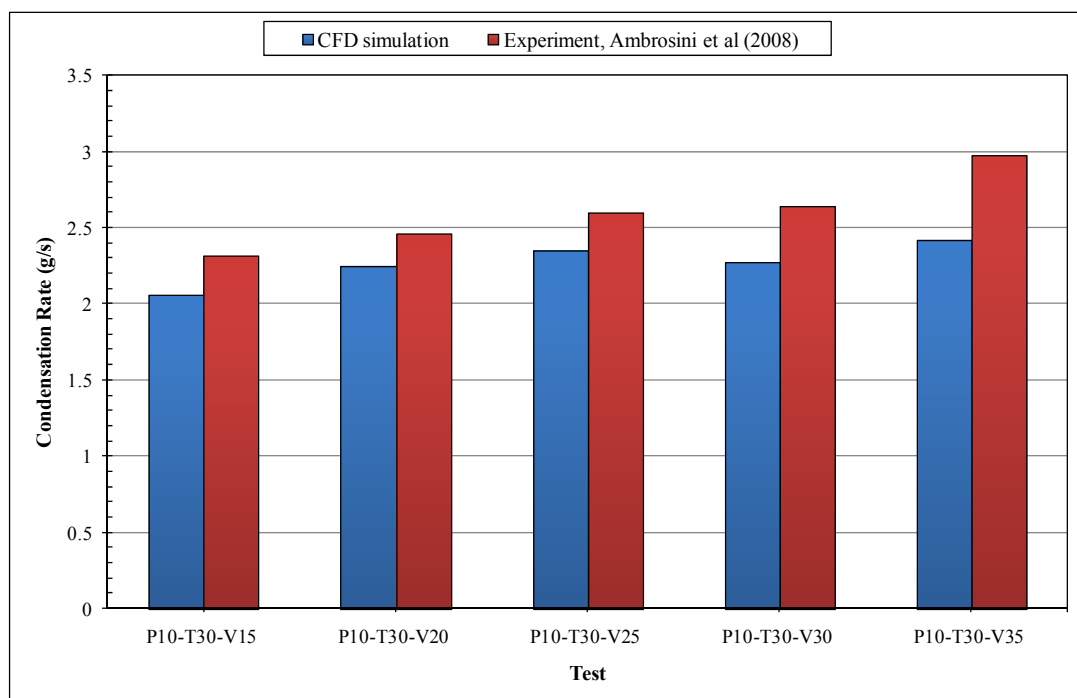


Figure 5.7: Comparison of calculated and experimental values of condensation rate.

Figure 5.6 shows that there is reasonable agreement between the predicted heat flux at the condensing surface. Near the entrance of the air-steam mixture, the predicted heat fluxes are in general lower than those that were obtained experimentally. The same phenomenon has been observed by other researchers in the condensation Benchmark tests (Ambrosini et al. 2008). In fact, the under-prediction of the heat flux near the entrance of the air-steam mixture shown in Figure 5.6 was less than that of Ambrosini and thus the heat fluxes obtained from the present CFD simulations are much closer to the experimental results than were those obtained in Ambrosini et al.'s study. Figure 5.7 shows the comparison of the condensate rates from the CFD and the experimental data. The agreement is acceptable, but differences in the condensation rates between the CFD predictions and the experimental results can be as high as 30%.

5.2.1.3. Step 2

In this step, the complete condensing system of Ambrosini et al. (2008) was simulated (simplified to a 2D problem). The system consists of two fluid streams separated by a solid wall. Cooling water flows vertically upwards inside one of the channels, while a mixture of air and water vapour flows vertically on the other channel, as shown in Figure 5.8. The water vapour condenses on the cold wall and a liquid film forms that flows downwards. Again, we neglect the effect of the condensate film and assume that the air-steam mixture extends to the condensing surface: the aluminium wall.

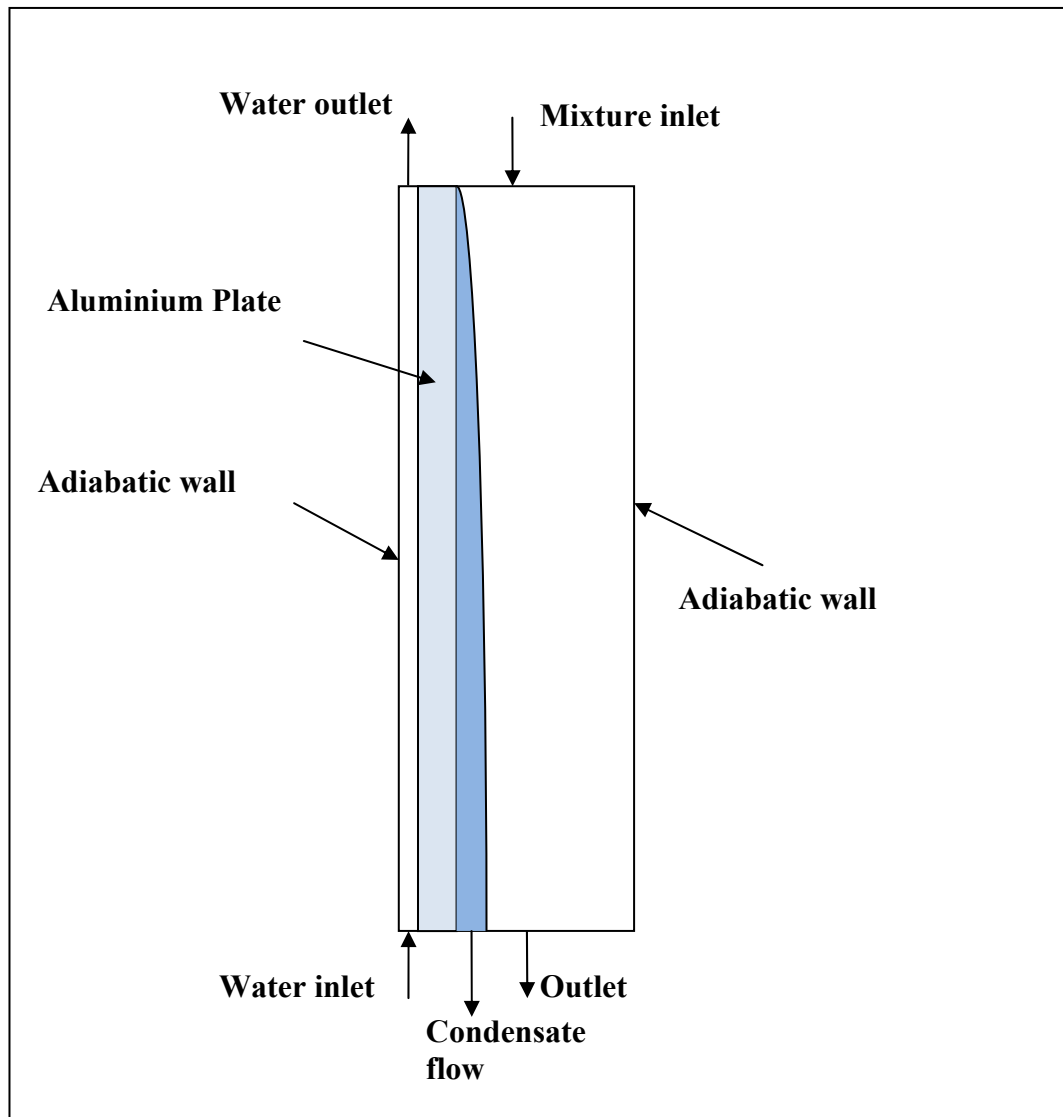


Figure 5.8: Computational domain for step 2.

In using FLUENT[®] for predicting the heat and mass transfer in both the air-vapour mixture channel and the cooling water channel simultaneously, many difficulties were encountered. First, as stated the FLUENT[®] User's Guide (2010), in modelling heat transfer in two separated fluid regions involving multi-species, only a single-mixture material for the entire domain can be used. As a result, the two flows in the present situation including the air-vapour mixture and the cooling water cannot be simulated simultaneously using FLUENT[®] because the flow in one channel is a mixture of air and water vapour and in the other channel the flow is water liquid. FLUENT[®] can

model two flows separated by a solid wall only if one flow is water, say, and the other is air.

One possible solution is to model the present problem using two fluids, one being water and the other being air. The water vapour is introduced in the air channel as a user-defined scalar (UDS). However, the UDS in FLUENT[®] is treated as being passive. In the vapour condensation in the presence of non-condensable gas, water vapour is strongly coupled with the airflow. To couple the water vapour and the air, all the properties of the air-steam mixture (including the density) need to be redefined. However, FLUENT[®] does not allow the specific heat of the mixture to be calculated externally. Various methods of trying to overcome these difficulties using UDS were attempted, but we found it impossible to solve this problem using UDS with the current FLUENT[®] setup.

A second method is to separate the simulations into two and carry them out asynchronously. Heat and mass transfer is analysed in the air-steam mixture channel only (very much like that in step 1) and the second simulation is confined to the cooling water channel and the aluminium plate. The two simulations are coupled at the condensing surface of the aluminium plate. The latest version of ANSYS[®] includes FLUENT[®] and other packages for the analysis of mechanical systems and provides the possibility of interactions between systems defined by different branches of physics. However, it cannot yet provide the interaction between two simulations involving two flows. To overcome this difficulty, the two flows were simulated using two standalone FLUENT[®] models running sequentially.

The flow in the air-steam mixture channel was simulated first. A wall temperature from a pre-written file (this file includes the temperature at the condensing surface at each grid centre and initially it can assume the temperature of the cooling water) at the condensing surface was read and the simulation was carried out until convergence was approached. A separate file was written for the heat flux at the condensing surface as an output of this simulation. Heat transfer in the cooling water channel and the aluminium plate was then simulated using the heat flux file written previously as the input boundary conditions. The simulation was again carried to convergence and a file for the temperature at the condensing surface was written as an output of this second simulation. These two sequential simulations were repeated and two journal files were written to save the setting up of the problems at every iteration. It was found that only a few iterations were required to achieve convergent results for both simulations.

As in step 1, a gas mixture of air and water vapour was introduced at the inlet with a given velocity, temperature and relative humidity. All the thermal properties of the air and water vapour were assumed functions of temperature and were calculated in the UDFs. The flow was assumed turbulent and an RNG $k-\varepsilon$ model with enhanced wall treatment was implemented. A diffusion energy source was allowed. The mass transfer and condensation rates were calculated the same way as in step 1, and the heat flux at the condensing wall was calculated using Equation 5.12.

In simulating the flow in the cooling channel, water was introduced at the inlet (from the bottom, as shown in Figure 5.8) at the prescribed velocity and temperature. Buoyancy effects were included in modelling the heat transfer as recommended by Li

et al. (2010) because buoyancy effects cannot be generally neglected in the cooling channel. However, in the conditions encountered in this problem, buoyancy effects are small since the surface temperature of the aluminium plate facing the water is close to the bulk temperature of the coolant. To use the wall temperature profile (written in a file in the simulations for cooling channel and aluminium plate) in the simulation of flows in the air-steam mixture channel and to use the heat flux profile (written in a file in the simulations for mixture flow) in the simulation of cooling water and aluminium plate, the grids on the surface of the condensing wall common to both simulations need to be matched. Further, in general, FLUENT[®] performs CFD simulations starting from the inlet of the fluid domain and the positions at the condensing surface in the two simulations need to be carefully matched.

Figures 5.9 and 5.10 show the results from the CFD predictions using this strategy of simulating two separate flows. Figure 5.9 shows the predicted and the experimental condensate rates corresponding to the five experimental conditions as listed in Table 5.1. The figure shows that agreement between the CFD and experimental results is reasonable. In comparison with the results shown in Figure 5.7, the CFD results shown in Figure 5.9 are in general higher than the experimental results, while the predicted results as shown in Figure 5.7 are in general lower than the experimental results. Nevertheless, we cannot conclude that the new strategy has improved the prediction of the condensation rates since the magnitudes of the differences shown in Figures 5.7 and 5.9 are similar.

Figure 5.10 shows the comparison of the predicted and experimental heat fluxes at the condensing wall for all five experimental conditions as listed in Table 5.1. Here, the

heat fluxes near the entrance of the air-steam mixture agree well with the experimental data, but the predicted fluxes are in general less than the experimental results beyond $x = 1$ m. This is in contrast to the results shown in Figure 5.6 in which the agreement near the entrance is poor but which is good beyond $x = 0.5$ m. As a result, we still cannot conclude that the simulation in step 2 has improved the agreement between the CFD predictions and the experimental results.

However, it should be noted that the simulations in step 1 were performed by assuming a constant heat resistance from the aluminium plate and the cooling flow. In practice, this is normally unknown. In step 2 CFD simulations, the inputs are the cooling water flow rates and inlet temperatures and the material properties and thickness of the cooling plate. These conditions are normally given for condensers. Thus, the simulations in step 2 are closer to reality.

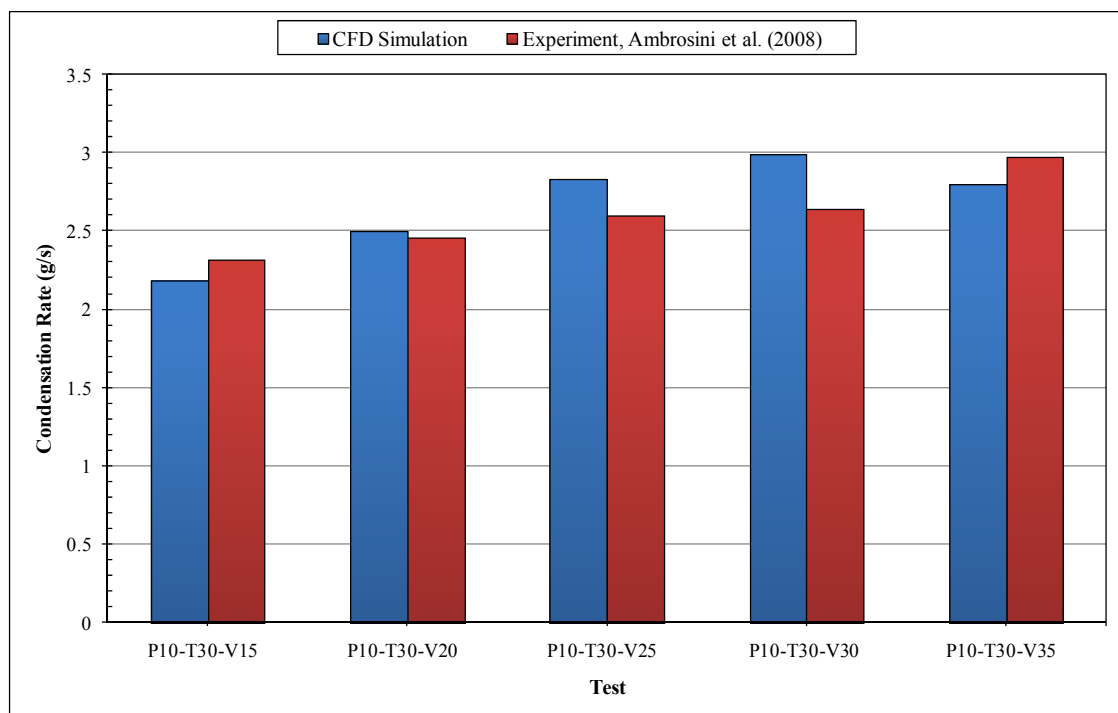


Figure 5.9: Comparison of calculated and experimental values of condensation rate from step 2.

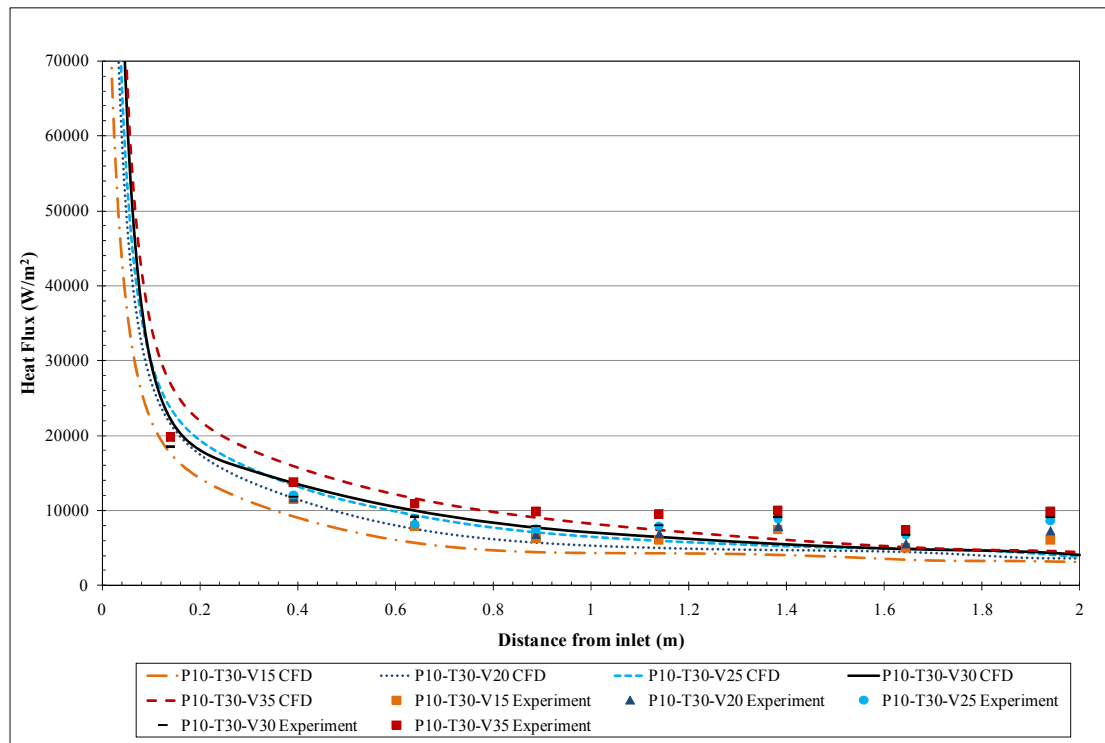


Figure 5.10: Comparison of calculated and experimental values of heat flux from step 2.

5.3. Conclusions and Discussion

CFD simulations of the condensation of vapour in the presence of a non-condensable gas were performed using three different approaches. The results were compared with existing correlations and the experimental results of Ambrosini et al. (2008). The CFD simulations were conducted in three steps:

- Step 0: Flow in the air-steam channel with a constant wall temperature
- Step 1: Flow in the air-steam channel with a constant HTC at the condensing wall
- Step 2: Flows in both the air-steam channel and the cooling channel

It was found that the results from the step 0 simulation agree with the well-known existing correlations, apart from the entrance regions. The condensate rates and the heat flux at the condensing wall predicted from the step 1 CFD simulation agree reasonably well with the experimental results of Ambrosini et al. In the step 2 CFD simulations, a unique strategy of simulating heat and mass transfer in the two channels separately was applied to overcome the shortcomings of the current commercial CFD package. It is found that, with this strategy, the CFD predictions agree reasonably well with the experimental results. Although it cannot be concluded that the results in the step 2 CFD simulations agree better with the experimental results than those from step 1, the strategy adopted in step 2 can be applied in practice because the HTC at the condensing wall is not known a priori.

Chapter 6: Conclusions and Recommendations

6.1. Conclusions

Experimental and simulation studies of heat transfer in a Polypropylene compact heat exchanger with counter-flow configuration were performed. Experimental setup was fabricated to study water-to-air heat transfer in the Polypropylene compact heat exchanger. This study investigated the effect of air and water flow rates on the heat rejected by the compact heat exchanger. The results obtained during the experiments showed that the heat rejection rate increases as the air and water mass flow rate increases. Results also indicated that the outlet water temperature was close to the ambient air temperature, meaning that the compact heat exchanger was performing well and could reduce the water temperature effectively. Heat transfer of the Polypropylene compact heat exchanger was also studied using CFD software FLUENT[®] to produce numerical results. The CFD predictions of the heat rejected by the compact heat exchanger were compared with those calculated in the experimental results and found to be in reasonably good agreement. To compare the Polypropylene heat exchanger with the aluminium heat exchanger, both heat exchangers were simulated to obtain the heat rejection rate. In the comparison, the Polypropylene heat exchanger achieved almost the same performance as that of the aluminium heat exchanger, with low cost and requiring little maintenance. Hence, it was concluded

that the constructed Polypropylene compact heat exchanger would be a good substitute the conventional metal heat exchangers in many future applications.

The mathematical model employed to model heat and mass transfer in a plate heat exchanger and tube condensers, in which a mixture of water vapour and non-condensable gas is cooled by liquid water, was reported in this thesis. A set of differential and algebraic equations were derived. In combination with models based on analogies between heat and mass transfer, these equations were solved simultaneously for the water-vapour mixture, the condensate and the coolant flows. Numerical predictions for condensation rate, heat flux and outlet water temperature in the plate heat exchanger were compared with experimental results from the literature and good agreement was found.

The model was also used for tube condensers to predict the condensation rate, the bulk temperatures of the coolant and the gas-vapour mixture and the surface temperatures of the condenser wall. The predicted results for counter-flow tube condensers were compared with three sets of published experimental data for systems in which air is the non-condensable gas. It was found that the predicted condensation rates and coolant bulk temperatures agreed very well with the three sets of experimental data. The predicted wall temperatures agreed reasonably well with the experimental results, and the agreement between the predictions and the experimental results on the bulk temperature of the air-vapour mixture was excellent for one set of the experimental data, reasonable for the second set of experimental data, but poor for the third set of experimental data. It was suggested that the poor agreement between

the predicted and measured bulk temperatures of the mixture for the third set of experimental data arose from experimental errors in the original study.

In this research, it was revealed that when modelling vapour condensation in the presence of a non-condensable gas, a simple model for the mixture channel alone may not be sufficient since neither the temperature nor the heat flux at the wall can be assumed to be constant. The results also show that the wall temperature in the coolant channel can be quite high, and careful modelling of the heat transfer in the coolant channel is needed to achieve good agreement between the model predictions and the experimental results.

Condensation from vapour and non-condensable gas mixture was also investigated, using CFD. The simulations were conducted using FLUENT[®] for three different cases. In the first case, convective heat and mass transfer and vapour condensation at a constant wall temperature were simulated in plane channel with the aim of comparing the CFD results with well-established correlations. The comparisons were in good agreement. In the second case, CFD simulations of heat and mass transfer and water-vapour condensation in the presence of non-condensable air were carried out for constant HTC's for the condensation wall and coolant with different mass fractions of water vapour and inlet velocities. The predictions obtained from this were compared with experimental data and reasonable agreement was found for the condensation rates of water vapour and heat flux. In the third case, for a more realistic model, the condensation of the water vapour was simulated in a heat exchanger including both the cooling water and vapour-air mixture channels separated by solid walls. In this simulation, no assumptions were required for the temperature or heat-

transfer coefficient at the condensing wall. It was found that the CFD predictions agreed reasonably well with the experimental results.

6.2. Recommendations

For future work, it is recommended to develop a 3D CFD model for condensation of water vapour in plate heat exchangers. It is probable that more accurate physical modelling of heat exchangers in CFD software programs will lead to simulation results that more closely match the experimental values.

Further research is needed to investigate the heat transfer in the Polypropylene compact heat exchanger during extreme operation conditions and study the tightness of the heat exchanger to eliminate any leakage.

REFERENCES

- Ambrosini, W, Bucci, M, Forgone, N, Oriolo, F, Paci, S, Magnaud, Jp, Studer, E, Reinecke, E, Kelm, S & Jahn, W 2008, 'Comparison and analysis of the condensation benchmark results', The 3rd European review meeting on severe accident research (ERMSAR-2008), Nesseber, Bulgaria, 23–25 September 2008.
- Baehr, Hd & Stephan K 2006, *Heat and mass transfer*, 2nd ed., Springer, Berlin, Heidelberg.
- Benelmir, R, Mokraoui, S & Souayed, A 2009, 'Numerical analysis of filmwise condensation in a plate fin-and-tube heat exchanger in presence of non-condensable gas', *Heat and Mass Transfer*, vol. 45, pp. 1561–1573.
- Bigg, DM, Stickford, GH & Talbert, SG 1989, 'Applications of polymeric materials for condensing heat exchangers', *Polymer Engineering and Science*, vol. 29, pp. 1111–1116.
- Bird, RB, Stewart, WE & Lightfoot, EN 2007, *Transport phenomena*, 2nd ed, John Wiley & Sons, UK.

- Bromley, LRA 1952, 'Heat transfer in condensation—Effect of heat capacity of condensate', *Industrial Engineering Chemistry Research*, vol. 44, pp. 2966–2969.
- Brouwers, HJH & Van Der Geld, CWM 1996, 'Heat transfer, condensation and fog formation in crossflow plastic heat exchangers', *International Journal of Heat and Mass Transfer*, vol. 39, pp. 391–405.
- Bucci, M, Sharabi, M, Ambrosini, W, Forgione, N, Oriolo, F & He, S 2008, 'Prediction of transpiration effects on heat and mass transfer by different turbulence models', *Nuclear Engineering and Design*, vol. 238, pp. 958–974.
- Bum-Jin, C, Sin, K, Min Chan, K & Ahmadinejad, M 2004, 'Experimental comparison of film-wise and drop-wise condensations of steam on vertical flat plates with the presence of air', *International Communications in Heat and Mass Transfer*, vol. 31, pp. 1067–1074.
- Cengel, YA & Boles, MA 2008, *Thermodynamics—An engineering approach*, 6th ed., McGraw Hill, UK.
- Churchill, SW 1977, 'A comprehensive correlating equations for laminar assisting forced and free convection', *AIChE Journal*, vol. 23, pp. 10–16.
- Colburn, AP & Hougen, OA 1934, 'Design of cooler condensers for mixtures of vapours with noncondensing gases', *Industrial and Engineering Chemistry*, vol. 26, no. 11, pp. 1178–1182.

- Corradini, ML 1984, 'Turbulent condensation on a cold wall in the presence of a noncondensable gas', *Nuclear Technology*, vol. 64, pp. 186–195.
- Davidson, J, Oberreit, D, Liu, XW & Mantell, S 1999, 'Are plastic heat exchangers feasible for solar water heaters? Part 1: A review of the technology, codes and standards, and commercial products', ASME–KSME–JSME–ASHRAE–JES International renewable and advanced energy systems for the 21st century, Hawaii, April 1999.
- Dehbi, A & Guentay, S 1997, 'A model for the performance of a vertical tube condenser in the presence of noncondensable gases', *Nuclear Engineering and Design*, vol. 177, pp. 41–52.
- Desrayaud, G & Lauriat, G 2001, 'Heat and mass transfer analogy for condensation of humid air in a vertical channel', *Heat and Mass Transfer*, vol. 37, pp. 67–76.
- Dharma Rao, V, Murali Krishna, V, Sharma, KV & Rao, PVJM 2008, 'Convective condensation of vapour in the presence of a non-condensable gas of high concentration in laminar flow in a vertical pipe', *International Journal of Heat and Mass Transfer*, vol. 51, pp. 6090–6101.
- Dharma Rao, V, Phanikumar, D, Sarma, PK & Sivannarayana, P 2002, 'Effect of the presence of a non-condensable gas on condensation rates during external condensation', *Proceedings of Andhra Pradesh Akademi of Sciences*, vol. 6, pp. 251–260.

EngineeringToolBox 2010, *Steam and Vapor Enthalpy*, EngineeringToolBox, viewed at http://www.engineeringtoolbox.com/steam-vapor-enthalpy-d_160.html

FLUENT[®] 6.3 User's guide 2010.

Ganzevles, F & Van Der Geld, CWM 2002, *Drainage and condensate heat resistance in dropwise condensation of multicomponent mixtures in a plastic plate heat exchanger*, PhD theses, Eindhoven University of Technology, Netherlands.

Groff, MK, Ormiston, SJ & Soliman, HM 2007, 'Numerical solution of film condensation from turbulent flow of vapour-gas mixture in vertical tubes', *International Journal of Heat and Mass Transfer*, vol. 50, pp. 3899–3912.

Haaland, SE 1983, 'Simple and explicit formulas for the friction factor in turbulent pipe flow', *Journal of Fluids Engineering*, vol. 105, pp. 89–90.

Hetsroni, G & Mosyak, A 1994, 'Heat transfer and pressure drop in a plastic heat exchanger with triangular channels', *Chemical Engineering and Processing: Process Intensification*, vol. 33, pp. 91–100.

Holman, JP 1992, *Heat transfer*, 7th ed., McGraw-Hill, UK.

Jachuck, R & Ranshaw, C 1994, 'Process intensification: Polymer film compact heat exchanger (PFCHE)', *Chemical Engineering Research & Design*, vol. 72, pp. 255–262.

- Karapantsios, TD, Kostoglou, M & Karabelas, AJ 1995, 'Local condensation rates of steam-air mixtures in direct contact with a falling liquid film', *International Journal of Heat and Mass Transfer*, vol. 38, pp. 779–794.
- Karkoszka, K & Anglart, H 2006, 'CFD modelling of laminar film and spontaneous condensation in presence of noncondensable gas', *Archives of Thermodynamics*, vol. 27, pp. 23–36.
- Kays, W & Moffat, R 1975, 'The behavior of transpired turbulent boundary layers', *NASA STI/Recon Technical Report N*, vol. 75, p. 32383.
- Kays, WM, Crawford, ME & Weigand, B 2005, *Convective heat and mass transfer*, 4th ed., McGraw-Hill, UK.
- Kim, M & Kang, H 1993, 'Condensation phenomena with wavy interface in the presence of a noncondensable gas', *ASME Conference Proceedings*, pp. 219–230.
- Kim, MH & Corradini, ML 1990, 'Modeling of condensation heat transfer in a reactor containment', *Nuclear Engineering and Design*, vol. 118, pp. 193–212.
- Kuhn, SZ 1995, *Investigation of heat transfer from condensation steam-gas mixture and turbulent films flowing downward inside a vertical tube*, University of California Press, Berkeley.

- Lebedev, PD, Baklastov, AM & Sergazin, ZF 1969, 'Aerodynamics, heat and mass transfer in vapour condensation from humid air on a flat plate in a longitudinal flow in asymmetrically cooled slot', *International Journal of Heat and Mass Transfer*, vol. 12, pp. 833–841.
- Lee, K-Y & Kim, MH 2008, 'Modeling of condensation heat transfer for a PRHRS heat exchanger in a SMART-P plant', *Nuclear Engineering and Design*, vol. 238, pp. 3253–3262.
- Levy, E, Bilirgen, H, Jeong, K, Kessen, M, Samuelson, C & Whitcombe, C 2008a, 'Recovery of water from boiler flue gas', *DOE Final Technical Report (952467)*.
- Levy, E, Bilirgen, H, Samuelson, C, Jeong, K, Kessen, M & Whitcomb, C 2008b, 'Separation of water and acid vapours from boiler flue gas in a condensing heat exchanger', Proceedings of the 33rd international technical conference on coal utilization and fuel systems, Clearwater, Florida, 1 June to 5 June, 2008.
- Li, JD, Saraireh, M & Thorpe, GR 2011, 'Condensation of vapour in the presence of non-condensable gas in condensers', *International Journal of Heat and Mass Transfer*, vol. 54, pp. 4078–4089.
- Lux, JJ, Jr, Razgaitis, R, Ball, DA & Locklin, DW 1983, 'Development of an analytical design technique for condensing flue-gas heat exchangers', International gas research conference, London.

- Malalasekera, WMG, James, EH, Tayali, NE & Lee, LEK 1993, 'Flow and heat transfer in the secondary heat exchanger of a condensing boiler', American society of mechanical engineers, 29th national heat transfer conference, Atlanta, Georgia, August 1993.
- Mamyoda, T & Asano, K 1994, 'Experimental study of condensation of vapours in the presence of non-condensable gas on a short horizontal tube', *Journal of Chemical Engineering*, vol. 27, pp. 485–490.
- Martin-Valdepenas, JM, Jimenez, MA, Martin-Fuertes, F & Fernandez-Benitez, JA 2005, 'Comparison of film condensation models in presence of non-condensable gases implemented in CFD code', *Heat and Mass Transfer*, vol. 41, pp. 961–967.
- Minkowycz, WJ & Sparrow, EM 1966, 'Condensation heat transfer in the presence of noncondensables, interfacial resistance, superheating, variable properties, and diffusion', *International Journal of Heat and Mass Transfer*, vol. 9, pp. 1125–1144.
- Norris, RH 1970, 'Some simple approximate heat transfer correlations for turbulent flow in ducts with rough surfaces', *Augmentation of Convective Heat and Mass Transfer*, ASME, New York, p. 66.
- Nusselt, W 1916, 'Des Oberflächenkondensation des Wasserdampfes', *Zeitschrift Des Vereines Deutscher Ingenieure*, vol. 60, pp. 541–564, 569–575.

- Oh, S & Revankar, ST 2006, 'Experimental and theoretical investigation of film condensation with noncondensable gas', *International Journal of Heat and Mass Transfer*, vol. 49, pp. 2523–2534.
- Patankar, SV & Sparrow, EM 1979, 'Condensation on an extended surface', *Journal of Heat Transfer*, vol. 101, pp. 434–440.
- Pele, C, Baudoin, B & Barrand, JP 1994, 'Effect of humid air flow rate on the filmwise condensation inside a vertical cooled pipe: Numerical and experimental study', *International Journal of Heat and Mass Transfer*, vol. 37, pp. 1829–1837.
- Perry, CR, Dietz, LHS & Shannon, RL 1983, 'Heat exchange apparatus having thin film flexible sheets', *The Boeing Company US*, Patent No. 4411310.
- Reay, DA 2000, *Polymer heat exchangers: Exploitation of the technology—A discussion of some options*, David Reay & Associates, Newcastle, UK.
- Reynolds, HC, Swearngen, TB & McEligot, DM 1969, 'Thermal entry for low Reynolds number turbulent flow', *Journal of Basic Engineering*, vol. 91, p. 87.
- Rohsenow, WJ 1973, *Condensation handbook of heat transfer*. McGraw-Hill, New York.

- Sarma, PK, Anjaneya Reddy, M, Bergles, AE & Kakac, S 2001, 'Condensation of vapours on a fin in the presence of non-condensable gas', *International Journal of Heat and Mass Transfer*, vol. 44, pp. 3233–3240.
- Schnon, SG 1988, *Plastic film plate type heat exchanger*, US Patent No. 4744414.
- Siddique, M 1992, 'The effects of noncondensable gases on steam condensation under forced convection conditions', *Department of Nuclear Engineering*, Massachusetts Institute of Technology, Cambridge, MA.
- Siddique, M, Golay, MW & Kazimi, MS 1994, 'Theoretical modeling of forced convection condensation of steam in a vertical tube in the presence of a noncondensable gas', *Nuclear Technology*, vol. 106, pp. 202–215.
- Sparrow, EM & Lin, SH 1964, 'Condensation heat transfer in the presence of a noncondensable gas', *Journal of Heat Transfer*, vol. 86, pp. 430–436.
- Sparrow, EM, Minkowycz, WJ & Saddy, M 1967, 'Forced convection condensation in the presence of noncondensables and interfacial resistance', *International Journal of Heat and Mass Transfer*, vol. 10, pp. 1829–1845.
- Takarada, M, Ikeda, S, Izumi, M, Shimada, R, Sasaki, S & Yamakawa, S 1997, 'Forced convection heat and mass transfer from humid air under condensation conditions', *Proceedings of Experimental Heat Transfer, Fluid Mechanics and Thermodynamics*, vol. 2, pp. 1103–1116.

- Tanrikut, A & Yesin, O 1998, 'Experimental research on in-tube condensation in the presence of air', *Proceedings of a technical committee meeting, IAEA TECDOC-1149*, Switzerland.
- Tanrikut, A & Yesin, O 2005, 'Experimental research on in-tube condensation under steady-state and transient conditions', *Nuclear Technology*, vol. 149, pp. 88–100.
- Terekhov, VI, Terekhov, VV & Sharov, KA 1998, 'Heat and mass transfer in condensation of water vapour from moist air', *Journal of Engineering Physics and Thermophysics*, vol. 71, pp. 771–777.
- Valencia, MPP 2004, *Condensation of water vapour and acid mixtures from exhaust gases*, PhD thesis, Technical University of Berlin, Germany.
- Volchkov, EP, Terekhov, VV & Terekhov, VI 2004, 'A numerical study of boundary-layer heat and mass transfer in a forced flow of humid air with surface steam condensation', *International Journal of Heat and Mass Transfer*, vol. 47, pp. 1473–1481.
- Wang, C-Y & Tu, C-J 1988, 'Effects of non-condensable gas on laminar film condensation in a vertical tube', *International Journal of Heat and Mass Transfer*, vol. 31, pp. 2339–2345.

- Webb, RL & Wanniarachchi, AS 1980, 'The effect of non-condensable gases in water chiller condensers—Literature survey and theoretical prediction', *ASHRAE Transactions*, vol. 80, pp. 142–159.
- Zaheed, L & Jachuck, RJJ 2005, 'Performance of a square, cross-corrugated, polymer film, compact, heat-exchanger with potential application in fuel cells', *Journal of Power Sources*, vol. 140, pp. 304–310.
- Zarkadas, DM & Sirkar, KK 2004, Polymeric hollow fiber heat exchangers: An alternative for lower temperature applications, *Industrial and Engineering Chemistry Research*, vol. 43, pp. 8093–8106.

APPENDICES

Appendix A: Tables of Experimental Data

Symbols used in the tables of experimental data:

$T_{a \text{ in}}$ inlet air temperature ($^{\circ}\text{C}$)

$T_{w \text{ in}}$ inlet water temperature ($^{\circ}\text{C}$)

$T_{w \text{ out}}$ outlet water temperature ($^{\circ}\text{C}$)

m_w mass flow rate of water (l/s)

ΔP_a pressure drop across the compact heat exchanger (Pa)

m_{air} mass flow rate of air (kg/s)

Q_{exp} heat rejection rate (kW)

Test for the period 24 to 25 January 2011

Time (s)	Date and Time	T _a in (°C)	T _w in (°C)	T _w out (°C)	m _w (l/s)	ΔP _a (Pa)	m _{air} (kg/s)	Q _{exp} (kW)
0	1/24/11 8:30	18.616	40.928	23.336	0.1728	120.410	1.344	12.725
12.222	1/24/11 8:30	19.898	40.992	23.336	0.1731	121.620	1.359	12.792
24.444	1/24/11 8:30	18.189	40.992	23.208	0.1737	124.150	1.390	12.930
36.667	1/24/11 8:30	19.288	40.928	23.304	0.1716	123.120	1.378	12.661
48.889	1/24/11 8:30	18.494	40.864	23.176	0.1575	124.220	1.391	11.660
61.111	1/24/11 8:31	19.166	40.800	23.208	0.1522	120.920	1.350	11.205
73.333	1/24/11 8:31	18.922	40.736	23.272	0.1532	121.550	1.358	11.201
85.556	1/24/11 8:31	18.983	40.736	23.176	0.1527	121.880	1.362	11.226
97.778	1/24/11 8:31	19.898	40.672	23.112	0.1528	124.370	1.393	11.232
110	1/24/11 8:31	18.494	40.672	22.984	0.1532	125.500	1.407	11.344
122.222	1/24/11 8:32	18.555	40.672	23.176	0.1516	122.420	1.369	11.105
134.444	1/24/11 8:32	20.326	40.608	23.112	0.1530	122.570	1.371	11.204
146.667	1/24/11 8:32	19.044	40.608	22.984	0.1526	122.640	1.372	11.258
158.889	1/24/11 8:32	18.311	40.608	23.080	0.1525	123.270	1.379	11.188
171.111	1/24/11 8:32	18.739	40.544	22.984	0.1518	122.420	1.369	11.161
183.333	1/24/11 8:33	19.410	40.480	22.952	0.1522	122.420	1.369	11.164
195.556	1/24/11 8:33	19.837	40.416	22.600	0.1524	126.750	1.423	11.363
207.778	1/24/11 8:33	19.593	40.480	22.728	0.1517	123.450	1.382	11.271
220	1/24/11 8:33	18.372	40.352	23.016	0.1526	120.810	1.349	11.071
232.222	1/24/11 8:33	18.861	40.288	22.920	0.1514	121.140	1.353	11.009
244.444	1/24/11 8:34	18.494	40.352	22.888	0.1520	121.360	1.356	11.114
256.667	1/24/11 8:34	18.433	40.416	22.888	0.1526	122.640	1.372	11.200
268.889	1/24/11 8:34	18.861	40.480	23.016	0.1519	121.620	1.359	11.103
281.111	1/24/11 8:34	18.067	40.544	23.016	0.1518	120.520	1.345	11.135
293.333	1/24/11 8:34	17.945	40.608	22.920	0.1521	121.110	1.353	11.263
305.556	1/24/11 8:35	18.494	40.544	22.729	0.1522	124.110	1.390	11.347
317.778	1/24/11 8:35	17.823	40.416	22.696	0.1533	121.110	1.353	11.370
330	1/24/11 8:35	18.922	40.352	22.569	0.1539	121.950	1.363	11.460
342.222	1/24/11 8:35	18.311	40.224	22.569	0.1538	121.730	1.360	11.368

.

98657.78	1/25/11 11:54	21.058	40.672	24.710	0.1533	123.930	1.388	10.240
98670	1/25/11 11:54	21.607	40.608	24.678	0.1523	124.040	1.389	10.154
98682.22	1/25/11 11:54	21.729	40.672	24.806	0.1537	123.230	1.379	10.205
98694.44	1/25/11 11:54	21.913	40.672	24.806	0.1529	123.230	1.379	10.156
98706.67	1/25/11 11:55	21.424	40.672	24.774	0.1537	123.300	1.380	10.229
98718.89	1/25/11 11:55	22.218	40.672	24.742	0.1541	124.800	1.398	10.276
98731.11	1/25/11 11:55	21.668	40.672	24.838	0.1537	123.600	1.384	10.185
98743.33	1/25/11 11:55	22.950	40.672	24.934	0.1537	122.240	1.367	10.128
98755.56	1/25/11 11:55	22.401	40.736	24.966	0.1533	122.900	1.375	10.119
98767.78	1/25/11 11:56	22.706	40.736	24.998	0.1535	122.830	1.374	10.114
98780	1/25/11 11:56	21.790	40.800	24.998	0.1540	121.510	1.358	10.188
98792.22	1/25/11 11:56	21.913	40.736	24.998	0.1528	123.710	1.385	10.069
98804.44	1/25/11 11:56	22.218	40.672	24.934	0.1528	124.070	1.389	10.066
98816.67	1/25/11 11:56	22.706	40.736	24.998	0.1534	123.780	1.386	10.104

Test for the period 25 to 27 January 2011

Time (s)	Date and Time	T _a in (°C)	T _w in (°C)	T _w out (°C)	m _w (l/s)	ΔP _a (Pa)	m _{air} (kg/s)	Q _{exp} (kW)
7162.22	1/25/11 18:00	16.235	41.887	17.664	0.1278	121.510	1.358	12.957
7186.67	1/25/11 18:00	16.267	42.015	17.664	0.1298	121.360	1.356	13.228
7211.11	1/25/11 18:01	16.267	42.015	17.573	0.1298	121.580	1.358	13.281
7235.56	1/25/11 18:01	16.314	42.015	17.573	0.1293	123.670	1.384	13.228
7260	1/25/11 18:01	16.408	42.015	17.573	0.1300	121.770	1.361	13.299
7284.44	1/25/11 18:02	16.314	42.015	17.664	0.1297	121.510	1.358	13.216
7308.89	1/25/11 18:02	16.345	41.951	17.573	0.1294	122.680	1.372	13.206
7333.33	1/25/11 18:03	16.282	42.015	17.664	0.1297	122.750	1.373	13.224
7357.78	1/25/11 18:03	16.235	42.015	17.664	0.1293	121.950	1.363	13.179
7382.22	1/25/11 18:03	16.235	42.079	17.481	0.1293	121.330	1.355	13.313
7406.67	1/25/11 18:04	16.298	42.079	17.573	0.1294	122.680	1.372	13.271
7431.11	1/25/11 18:04	16.016	41.951	17.481	0.1297	123.270	1.379	13.280
7455.56	1/25/11 18:05	15.781	41.951	17.390	0.1299	124.040	1.389	13.359
7480	1/25/11 18:05	15.703	41.887	17.390	0.1292	123.300	1.380	13.245
7504.44	1/25/11 18:05	15.703	41.887	16.932	0.1295	122.390	1.368	13.531
7528.89	1/25/11 18:06	15.641	41.951	16.932	0.1286	123.120	1.378	13.463
7553.33	1/25/11 18:06	15.687	41.951	16.841	0.1284	124.370	1.393	13.495
7577.78	1/25/11 18:07	15.687	42.015	16.658	0.1286	122.460	1.369	13.645
7602.22	1/25/11 18:07	15.719	41.951	16.566	0.1283	121.910	1.363	13.630
7626.67	1/25/11 18:07	15.672	41.951	16.566	0.1279	122.570	1.371	13.595
7651.11	1/25/11 18:08	15.641	41.887	16.566	0.1275	122.420	1.369	13.514
7675.56	1/25/11 18:08	15.687	41.823	16.566	0.1288	122.020	1.364	13.622
7700	1/25/11 18:09	15.656	41.823	16.566	0.1289	122.640	1.372	13.626
7724.44	1/25/11 18:09	15.594	41.887	16.566	0.1287	122.680	1.372	13.644
7748.89	1/25/11 18:09	15.609	41.823	16.566	0.1286	121.910	1.363	13.601
7773.33	1/25/11 18:10	15.594	41.887	16.383	0.1300	123.340	1.380	13.877
7797.78	1/25/11 18:10	15.547	41.887	16.200	0.1297	122.350	1.368	13.949
7822.22	1/25/11 18:11	15.500	41.759	16.383	0.1293	121.980	1.363	13.734
7846.67	1/25/11 18:11	15.594	41.759	16.292	0.1298	123.120	1.378	13.834
.
.
.
143611	1/27/11 7:54	14.639	39.201	16.932	0.1293	125.430	1.406	12.056
143636	1/27/11 7:54	14.811	39.201	17.115	0.1298	125.500	1.407	11.997
143660	1/27/11 7:55	14.811	39.073	16.932	0.1284	123.160	1.378	11.896
143684	1/27/11 7:55	14.639	39.137	17.024	0.1284	123.850	1.387	11.884
143709	1/27/11 7:55	14.639	39.137	16.841	0.1292	123.780	1.386	12.058
143733	1/27/11 7:56	14.639	39.201	16.932	0.1294	124.070	1.389	12.060
143758	1/27/11 7:56	14.670	39.137	17.115	0.1293	123.960	1.388	11.918
143782	1/27/11 7:57	14.764	39.073	17.024	0.1297	125.280	1.404	11.974
143807	1/27/11 7:57	14.795	39.137	16.932	0.1288	126.670	1.422	11.968
143831	1/27/11 7:58	14.685	39.009	17.024	0.1284	123.710	1.385	11.812
143856	1/27/11 7:58	14.560	39.009	17.024	0.1290	123.670	1.384	11.872
143880	1/27/11 7:58	14.623	39.009	16.749	0.1284	123.710	1.385	11.967
143904	1/27/11 7:59	14.654	39.073	16.749	0.1289	123.120	1.378	12.047
143929	1/27/11 7:59	14.717	39.009	16.749	0.1297	123.120	1.378	12.088
143953	1/27/11 8:00	14.858	39.073	16.749	0.1282	124.260	1.392	11.975

Test for the period 4 to 11 February 2011

Time (s)	Date and Time	T _{a in} (°C)	T _{w in} (°C)	T _{w out} (°C)	m _w (l/s)	Δ P _a (Pa)	m _a (kg/s)	Q _{exp} (kW)
0.000	2/4/11 2:36 PM	21.261	44.253	24.898	0.16413	120.850	1.349	13.298
111.100	2/4/11 2:37 PM	21.292	44.317	24.898	0.16686	120.630	1.347	13.564
222.200	2/4/11 2:39 PM	21.089	44.317	24.807	0.16474	120.850	1.349	13.454
333.300	2/4/11 2:41 PM	21.089	44.253	24.715	0.16503	120.960	1.351	13.497
444.400	2/4/11 2:43 PM	21.261	44.253	25.081	0.16596	121.290	1.355	13.319
555.600	2/4/11 2:45 PM	21.136	44.381	24.990	0.16552	120.450	1.344	13.435
666.700	2/4/11 2:47 PM	21.073	44.317	24.807	0.16446	122.310	1.367	13.431
777.800	2/4/11 2:49 PM	21.120	44.317	24.807	0.16474	120.920	1.350	13.454
888.900	2/4/11 2:50 PM	21.026	44.317	24.715	0.16491	122.680	1.372	13.532
1000.000	2/4/11 2:52 PM	21.026	44.253	24.715	0.16543	122.460	1.369	13.530
1111.100	2/4/11 2:54 PM	20.979	44.381	24.898	0.16584	121.220	1.354	13.525
1222.200	2/4/11 2:56 PM	20.979	44.445	24.715	0.16543	121.800	1.361	13.663
1333.300	2/4/11 2:58 PM	21.073	44.445	24.715	0.16495	121.290	1.355	13.623
1444.400	2/4/11 3:00 PM	21.136	44.317	24.990	0.16487	121.000	1.351	13.338
1555.600	2/4/11 3:01 PM	21.105	44.317	24.898	0.16511	121.030	1.352	13.421
1666.700	2/4/11 3:03 PM	21.073	44.317	25.081	0.16556	121.400	1.356	13.331
1777.800	2/4/11 3:05 PM	21.058	44.317	24.990	0.16552	120.780	1.348	13.391
1888.900	2/4/11 3:07 PM	21.151	44.381	24.990	0.16564	121.400	1.356	13.445
2000.000	2/4/11 3:09 PM	21.073	44.381	25.264	0.16543	121.510	1.358	13.238
2111.100	2/4/11 3:11 PM	21.355	44.445	25.448	0.16523	120.010	1.339	13.139
2222.200	2/4/11 3:13 PM	21.308	44.381	25.631	0.16499	120.960	1.351	12.950
2333.300	2/4/11 3:14 PM	21.339	44.381	25.722	0.16495	121.580	1.358	12.884
2444.400	2/4/11 3:16 PM	21.355	44.509	25.814	0.16507	121.660	1.359	12.918
2555.600	2/4/11 3:18 PM	21.418	44.509	25.905	0.1647	120.810	1.349	12.826
2666.700	2/4/11 3:20 PM	21.590	44.637	26.180	0.16564	120.780	1.348	12.798
2777.800	2/4/11 3:22 PM	21.543	44.701	26.180	0.16698	121.840	1.362	12.946
2888.900	2/4/11 3:24 PM	21.574	44.765	26.180	0.16613	120.810	1.349	12.924
3000.000	2/4/11 3:26 PM	21.778	44.829	26.180	0.16458	120.150	1.341	12.848
3111.100	2/4/11 3:27 PM	21.621	44.765	26.180	0.16483	121.840	1.362	12.823
3222.200	2/4/11 3:29 PM	21.543	44.637	26.088	0.16503	122.460	1.369	12.814
3333.300	2/4/11 3:31 PM	21.668	44.829	26.271	0.1656	120.450	1.344	12.864
3444.400	2/4/11 3:33 PM	21.872	44.829	26.729	0.16572	120.480	1.345	12.556
3555.600	2/4/11 3:35 PM	22.044	44.893	26.912	0.16503	120.560	1.346	12.422
3666.700	2/4/11 3:37 PM	22.091	45.021	27.095	0.16487	119.790	1.336	12.372
3777.800	2/4/11 3:39 PM	22.122	45.085	27.278	0.16507	122.460	1.369	12.304
3888.900	2/4/11 3:40 PM	22.451	45.276	27.644	0.16568	121.250	1.354	12.228
4000.000	2/4/11 3:42 PM	22.467	45.340	27.918	0.16523	121.140	1.353	12.050
4111.100	2/4/11 3:44 PM	22.561	45.404	28.101	0.16507	120.190	1.341	11.956

.

603111.100	2/11/11 2:07 PM	22.498	44.125	25.905	0.1632	125.790	1.411	12.447
603222.200	2/11/11 2:09 PM	22.326	44.189	25.722	0.16361	125.610	1.409	12.648
603333.300	2/11/11 2:11 PM	22.388	44.189	25.631	0.16499	127.730	1.435	12.817
603444.400	2/11/11 2:13 PM	22.247	44.189	25.722	0.16539	127.920	1.438	12.785
603555.600	2/11/11 2:15 PM	22.169	44.253	25.539	0.16499	126.120	1.415	12.925
603666.700	2/11/11 2:17 PM	22.153	44.253	25.356	0.16564	129.270	1.455	13.103
603777.800	2/11/11 2:19 PM	22.279	44.189	25.448	0.16584	127.880	1.437	13.010
603888.900	2/11/11 2:20 PM	22.404	44.253	25.631	0.16592	129.350	1.456	12.934
604000.000	2/11/11 2:22 PM	22.294	44.253	25.539	0.16637	128.430	1.444	13.033
604111.100	2/11/11 2:24 PM	22.482	44.253	25.722	0.1673	126.490	1.420	12.978
604222.200	2/11/11 2:26 PM	22.388	44.189	25.814	0.16637	134.030	1.515	12.797
604333.300	2/11/11 2:28 PM	22.122	44.125	25.722	0.16686	125.830	1.411	12.854
604444.400	2/11/11 2:30 PM	22.075	44.253	25.539	0.16673	127.660	1.434	13.061
604555.600	2/11/11 2:31 PM	22.060	44.125	25.264	0.16673	127.510	1.432	13.164
604666.700	2/11/11 2:33 PM	22.107	44.061	25.356	0.16633	125.940	1.413	13.023
604777.800	2/11/11 2:35 PM	22.263	44.061	25.448	0.16637	125.320	1.405	12.963

Test for the period 15 to 24 February 2011

Time (s)	Date and Time	T _{a in} (°C)	T _{w in} (°C)	T _{w out} (°C)	m _w (l/s)	ΔP _a (Pa)	m _{air} (kg/s)	Q _{exp} (kW)
17000	2/15/11 4:20 PM	21.332	45.468	25.569	0.1836	117.040	1.302	15.293
17111.1	2/15/11 4:22 PM	21.355	45.468	25.633	0.1836	116.820	1.300	15.243
17222.2	2/15/11 4:23 PM	21.245	45.596	25.569	0.1835	118.980	1.326	15.381
17333.3	2/15/11 4:25 PM	21.050	45.532	25.441	0.1838	117.740	1.311	15.454
17444.4	2/15/11 4:27 PM	21.245	45.468	25.377	0.1832	115.720	1.286	15.410
17555.6	2/15/11 4:29 PM	21.292	45.532	25.569	0.1831	117.080	1.303	15.301
17666.7	2/15/11 4:31 PM	21.355	45.468	25.697	0.1832	116.460	1.295	15.164
17777.8	2/15/11 4:33 PM	21.347	45.468	25.697	0.1829	115.500	1.283	15.137
17888.9	2/15/11 4:35 PM	21.433	45.340	25.761	0.1833	117.700	1.310	15.020
18000	2/15/11 4:36 PM	21.425	45.340	25.888	0.1829	113.560	1.259	14.890
18111.1	2/15/11 4:38 PM	21.379	45.276	25.888	0.1823	115.690	1.286	14.791
18222.2	2/15/11 4:40 PM	21.316	45.213	25.633	0.1836	116.530	1.296	15.051
18333.3	2/15/11 4:42 PM	21.269	45.149	25.697	0.1838	118.100	1.315	14.962
18444.4	2/15/11 4:44 PM	21.379	45.021	25.761	0.1827	114.290	1.268	14.733
18555.6	2/15/11 4:46 PM	21.504	45.021	25.824	0.1831	116.820	1.300	14.710
18666.7	2/15/11 4:48 PM	21.394	44.893	25.761	0.1836	118.870	1.325	14.700
18777.8	2/15/11 4:49 PM	21.253	44.829	25.697	0.1835	118.030	1.314	14.693
18888.9	2/15/11 4:51 PM	21.402	44.893	25.824	0.1839	118.070	1.315	14.677
19000	2/15/11 4:53 PM	21.457	44.765	25.952	0.1829	118.400	1.319	14.400
19111.1	2/15/11 4:55 PM	21.402	44.637	25.697	0.1826	118.870	1.325	14.475
19222.2	2/15/11 4:57 PM	21.457	44.701	25.761	0.1830	117.520	1.308	14.507
19333.3	2/15/11 4:59 PM	21.253	44.573	25.633	0.1829	116.640	1.297	14.504
19444.4	2/15/11 5:00 PM	21.245	44.445	25.569	0.1831	112.980	1.252	14.464
19555.6	2/15/11 5:02 PM	21.394	44.445	25.697	0.1829	116.750	1.299	14.351
19666.7	2/15/11 5:04 PM	21.386	44.637	25.761	0.1827	113.230	1.255	14.436
19777.8	2/15/11 5:06 PM	21.277	44.701	25.569	0.1825	117.190	1.304	14.612
19888.9	2/15/11 5:08 PM	21.371	44.701	25.633	0.1821	113.820	1.263	14.537
20000	2/15/11 5:10 PM	21.433	44.829	25.697	0.1812	112.790	1.250	14.514
20111.1	2/15/11 5:12 PM	21.379	44.893	25.697	0.1803	114.000	1.265	14.485
20222.2	2/15/11 5:13 PM	21.488	45.085	25.824	0.1802	112.570	1.247	14.531
20333.3	2/15/11 5:15 PM	21.590	45.213	25.888	0.1793	112.610	1.248	14.507
20444.4	2/15/11 5:17 PM	21.535	45.340	25.888	0.1805	117.190	1.304	14.697
20555.6	2/15/11 5:19 PM	21.551	45.276	26.016	0.1821	113.120	1.254	14.677
20666.7	2/15/11 5:21 PM	21.543	45.404	26.080	0.1834	113.230	1.255	14.838
20777.8	2/15/11 5:23 PM	21.472	45.468	26.016	0.1825	119.930	1.338	14.856
20888.9	2/15/11 5:25 PM	21.535	45.532	26.016	0.1811	119.680	1.335	14.796
21000	2/15/11 5:26 PM	21.606	45.532	25.952	0.1811	114.180	1.267	14.844
21111.1	2/15/11 5:28 PM	21.613	45.468	26.016	0.1814	113.120	1.254	14.771
21222.2	2/15/11 5:30 PM	21.676	45.468	26.080	0.1816	117.520	1.308	14.738

771556	2/24/11 9:56 AM	13.738	38.945	15.537	0.1772	129.240	1.454	17.360
771667	2/24/11 9:58 AM	13.637	39.009	15.346	0.1768	129.240	1.454	17.510
771778	2/24/11 9:59 AM	13.449	39.073	15.154	0.1767	127.950	1.438	17.695
771889	2/24/11 10:01 AM	13.480	39.073	15.090	0.1764	128.060	1.439	17.709
772000	2/24/11 10:03 AM	13.308	39.137	14.962	0.1775	128.580	1.446	17.962
772111	2/24/11 10:05 AM	13.269	39.073	15.026	0.1769	128.580	1.446	17.810
772222	2/24/11 10:07 AM	13.441	39.073	15.218	0.1773	129.020	1.451	17.709
772333	2/24/11 10:09 AM	13.668	39.201	15.537	0.1772	129.200	1.454	17.550
772444	2/24/11 10:10 AM	13.824	39.201	15.665	0.1768	130.370	1.468	17.416
772556	2/24/11 10:12 AM	14.044	39.265	15.857	0.1768	130.080	1.465	17.321
772667	2/24/11 10:14 AM	14.075	39.393	15.857	0.1770	129.460	1.457	17.435

Appendix B: Thermophysical Properties of Fluids

A.1. Water Liquid

The following correlations are based on the data from Holman (1992). The properties are valid from 0°C to 288°C .

Thermal Conductivity

$$k = 0.56611 + 0.002048T - 1.0205 \times 10^{-5}T^2 + 1.1897 \times 10^{-8}T^3 \quad (\text{A1})$$

Specific Heat

$$C_p = \exp(1.4423 - 8.4025 \times 10^{-4}T + 1.41 \times 10^{-5}T^2 - 7.3846 \times 10^{-8}T^3 + 1.4856 \times 10^{-10}T^4) \quad (\text{A2})$$

Density

$$\rho = 1002.6 - 0.2177T - 0.0020099T^2 - 1.6478 \times 10^{-6}T^3 \quad (\text{A3})$$

Dynamic Viscosity

$$\mu = \exp(-6.3933 - 0.026299T + 9.7341 \times 10^{-4}T^2 - 1.3986 \times 10^{-7}T^3) \quad (\text{A4})$$

A.2. Dry Air

The following correlations are based on data from Holman (1992). The properties are valid from 0 °C to 400 °C .

Thermal Conductivity

$$k = 0.02428 + 6.939 \times 10^{-5}T + 2.515 \times 10^{-8}T^2 - 7.194 \times 10^{-11}T^3 \quad (\text{A5})$$

Specific Heat

$$C_p = 1.005 - 1.473 \times 10^{-5}T + 7.002 \times 10^{-7}T^2 - 6.846 \times 10^{-10}T^3 \quad (\text{A6})$$

Density

$$\rho = \frac{101.325}{0.287(T + 273.15)} \quad (\text{A7})$$

Dynamic Viscosity

$$\mu = (13.29 + 0.0879T + 0.0001029T^2 - 3.749 \times 10^{-8}T^3) \times 10^{-6} \text{ m} \quad (\text{A8})$$

A.3. Water Vapour

The temperature is in the range of 0 to 200 °C .

Thermal Conductivity

$$k = 0.017071 + 5.3167 \times 10^{-5}T + 2.322 \times 10^{-7}T^2 + 3.8962 \times 10^{-10}T^3 \quad (\text{A9})$$

Specific Heat

$$C_p = 1.8653 + 1.0881 \times 10^{-5}T - 4.4902 \times 10^{-6}T^2 + 1.0183 \times 10^{-7}T^3 \quad (\text{A10})$$

Dynamic Viscosity

$$\mu = 10^{-6} \times (9.1445 + 0.029257T + 1.9067 \times 10^{-6}T^2) \quad (\text{A11})$$

To calculate the properties for mixture, the following relationships from Dharma Rao et al. (2008) are used:

$$\mu_g = \frac{\sum_{\alpha=1}^2 Y_{\alpha} \mu_{\alpha}}{\sum_{\beta} Y_{\beta} \Phi_{\alpha\beta}} \quad (\text{A12})$$

$$k_g = \frac{\sum_{\alpha=1}^2 Y_{\alpha} k_{\alpha}}{\sum_{\beta} Y_{\beta} \Phi_{\alpha\beta}} \quad (\text{A13})$$

$$\Phi_{\alpha\beta} = \frac{1}{\sqrt{8}} \left(1 + \frac{M_{\alpha}}{M_{\beta}}\right)^{-1/2} \left[1 + \left(\frac{\mu_{\alpha}}{\mu_{\beta}}\right)^{1/2} \left(\frac{M_{\beta}}{M_{\alpha}}\right)^{1/4}\right]^2 \quad (\text{A14})$$

$$C_p = Y_v C_{p,v} + Y_a C_{p,a} \quad (\text{A15})$$

$$D_{av} = \frac{1.87 \times 10^{-10} \times T^{2.072}}{P} \quad (\text{A16})$$

$$h_{fg} = 2,755,400 - 3.464(T - 5)^2 \quad (\text{A17})$$

$$P_v^* = \exp\left(18.79 - 0.0075T - \frac{5965.6}{T}\right) \quad (\text{A18})$$

Here, μ_g , k_g , C_p are the viscosity, the thermal conductivity and the specific heat of the air-vapour mixture, respectively, Y_{α} is the mole fraction of species α , Y_{β} is the mole fraction of species β , M is the molecular weight, Y_v is the mass fraction of vapour, Y_a is the mass fraction of air, D_{av} is the mass diffusivity between vapour and air, h_{fg} is the latent heat of water vapour, P_v^* is the saturation vapour pressure in bar, and T is the temperature in Kelvin.